

THE UNIVERSITY OF HULL

**Optical and Ion Beam Studies of Excimer Laser
Irradiated Hexagonal Silicon Carbide**

being a Thesis submitted for the Degree of

Doctor of Philosophy

By

Christopher Derek Walton B.Sc (Hons)

September, 2000

*In memory of
Esther Frances Walton.*

Acknowledgements

During the last four years I have received help from many people from both academic and social backgrounds. It is difficult for me to thank everybody adequately, however, what I can do here is no more than record my gratitude to all those concerned.

Firstly I would like to show my appreciation to Professor Peter Dyer, If it were not for Pete, firstly, for giving me the opportunity and secondly giving me the support towards the end, this thesis might not have been made possible. At the same time I would like to say thank you to all the members of staff within the physics department and especially to Judy and Margaret for their secretarial work.

My thanks go to my supervisor Dr David Sands for his continued help and advice. I would especially like to thank David for his personal support at the beginning of this work. I would also like to show my appreciation for having been given the opportunity to attend the international conference on Silicon Carbide and Related Materials in Raleigh, North Carolina. Here I was fortunate to meet one of the world leaders in Silicon Carbide research, Professor Wolfgang Jim Choyke.

My thanks go to Paul Monk, Bryan Tait, Gordon Sowersby, Terry Aspinwell, Anthony Sinclair and the team in the mechanical workshop for their excellent technical assistance and expertise. Without their help this work would not have been possible.

I am particularly indebted to Dr Howard Snelling for the stimulating discussions and his rhetorical questions for which, looking back, were an important part of my training.

Martin deserves a special mention. Working on the same material we were able to share ideas and discuss a variety of topics. Some, I might add, were related to Silicon Carbide and many others not. All in all, I enjoyed our discussions and it was a pleasure working together. Thank you.

Nancy, Phil, James, Fabien, Petros, Saher and Ali without doubt provide me with many happy memories. However, I do offer my sincere apologies for the times when I became so enthralled with my research that it appeared I had little time for anything else other than 'Silicon Carbide'.

I also thank Professor Winston Hagston for sharing with me his valuable time. An afternoon I will always remember was a conversation during the summer about atomic diffusion explaining the violent interactions that can occur within solids. This and similar discussions that took place stimulated my interests in solid state physics, particularly in the area of light interaction with matter.

I would like to thank Professor Paul Coleman and Faiz Malik for the positron annihilation results and also their kind hospitality during our meetings.

The financial support from EPSRC and DERA-Malvern is gratefully acknowledged as is the help and useful discussions from Dr Mike Uren and his colleagues.

On a lighter note, one cannot forget 'Google', for supplying many of the topics for our lunchtime discussions. A search engine that helped answer many questions and found many interesting articles which provided hours of enjoyable reading.

Finally, I am indebted to my family and friends back home who have been extremely supportive and understanding throughout my studies. I now look forward in being able to share with them a little more time together.

CONTENTS

Chapter 1

Introduction.

1.1 Silicon Carbide	1
1.2 References	8

Chapter 2

Excimer Laser Interaction with Silicon Carbide: Determination of Irradiation Parameters

2.1 Introduction	10
2.2 Optical Propagation in Semiconductors	12
2.2.1 Propagation in Free Space	13
2.2.2 Propagation in Semiconductors	15
2.3 Optical Measurements	21
2.3.1 Refractive Index Measurements	21
2.4 Experimental Procedure	25
2.4.1 Introduction	25
2.4.2 Sample Information	26
2.5 Experimental Results	27
2.5.1 ArF Irradiated Epitaxial 4H-SiC: In Vacuum	27
2.5.2 ArF Irradiated Epitaxial 4H-SiC: In Oxygen	31
2.5.3 XeCl Irradiated Bulk 4H-SiC: In Argon	35
2.5.4 Laser Induced Surface Modifications	38
2.6 Conclusion	41
2.7 References	42

CONTENTS

Chapter 3

Photoluminescence Measurements of Excimer Laser Irradiated and Hydrogenated 4H-Silicon Carbide

3.1 Introduction	44
3.2 Radiative Transition in Silicon Carbide	47
3.2.1 Donor Species in Silicon Carbide	49
3.2.2 Acceptors Species in Silicon Carbide	49
3.2.3 Band-Acceptor Transitions. (A_0 peaks)	50
3.2.4 Donor-Acceptor Pair (DAP) Recombination: (B_0 and C_0 peaks)	52
3.3 Experimental Procedure	53
3.4 Experimental Results	55
3.4.1 Photoluminescence Interpretation of As-Received Material	55
3.4.2 Broad Band Photoluminescence Spectra	56
3.4.3 ArF Laser Irradiated 4H-SiC	63
3.4.4 Hydrogen Passivation of Epitaxial 4H-SiC	65
3.4.5 XeCl Laser Irradiated Bulk 4H-SiC.	70
3.5 Conclusion	73
3.6 References	74

CONTENTS

Chapter 4

Positron Annihilation Studies of Excimer Laser Irradiated 4H-Silicon Carbide

4.1 Introduction	76
4.2 Positron Annihilation Spectroscopy	76
4.3 The Momentum Distribution Technique: Doppler Broadening	78
4.3.1 Interpretation of S and W Parameters	80
4.3.2 Positron Implantation and Diffusion	81
4.4 Experimental Procedure	83
4.5 Experimental Results	85
4.5.1 XeCl Laser Irradiated 4H-SiC	86
4.5.2 ArF Laser Irradiated Epitaxial 4H-SiC	88
4.6 Conclusion	93
4.7 References	94

CONTENTS

Chapter 5

Excimer Laser Annealing of Ion-Implanted 4H- and 6H-Silicon Carbide

5.1 Introduction.	96
5.2 Lattice Recovery.	98
5.2.1 Ion-Implantation Damage.	98
5.2.2 Pulsed Laser Annealing.	100
Thermal Model	101
Plasma Model	102
5.3 Infrared Reflectivity in Silicon Carbide: The Reststrahlen Band.	104
5.3.1 The Lorentz-Drude Model.	105
5.4 Experimental Procedure.	107
5.4.1 Infrared Measurements.	107
5.4.2 XeCl Excimer Laser Annealing.	108
5.5 Experimental Results:	110
5.5.1 Reflectivity of As-received and Ion-Implanted 4H-SiC	110
5.5.2 Near Normal Reflectivity of Laser Irradiated 4H-SiC	116
5.5.3 Spatial Dispersion Effects of Laser Irradiated 6H-SiC	123
5.5.4 Lorentz-Drude Interpretation of Laser Annealed 4H-SiC	133
5.5.5 Dopant Activation.	143
5.5.6 Structural Modifications of XeCl Laser Annealed 4H-SiC	148
5.6 Conclusion	151
5.7 References.	153

CONTENTS

Chapter 6

Summary and Conclusion

6.1 Summary	156
6.2 Conclusion	167
6.3 References	169

Publications and Presentations

Publications	170
Presentations	171

Abstract

The realisation of doped regions, specifically Nitrogen, in Silicon Carbide (SiC) for transistor and p-n junction applications is a serious problem. Difficulty arises because of the low value of the diffusion coefficient and consequently the excessive temperatures required for substantial diffusion to take place can cause dissociation of the material. Coincidentally, the robustness of Silicon Carbide makes it a suitable material for use in harsh environments, where excessive radiation and temperatures exist especially for high power and high frequency applications. Diffusion and activation using thermal processes in equilibrium is not a practicable solution and therefore one feasible alternative technique is that of ion-implantation and laser annealing. However, the incorporation of dopants by ion implantation can cause damage to the crystal lattice. In the work that follows, excimer laser processing of Silicon Carbide has been employed to address these problems from two quite different approaches.

Experimental investigations are carried out to investigate the laser interaction of Silicon Carbide over a range of laser fluence close to the ablation threshold. These experiments serve as preliminary investigations to establish the experimental process parameters for the fourth coming work. As a first approach, work was carried out in an attempt to introduce vacancy type defects into the lattice of 4H-SiC using both Argon Fluoride (193nm) and Xenon Chloride (308nm) excimer lasers, a technique we refer to here as "Laser Induced Defect Mediated Diffusion". The introduction of defects using ion beams to displace host atoms has previously been undertaken by other workers where it has been shown that the diffusion of dopant species can be enhanced, however, no such studies on Silicon Carbide exist at the present time using an excimer laser to specifically disrupt the lattice in this way. Photoluminescence (PL) and Positron Annihilation (PA) measurements are adopted as the diagnostic techniques to measure and quantify the response of Silicon Carbide subsequent to laser irradiation, hence help determine the nature of any defects that might have been introduced. PL measurements of ArF laser irradiated Silicon Carbide revealed the evolution of an emission band that correlates with the laser fluence which was tentatively associated with laser induced damage below the ablation threshold. Work is driven by these latter results and a technique for gaining further information on the nature of this band was adopted. The technique of PA is

carried out on both ArF and XeCl laser irradiated material. On a microscopic scale the laser induced 'damage' consists of di-vacancy clusters at the near surface. The damage consists of large voids, essentially holes, which are not suitable for mediating the diffusion of dopant species in Silicon Carbide.

Secondly, an alternative way of introducing Nitrogen dopants is carried out. Samples of 4H- and 6H-SiC were implanted with Nitrogen ions and later annealed using a Xenon Chloride excimer laser. The laser annealing experiments serve the purpose of removing/reducing implantation damage. Fourier Transform Infrared Reflection (FTIR) spectrometric and visible reflection measurements have been undertaken in an attempt to determine the optimum parameters for lattice recovery. We show that excimer laser annealing can be considered as an alternative method of removing ion-implantation damage when annealed at a optimum laser fluence and above this optimum the photon flux imparts detrimental damage to the lattice.

Chapter 1

Introduction

1.1	Silicon Carbide	1
1.2	References.	8

Chapter 1

Introduction

1.1 Silicon Carbide

The first reports on Silicon Carbide (SiC) came as long ago as 1824 by the Swedish scientist of the name Jons Jacob Berzelious. He published a paper that suggested there might be a bond between the elements Carbon and Silicon. A short time later in 1895, E. G. Acheson synthesized the very first compound of SiC. Consequently, in 1907, the electroluminescent properties of SiC were discovered and the very first light emitting diode was produced [1]. At the time the properties and potential of this material were not known and a null in research activities seems to have existed. However, recently there has been a resurgence in SiC device technology.

The international conference on Silicon Carbide and Related Materials 1999, (ICSCRM99), held in Raleigh North Carolina was opened by Prof. W. J. Choyke[¶]. His opening speech was titled 'the semiconductor of the future'. Possibly a little ambitious, but nevertheless, such a bold statement from an eminent scientist gives an indication of the potential this material might have in the future. Not surprisingly, GaAs had similar expectations and only recently it has begun to realize the small niche market. The motivation for work on SiC is founded in markets where Silicon has reached limits in nature and not in technology. Because SiC bares some similarities to silicon, the already established processing technology adopted for silicon can be employed to SiC and it is this as well as the advanced properties that have excited the SiC community.

[¶] Prof W. J. Choyke has been fortunate to work on SiC throughout his entire life, his first paper on SiC was in the early 1950's and he is continuing to make influential research contributions in this area.

SiC is the only known compound of Silicon and Carbon, the basic unit consists of a covalently bonded tetrahedron of Silicon and Carbon atoms with either Silicon or Carbon at a centroidal position. SiC exhibits a one-dimensional polymorphism called polytypism. Silicon and Carbon bi-layers can take up one of three positions in the sub-lattice, thus in hexagonal material, produce a number of stacking sequences, so called polytypes where more than 200 have already been discovered [2]. Several notations are in common use to identify the various polytypes [3]. The most widely adopted notation is that introduced by Ramsdel [4] and will be adopted in this thesis. The prefix letters 'C', 'H' and 'R' refer to the Cubic, Hexagonal and Rhombohedral structures respectively and a numerical prefix (e.g 4H-SiC) refers to the number of Si-C bi-layers along the 'c' axis before the structure is repeated. Another nomenclature that is commonly used, especially in some of the references within this thesis is the 'Ramsdell zigzag'. The position of the three possible bi-layers are depicted by unique positions, 'A', 'B', and 'C', e.g., 4H-SiC and 6H-SiC can be represented by the stacking sequence 'ABCB' and 'ABCBCA' respectively.

It has been known for many years that SiC possesses enhanced properties. There has been resurgence in research interests over the last few decades, see fig 1. Much of the work takes place in the field of device technology and has emerged partly due to the improved techniques in crystal growth. High quality 6H- and 4H-SiC wafers became commercially available in 1991 and 1994 from Cree [5] and ATMI in 1995 [6] respectively.

SiC is a very versatile material. One of the early recognized properties is its mechanical hardness, (Mohs hardness ~9.5), the high cohesive atomic bond energies enable carborundum to be used as an abrasive material. [7]. Optical engineers have developed SiC mirrors for use with VUV lasers [8,9] and have exhibited relatively high reflection coefficient at a wavelength ~ 60nm. They again, exhibit extreme robustness with structural stability at energy densities up to 1.0 J.cm^{-2} and have remained structurally stable over many hours of operation. A rather novel application of SiC is the use as a slow positron field assisted moderator (FAM). Research carried out by Prof. P. G. Coleman et al, who carries out the defect studies in this work,

discovered copious slow-positron re-emission in virgin 6H-SiC material [10]. The intrinsic nature of the periodic structure of the various polytypes introduces exciting device applications.

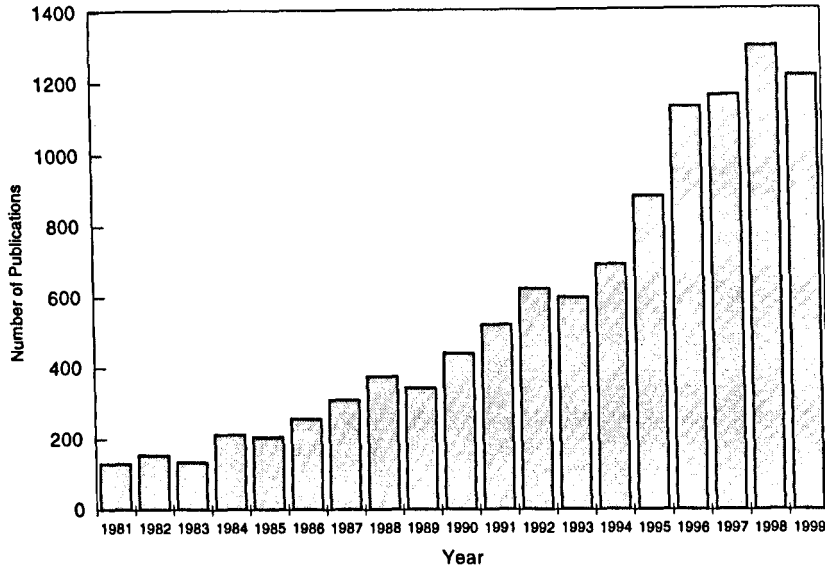


Figure 1:1. Research Interest in Silicon Carbide between 1981 and 1999. (Data taken from the University of Bath data base : BIDS).

Bloch oscillations connected with the Bragg reflection of electrons have been experimentally observed [11] in SiC. Direct measurements have allowed observation of negative differential resistance for some of the more common hexagonal polytypes including 4H-SiC.

From a device aspect, SiC is expected to be a promising material for high voltage semiconductor power devices. Properties such as high avalanche electric breakdown field ($\sim 3 \times 10^6 \text{ V cm}^{-1}$), large bandgap (4H-SiC : 3.285 eV, at 2 kelvin), a thermal conductivity that approaches, or if not exceeds that of copper (4H-SiC : $4.7 \text{ W cm}^{-1} \text{ K}^{-1}$) and also high radiation resistance make it a good candidate for high voltage high temperature [12,13] and high power applications [14]. In addition, chemical inertness and low dopant diffusivities of SiC also provide stable operation at elevated temperatures with low leakage currents.

However, the reliability and yield of such devices has been hampered by the existence of microchannel defects termed micro-pipes [15]. They are hollow tubes that penetrate along the growth direction, [16,17], and only recently have the micropipe defect densities reduced significantly [18], the latest figure reported to be $< 1 \text{ cm}^{-2}$ in 35mm diameter wafers [19]. With micropipes sizes being of the order of $\sim 5 \text{ }\mu\text{m}$ in diameter this might seem reasonably acceptable, but these figures are for selective wafers showing the importance of solving the aforementioned problem. For high power, high voltage vertical power devices, areas of $\sim \text{cm}^2$ may be required and therefore the existence of micropipes restricts the usable area of the wafer. Even a single micropipe would be sufficient in the active region to kill the device. In smaller devices this problem is not so detrimental and working SiC devices have been realized with some degree of success, see figure 1:2. However, there is still a great deal of research activity in the field of high frequency devices to optimize the electrical contacts, especially in harsh environments [20]. Devices are in their early design stages and there is much room for improvement in terms of optimizing processing techniques [21] and improving electrical properties. One particularly relevant aspect is to reduce the contact resistance, hence, very few devices are presently commercially unavailable. SiC devices do have the advantage of operating at temperature $> 250\text{C}$ where conventional Silicon devices begin to fail. This is particularly important for high power and high frequency devices that operate in high radiation environments.

A *p-n* junction plays an essential role in a semiconductor device. There are various ways of introducing dopant species into a material to produce such a junction. 1) a *vaporization* process can be used to transport dopant species into the material [22]. 2) diffusion from *deposited surface layers* and driven in via some external driving force, for example, a flash lamp [23] or a laser [24,25,26], 3) *ion implantation* doping [27,28,29] and 4) *insitu-doping* utilizing site competition epitaxy [30,31]

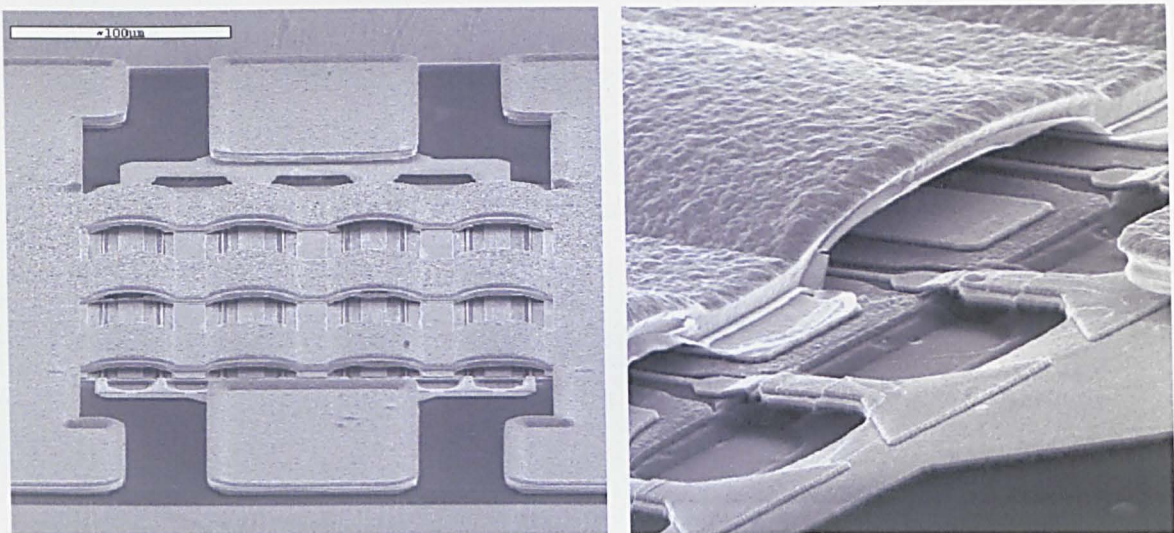


Figure 1:2 4H-SiC Air spaced 8×250 μm Power FET; Courtesy of DERA Malvern.

In essence, this work is driven by the non-trivial problem concerning the very low diffusivity of dopants in SiC, specifically, the *n*-type dopant nitrogen. Thermal diffusion has been readily employed in many semiconductors to modify the electrical and optical properties. However, in SiC, the nitrogen diffusion coefficient $\sim 10^{-20} \text{ cm}^2 \text{ s}^{-1}$ at 1500 C [32,33] and therefore with the present technology thermal diffusion is not feasible in practical timescales. High-dose nitrogen implants used for formation of source and drain contacts typically require anneal temperatures in excess of 1600 C and at these temperature levels SiC begins to decompose [34]. Sublimation occurs at $\sim 1850 \text{ C}$ and at these elevated increased temperatures the surface eventually becomes graphitic [35]. Therefore ways of suppressing ejected species and preventing graphitization becomes necessary. SiO_2 and Si_3N_4 dielectric capping layers have been used to prevent detrimental surface modifications, but they themselves begin to dissociate [36]. Recently AlN capping layers [37] which have a more stable at slightly higher temperatures compared with the latter have been used with some success but the processing steps can be considered as being rather numerous and unnecessarily complicated.

Ion implantation doping is a recognized technique which reduces the problems associated with decomposition at elevated temperatures and is currently the accepted doping technique [38]. Source, drain, gate and channel regions can be selectively modified with this process and it can

be considered as having the best overall results. Dopant concentrations, junction depths and their profiles can be controlled. Unfortunately, the collisional nature of the implantation process causes damage to the lattice structure and in the most severe case, high dose ion-implantation into a crystalline material can totally amorphize the material. Therefore, ways of restoring the lattice symmetry, whilst maintaining the stoichiometry [39] and preventing polytypic transformations [40] become essential. Implantation can be carried out at temperatures (600-800 °C) [41], but even at these temperatures the effect is only to reduce the amount of implantation damage.

Several techniques are available to anneal out any induced lattice damage. Thermal anneals exist but unfortunately the prolonged exposure causes detrimental loss of surface material. Rapid thermal annealing (RTA) techniques have been developed and are proving to be reasonably successful. However, as with most newly developed systems, initial problems arise that need to be addressed. In the case of RTA, problems with surface degradation and increased surface roughness exist and there is the difficulty in annealing selective areas.

In this work excimer laser processing is being adopted as an alternative way to address the aforementioned problems, essentially from two different angles. Firstly we address the low diffusion coefficient of dopants in SiC. Many diffusion mechanisms exist within the literature, but there is a great deal of controversy regarding the very nature of the diffusion processes. The mechanisms are extremely complex and certainly not fully understood, but, we accept that diffusion via vacancies might enhance the diffusion process. We therefore investigate the interaction process of excimer laser irradiation of SiC with photoluminescence and positron annihilation spectroscopy with the view of introducing vacancy type defects. Secondly we address the problem of annealing out induced implantation damage using an excimer laser. Excimer laser processing has been an adopted process for many years for annealing and activation of disordered semiconductors [42]. However very little work has been carried out on excimer laser interactions with SiC and especially 4H-SiC. Excimer laser processing offers several advantages over conventional techniques. Typical excimer laser pulse durations are in

the nano-second regime and at these relatively short time scales minimal heat is transferred into the un-irradiated regions. Therefore an advantage exists over conventional thermal anneals due to the duration of the thermal cycles in terms of unwanted lateral heat flow. Non-equilibrium heating reduces the time available for thermal decomposition and from a technologically point of view low thermal budgets can be realized. With device sizes continuously shrinking, 'self aligned processing' is becoming increasingly important. Here, excimer laser processing does to some extent offer advantages over existing processes in terms of spatial selection and throughput. Therefore a novel way of enhancing the diffusion coefficient would itself be a major contribution since it is one of the fundamental problems that impedes the development of SiC electronic devices. Secondly, as an alternative route, to investigate the possibilities of improving conventional processing techniques using excimer laser irradiation by removing implantation damage by laser annealing will be undertaken.

Both these routes are ultimately connected with the intrinsic nature of the extremely low value of the Nitrogen diffusion coefficient in SiC.

1.2 References.

-
- [1] H. J. Round, *Electrical World*. **19** 309, (1907).
- [2] G. Pensl and W. J. Choyke, *Phys. B* **185**, 264 (1993).
- [3] P. G. Baranov, N. G. Romanov, V. A. Vetrov, V.G. Oding., 20th . Conf. Physics of Semiconductors Ed E.M. Anastassakis, J.D Joannopoulos (World Scientific, Singapore, New Jersey, London, Hong Kong, 1990, 1885).
- [4] P. G. Baranov, N. G. Romanov., *Mater. Sci. Forum*. **83-87** 1207 (1992).
- [5] Cree. Research. Inc., Durham, NC 27713, USA.
- [6] Advanced Technology Materials, Inc, 7 Commerce Drive, Danbury, CT 06810-4169.
- [7] R. E. Kirk and D. F. Othmer, *Encyclopedia of Chemical Technology*, 3rd. ed. (Wiley, New York, 1978), Vol 4, pp.520-535.
- [8] M. Ohmukai, H. Naito, M. Okuda, K. Kurosawa, W. Sasaki, Y. Takigawa, T. Matsushita and Y. Tsunawaki. *Jpn. J. Appl. Phys.* **31** L686 (1992).
- [9] A. M. Keski-Kuha, J. F. Osantowski, D. B. Leviton, T. T. Saha, G. A. Wright, R. A. Boucarut, C. M. Fleetwood and T. J. Madison, *Opt. Eng.* **36** 157 (1997).
- [10] J. Stormer, A. Goodtear, W. Anwand, G. Brauer, P. G. Coleman and W. Triftshauser, *J. Phys. Condens Matter*, **8** L89 (1996).
- [11] V. Sankin and I. Stolichnov, *Superlattices and Microstructures*, **23**, (5), 999 (1998).
- [12] P. L. Dreike, D. M. Fleetwood, D. B. King, D. C. Sprauer and T. E. Zipperian, *IEEE Transactions on Components Packing and Manufacturing Technology Part A*, **17**, (4) 594 (1994).
- [13] V. E. Chelnokov and A. L. Syrkin, *Materials Science and Engineering*, **B46**, 248 (1997).
- [14] E. Janzen and O. Kordina, *Materials Science and Engineering*, **B46**, 203 (1997).
- [15] J. Heindl and H. P. Strunk, V. Heydemann and G. Pensl, *Phys. Status. Solidi (a)* **162**, 251 (1997).
- [16] S. V. Rendakova, L. P. Nikitina, A. S. Tregubova and V. A. Dmitreiv, *J. Electronic Materials*, **27**, 4 292 (1998).
- [17] J. Heindl and H. P. Strunk, *Phys. Status Solidi (b)* **193**, K1 (1996).
- [18] V. F. Tsetkov, S. T. Allen, H. S. Kong and C. H. Carter Jr., *Inst Phys. Conf. Ser.*, **142**, 17 (1996).
- [19] C. H. Carter, Jr, V. F. Tsvetkov, D. Henshall, O. Kordina, K. Irvine, R. Singh, S. T. Allen and J. W. Palmer, *Progress in SiC*, 2nd European Conference on SiC and Related Materials., France, (1998) p 1-2.
- [20] J. Crofton, P. A. Barnes. J. R. Williams. And J. A. Edmond, *Appl. Phys. Lett.* **62** 384 (1993).
- [21] K. Yamaski. K. Asai, K. Kurumada. *IEEE, Trans. Electron. Devices* **29** 1772 (1982).
- [22] S.Y. Chou, Y. Chang, K. H. Weiner, T. W. Sigmon, *Appl. Phys. Lett.* **56** 530 (1990).

-
- [23] H. Wirth, D. Panknin, W. Skorupa and E. Niemann, *Appl. Phys. Lett.* **74**, 979 (1999).
- [24] G. G. Bentini, M. Bianconi, C. Summonte: *Appl. Phys. A*, **45**, 317 (1988).
- [25] S. Krishnan, G. C. D' Couto, M. I. Chaudhry and S. V. Babu, *J. Matl. Res.* **10**, 11, 2723 (1995).
- [26] O. Eryu, Y. Okuyama, K. Nahashima, T. Nakata and M. Watanabe, *Appl. Phys. Lett.* **67**, 14, 2052 (1995).
- [27] W. Suttrop, H. Zhang, M. Schadt, G. Pensl, K. Dohnke and S. Leibenzeder, *Springer Proc. In Physics* **71**, 143 (1990).
- [28] M. Ghezzo, D. M. Brown, E. Downey, J. Kretchmer, W. Hennessy, D. L. Polla and H. Bakhru, *IEEE Electron Device Letters*, **13**, 639 (1992).
- [29] N. Inoue, A. Itoh, H. Matsunai, T. Nakata and M. Watanabe, *Inst. Phys. Conf. Ser.* **142**, 525 (1996).
- [30] D. J. Larkin, *Inst. Phys. Conf. Ser.*, **142**, 23 (1996).
- [31] D. J. Larkin, P. G. Neudeck, J. A. Powell and L. G. Matus, *Appl. Phys. Lett.* **65**, 1659 (1994).
- [32] L. T. Kroko and A. G. Milnes, *Solid State Electron.* **9**, 1129 (1966).
- [33] R. F. Davis, G. Kelner, M. Shur, J. W. Palmour and J. A. Edmond, *Proc. IEEE Electron Device Letters*, **18**, 349 (1997).
- [34] S. K. Iilov, *Diamond and Related Materials*, **4**, 1331 (1995).
- [35] S. V. Baranov, A. G. Vodop'yanov, G. K. Moiseev, and G. N. Kozhevnikov, **18**(8) 1097 (1982).
- [36] K. A. Jones, K. Xie, D.W. Eckart, and M.C. Wood, V. Talyank, R.D. Vispute, T. Venkatesan, K. Wongchotigul and M. Spencer. *J. Appl. Phys.* **53**, 8010 (1998).
- [37] K. A. Jones, M. A. Derenge, P. B. Shah, T. S. Zhel'ueva, M. H. Ervin, K. W. Kirchner, and M.C. Wood, *International Conf Proc, North Carolina*, 10th -15th Oct 1503 (1999).
- [38] H. Sonntag, S. Kalbitzer, *J. Appl Phys. A*. **61**, 363 (1995).
- [39] J. Pezoldt, A. A. Kalnin, D. R. Moskwina, and W. D. Savelyev. *Nuclear Instruments and Methods in Physics Research*, **B80/81** 943 (1993).
- [40] I. S. Vlaskina, and D. H. Shin, *Jpn. J. Appl. Phys.* **38**, L27 (1999).
- [41] H. G. Bohn, J. M. Williams, C. J. McHargue and G. M. Begun, *J. Mater. Res.* **2** (1), 107 (1987).
- [42] I. B. Khaibullin and I. S. Smirnov. *Sov. Phys. Semicond.* **19**(4). 353 (1985).

Chapter 2

Excimer Laser Interaction with Silicon Carbide: Determination of Irradiation Parameters

2.1 Introduction	10
2.2 Optical Propagation in Semiconductors	12
2.2.1 Propagation in Free Space	13
2.2.2 Propagation in Semiconductors	15
2.3 Optical Measurements	21
2.3.1 Refractive Index Measurements	21
2.4 Experimental Procedure	25
2.4.1 Introduction	25
2.4.2 Sample Information	26
2.5 Experimental Results	27
2.5.1 ArF Irradiated Epitaxial 4H-SiC: In Vacuum	27
2.5.2 ArF Irradiated Epitaxial 4H-SiC: In Oxygen	31
2.5.3 XeCl Irradiated Bulk 4H-SiC: In Argon	35
2.5.4 Laser Induced Surface Modifications	38
2.6 Conclusion	41
2.7 References	42

Chapter 2

Excimer Laser Interaction with Silicon Carbide: Determination of Irradiation Parameters

2.1 Introduction

The use of lasers in many applications requires an understanding of the fundamental processes involved during laser material interaction. Optical, thermal, mechanical and radiative response depend on parameters such as the energy density (fluence), pulse duration, the surface morphology of the material, the gas ambient and the wavelength (frequency) of radiation.

High quality crystalline 4H-SiC has only been commercially available since ~ 1994 [1]. At the time, little work existed in the literature on the laser processing of this material. A check shortly before the submission of this thesis revealed only thirty papers between the years 1981-2000 which were primarily concerned with *laser ablation/desorption* of Silicon Carbide. Many of which were concerned with thin film deposition techniques and not directly concerned with the target material. Furthermore, only four concerned laser irradiation above a damage threshold [2,3,4,5]. Although extensive work has been carried out in this area with other materials, very little work has been directly concerned with excimer laser processing of 4H-SiC. The main drive has been to produce 'high quality' crystalline material for electronic devices and subsequently the principle effort has been directed towards processes derived from standard CMOS/Si technology. Excimer lasers are not a standard tool for processing electronic devices and because of this, there has been very little work on processing Silicon Carbide by these means. However, if excimer lasers are to be adopted as a viable processing tool then the optical response of fundamental parameters such as reflectivity, absorption depths, (α^{-1}), and

Excimer Laser Interaction with Silicon Carbide:
Determination of Irradiation Parameters

ablation 'thresholds' have to be determined. The absorption of optical radiation, however, can be different between samples and therefore experimental verification is important. Various polishing techniques are available [6,7] inducing differences in the surface roughness [8] and therefore affecting the surface reflectivity. Also, the concentrations of dopants and depending on the way the dopants have been incorporated, can influence the optical absorption. Particularly, the damage induced by ion implantation doping [9] can severely modify the optical absorption thus making the absorption highly sample dependent. With this in mind, ablation/desorption experiments have been carried out to establish the processing regimes for subsequent annealing and irradiation of Silicon Carbide. Therefore, by establishing the processing 'window' in laser fluence we will ensure that subsequent annealing work will not detrimentally modify the material in anyway.

It has been reported that under equilibrium conditions, at a pressure of one atmosphere, Silicon Carbide does not melt but sublimates [10,11]. Such conditions can lead to the surface regions becoming carbon rich and graphitic in nature. However, Burdel *et al* [2], have reported Silicon Carbide melts under the action of an XeCl laser pulse [2]. Inspection of the surface revealed a black appearance and it was attributed to the creation of a defect surface layer but not with graphitisation, highlighting the importance between equilibrium and non-equilibrium processes. High temperature analogues in the carbon related group IV elements are the materials graphite and diamond. It has also been observed that a Ruby laser used to irradiate graphite also melted the surface [12]. Therefore, because melting is pressure dependent there exists interesting debate on the exact peritectic point in the phase diagrams of Silicon Carbide.

In this work Silicon Carbide has been irradiated under varying processing conditions using Argon Fluoride (ArF : $\lambda=193\text{nm}$) and Xenon Chloride (XeCl : $\lambda=308\text{nm}$) lasers. The beam energy density, (fluence: J cm^{-2}), and number of laser pulses were varied in vacuum conditions and in an oxygen environment to establish basic ablation characteristics. Etch rate

measurements have been performed in order to establish ablation threshold calculations, hence, obtain the processing parameters for the subsequent chapters, namely, defect, damage and annealing studies in Chapters 3,4 and 5 respectively. Due to cost and availability, ablation experiments, because of their deleterious nature, were limited in number. Therefore, a minimal set of ablation/desorption experiments were carried out. The main aim was to establish the processing regimes rather than a more complete characterization of ablation/desorption processes and their mechanisms. We begin with a description of the fundamental optical properties of Silicon Carbide which serves also as the basic theory for the optical characterisation of the material described in Chapter 2.3.

2.2 Optical Propagation in Semiconductors

Light is generally defined as an electromagnetic radiation at visible wavelengths in the range ~370-800nm. However, occasionally within this thesis, Ultra Violet (UV) laser radiation, which lies outside this range will be loosely referred to as laser 'light'. Throughout this work light has been used in some form or another, be it to modify the Silicon Carbide using a laser or to probe effects of laser processing via standard optical characterization techniques. Therefore, light-interaction with matter is fundamental to this work and a brief description explaining the origins of optical constants and the associated experimental measurables are outlined, thus serving as an introduction for the subsequent chapters. The relatively simple behaviour of electromagnetic (EM) waves in free space underlies their far more complicated interactions in solids. EM can be related to the behaviour in a semiconductor to the quantities characteristic of the microscopic nature of the solid, namely, the frequency dependent dielectric function $\epsilon(\omega) = \epsilon_r + i\epsilon_i$ and the absorption coefficient $\alpha(\omega)$. These can then be related to the experimental measurables, reflectance, transmittance and absorptance.

2.2.1 Propagation in Free Space

Maxwell's equations define the behaviour of EM waves. Their solutions in free space describe undamped transverse waves which are composed of transverse electric and magnetic fields that propagate at the fixed speed of light [13]

$$\nabla \times \mathbf{H} = \mathbf{j} + \frac{\partial \mathbf{D}}{\partial t} \quad (2:1)$$

$$\nabla \times \mathbf{E} = -\frac{\partial \mathbf{B}}{\partial t} \quad (2:2)$$

$$\nabla \cdot \mathbf{D} = \rho \quad (2:3)$$

$$\nabla \cdot \mathbf{B} = 0 \quad (2:4)$$

where \mathbf{H} is the magnetic field strength, \mathbf{j} is the current density, \mathbf{D} , is the displacement vector, \mathbf{E} is the electric field, \mathbf{B} is the magnetic induction, ρ , is the free carrier charge density and t is the time. Maxwell's equations give a very concise description but are not in solvable form until the exact relation between \mathbf{D} and \mathbf{E} , and, \mathbf{B} and \mathbf{H} are known. The basic relations are:

$$\mathbf{D} = \epsilon_0 \mathbf{E} + \mathbf{P} = \epsilon \epsilon_0 \mathbf{E} \quad (2:5)$$

$$\mathbf{B} = \mu_0 \mathbf{H} + \mathbf{M} = \mu \mu_0 \mathbf{H} \quad (2:6)$$

where ϵ_0 is the permittivity in free space, \mathbf{P} , is the electric dipole per unit volume, μ_0 is the permeability of free space, \mathbf{M} , is the magnetic dipole per unit volume, ϵ and μ are the permittivity and permeability of the medium other than vacuum respectively.

Excimer Laser Interaction with Silicon Carbide:
Determination of Irradiation Parameters

In the simplest medium, free space, where there are no free charge carriers $j = 0$ and $\rho = 0$ and excludes magnetic and electric polarisation, therefore, equations (2:5) and (2:6) become

$$D = \epsilon_0 E \quad (2:7)$$

$$B = \mu_0 H \quad (2:8)$$

when this information is inserted into equations (1-4) the electric field becomes:

$$\nabla^2 E = \epsilon_0 \mu_0 \frac{\partial^2 E}{\partial t^2} \quad (2:9)$$

The standard solution of the wave equation in equation (2:9) is an oscillatory disturbance which propagates at a speed determined by the medium. The oscillatory form is represented by the complex term:

$$e^{i(qr - \omega t)} \quad (2:10)$$

where q is the wave vector which points in the direction of propagation and has a magnitude of $2\pi/\lambda = 2\pi f$ where λ is the wavelength and $1/\lambda$ is the wave number (cm^{-1}) and ω is the radian frequency $2\pi\nu$, with ν , the frequency in Hertz. If the wave propagates in the z direction, with a wave velocity ω/q , the assumed solution for equation (2:9) is then

$$E = E_0 e^{i(qz - \omega t)} \quad (2:11)$$

where E_0 defines the direction and magnitude of the electric field. Substituting this into equation (2:9)

$$q^2 = \epsilon_0 \mu_0 \omega^2 \quad (2:12)$$

which gives an electric field

$$E = E_0 e^{i\omega(z\sqrt{\epsilon_0\mu_0}-t)} \quad (2:13)$$

In the above solution for a wave propagating in free space there is no term that causes loss of energy, therefore there is no loss of amplitude and is atypical of a real medium.

2.2.2 Propagation in Semiconductors

The situation is somewhat different in a solid. The propagation of an EM wave is perturbed by the constituent charges which do not exist in free space. The waves become damped as they interact with the charges within the solid such that new phenomena occur, i.e. the speed of propagation depends on the frequency ω and longitudinal and transverse waves may occur. Unlike free space, a semiconductor solid contains bound and free charges. The free charges are the conduction electrons and valence band holes. The bound charges arise from the atomic charges comprising the lattice itself and defect sites. Defects and their complexes will also contribute to different absorption mechanisms. Thus, current charge density due to free charges and polarisability of the bound charges at perfect and defect lattice sites all affect the use of Maxwell's equations.

If we consider only the bound charges a dipole moment per unit volume, P , is produced. To a first approximation the magnitude is proportional to the electric field, E .

$$P = \chi\epsilon_0 E \quad (2:14)$$

where χ is called the susceptibility. The relationship is in fact more complex, with P depending on higher orders of, E , however, considering the linear approximation, equation (2:7) becomes

$$D = \epsilon_0 E + P = \epsilon_0 (1 + \chi) E = \epsilon_{\text{lat}}(\omega) \epsilon_0 E \quad (2:15)$$

Excimer Laser Interaction with Silicon Carbide:
Determination of Irradiation Parameters

where ϵ_{lat} refers to the dielectric response due to the electrons bound into the lattice and the lattice atoms themselves. The polarisation depends on the frequency of the electric field which accounts for the frequency dependant term $\epsilon_{\text{lat}}(\omega)$. By considering the microscopic charge current of Ohm's law due to free carriers and holes can be represented as

$$\mathbf{j} = \sigma(\omega)\mathbf{E} \quad (2:16)$$

where $\sigma(\omega)$ is frequency dependant conductivity. Substituting equations (2:15) and (2:16) into Maxwell's equation (2:1-2:4) and manipulating to eliminate B , gives the wave equation for the electric field in a solid:

$$\nabla \times \nabla \times \mathbf{E} = \nabla^2 \mathbf{E} - \nabla(\nabla \cdot \mathbf{E}) = \epsilon_{\text{lat}} \epsilon_0 \mu_0 \frac{\partial^2 \mathbf{E}}{\partial t^2} + \sigma \mu_0 \frac{\partial \mathbf{E}}{\partial t} \quad (2:17)$$

This equation for E is different from that in free space in two ways, firstly the term, $\nabla \cdot E$, which was zero in free space but is finite here and secondly the last term on the right which accounts for the current of free charges. To understand these new features we assume a plane wave solution of the form $E = E_0 e^{i(qz - \omega t)}$, equation (2:17) gives

$$q^2 E - q(q \cdot E) = \epsilon_{\text{lat}} \epsilon_0 \mu_0 \omega^2 E + \sigma \mu_0 i \omega E = \omega^2 \epsilon(\omega) \epsilon_0 \mu_0 E \quad (2:18)$$

where the term $\epsilon(\omega)$ is the dielectric response function given by

$$\epsilon(\omega) = \epsilon_{\text{lat}}(\omega) + \frac{i\sigma(\omega)}{\epsilon_0 \omega} \quad (2:19)$$

Equation (2:19) is a central quantity that describes the electromagnetic-semiconductor interaction in the simplified linear response limit. It combines the polarisation due to the bound charges and the free carrier current effects. As can be it is frequency dependant because of the contribution due to lattice and conduction charges. However, equation (2:18) cannot be solved

Excimer Laser Interaction with Silicon Carbide:
Determination of Irradiation Parameters

immediately for q versus ω because of the term $q(q \cdot E)$ but the solution can be obtained if E is expressed as a sum of transverse and longitudinal term components:

$$E = E_t \hat{t} + E_q \hat{q} \quad (2:20)$$

\hat{t} is the unit vector in the x-y plane perpendicular to the direction of propagation, and \hat{q} is a unit vector along q . In this new form, equation (2:18) becomes:

$$\left[\left(\frac{\omega}{c} \right)^2 \epsilon(\omega) - q^2 \right] E_t \hat{t} + \left(\frac{\omega}{c} \right)^2 \epsilon(\omega) E_q \hat{q} = 0 \quad (2:21)$$

Because the two terms in the above are linearly independent, equation (2:21) is satisfied if the coefficients are each zero. Hence,

$$q^2 = \frac{\omega^2}{c^2} \epsilon(\omega) \quad (2:22)$$

is the generalised dispersion relation for transverse waves in a solid of total dielectric function $\epsilon(\omega)$ and

$$\epsilon(\omega) = 0 \quad (2:23)$$

is the condition for longitudinal modes to exist. Equations (2:22) and (2:23) play an important role in Infrared spectroscopy, particularly in the resonant phonon modes in semiconducting materials. Infrared studies are primarily concerned with such phonon modes and a more complete explanation of equations (2:22) and (2:23) is covered in Chapter 5.

The dielectric function is a complex quantity by its fundamental definition in equation (2:19) and can be written as $\epsilon_R + i\epsilon_I$. In fact ϵ_{lat} and σ can also be written in a similar manner since the imaginary components also include imaginary parts if the polarisation and conduction processes

Excimer Laser Interaction with Silicon Carbide:
Determination of Irradiation Parameters

in the semiconductor are lossy, which to some extent is always the case. This means that the magnitude of the wavevector, q , is also a complex quantity $q=q_R+iq_I$. If this is inserted into the plane wave solution which was used to solve equation (2:17) the result is:

$$E = E_0 e^{-q_I z} e^{i(q_R z - \omega t)} \quad (2:24)$$

Therefore the imaginary part of the wavevector derived from equation (2:22) is related to the damping of the electric field as it penetrates the medium, whereas the real part describes the propagation of the EM wave in the medium.

A more familiar usage of the latter observations is the quantity referred to as the complex refractive index:

$$\boxed{N = n + ik = \sqrt{\epsilon(\omega)}} \quad (2:25)$$

Combining equations (2:22), (2:24) and (2:25) gives

$$E = E_0 e^{-kqz} e^{i(nq_0 z - \omega t)} \quad (2:26)$$

where $q_0 = \omega/c$ is the wavevector in vacuum. Equation (2:26) shows that the real part of the refractive index is related to the propagation of the wave through the definition of propagation velocity $v = \omega/(nq_0)$. The imaginary part of (2:25) is related to the attenuation of a wave as it penetrates a medium and is referred to as the extinction coefficient, k .

Reflectance and transmittance depends on the angle of incidence, however, in this chapter, the laser light is incident normal to the sample surface at polarisation effects can be ignored. However the effects of non-normal incidence will be briefly covered in Chapter 5 where the incident angle of Infrared radiation is either near normal or increased to investigate the various phonon modes.

Excimer Laser Interaction with Silicon Carbide:
Determination of Irradiation Parameters

The Fresnel amplitude coefficients for reflectance and transmittance can be written as :

$$r = \frac{E_r}{E_i} = \frac{N_1 - N_2}{N_1 + N_2} \quad (2:27)$$

$$t = \frac{E_t}{E_i} = \frac{2N_1}{N_1 + N_2} \quad (2:28)$$

where E_i , E_r and E_t are the electric field amplitudes of the incident, reflected and transmitted waves and N_1 and N_2 are the complex refractive index of the incident of medium 1 and 2. From an experimental viewpoint what is actually measured is the intensity of the reflected wave denoted by R or what is transmitted denoted by T . Therefore $R = rr^* = |r|^2$ and $T = tt^* = |t|^2$. If medium 1 is air, $n_1 = 1$, and $k_1 = 0$, the measured reflectance is given as

$$R = \frac{(n-1)^2 + k^2}{(n+1)^2 + k^2} \quad (2:29)$$

The above gives the reflectance for an ideal bulk sample which is semi-infinite along the z axis, or when the back surface behaves as if it were infinitely distant. This can also be approximated by a finite sample which absorbs light heavily such that very little light reaches the back surface, i.e., for $k \gg 1$, (see Chapter 5). There are situations where the finite slab has virtually no absorption, i.e. where k is very small and reflections from the back surface have to be taken into account. This is particularly important for thin films on substrates or where an optical interface exists, i.e. where lattice damaged might occur due to ion implantation. These conditions, as we will see later, are pertinent in Chapter 5, where both conditions ($k \gg 1$ and $k \approx 0$) are encountered in the Reststrahlen region of the infrared part of the spectrum.

Excimer Laser Interaction with Silicon Carbide:
Determination of Irradiation Parameters

Transmittance experiments on optically thin material are generally carried out on samples which have been polished on both front and back surfaces. In such cases the transmittance can be expressed as

$$T = \frac{(1-R)^2 e^{-\alpha d}}{1-R^2 e^{-2\alpha d}} \quad (2:30)$$

Equation (2:30) shows that the transmitted intensity through a slab is effected by the front surface reflectance, R, and by the exponential loss, the so called absorption coefficient, α , given by:

$$\alpha = \frac{2\alpha k}{c} = \frac{4\pi k}{\lambda} \quad (2:31)$$

From equation (2:30), in the limit where the front surface reflectance $R = 0$, the intensity leaving the back surface I_t is ;

$$I_t = I_0 e^{-\alpha d} \quad (2:32)$$

This is a general equation for the intensity variation of light passing through a medium governed by absorption in the semiconductor often referred to as Beer's Law.

The latter simplified description of EM wave propagation serves purely as an introduction to some of the relevant equations in material - interaction processing. The last four equations, reflectivity, transmittance, absorption coefficient and the exponential decay of the electric field propagating within a material are important laser processing parameters, especially when deciding on a particular laser wavelength in order to achieve the required results.

2.3 Optical Measurements

The optical properties of 6H-SiC have been extensively studied when compared to that of the 4H polytype. The main reason for this is because the 6H-polytype has been commercially available for longer than 4H-material. The optical properties for 6H-SiC are well established [14], but, until quite recently, the optical properties and particularly the absorption coefficient for 4H-material, has had to have been estimated from 6H data. Experimental measurements were recently made by Choyke et al [15] to determine the depth to which electromagnetic radiation penetrates into 4H-material over the wavelength range 325.0-356.4 nm. These measurements were particularly chosen for more accurate determination of the absorption depth for photoluminescence experiments. Choyke *et al* points out that there is an element of uncertainty in the measured and calculated absorption depths due to the low value of the extinction coefficient $\sim 300\text{nm}$. From experimental measurements the absorption depth at a wavelength of 351nm was measured to be $\sim 35\ \mu\text{m}$ compared with 4-5 μm from expected n and k data [14,15]. The uncertainty arises because the value of k is very small at this wavelength and therefore detecting the signal becomes difficult, consequently, the uncertainty in the measurement is increased.

2.3.1 Refractive Index Measurements

Ellipsometry measurements, courtesy of DERA, Malvern, were carried out to determine the optical properties between 300 – 900 nm. A wealth of information can be obtained from n and k data, our main concern are the parameters affecting the amount of radiation coupling into the material, e.g. equations (2:29 - 2:32). The ellipsometric data in Figure 2.3:1 only went down to a wavelength of 300 nm and therefore did not cover the ArF laser wavelengths (193 nm). Figure 2.3:2 shows optical the properties of 4H-SiC from published data [16] covering the ArF region and this data was used to calculate the reflectivity and optical

Excimer Laser Interaction with Silicon Carbide:
Determination of Irradiation Parameters

absorption in the deep UV. The very low value of the extinction coefficient can be seen as previously mentioned [15]. Using the reciprocal of equation (2:31) and equation (2:29) the absorption depth, α^{-1} , and the reflectivity have been determined and are shown in Table 2.3:1.

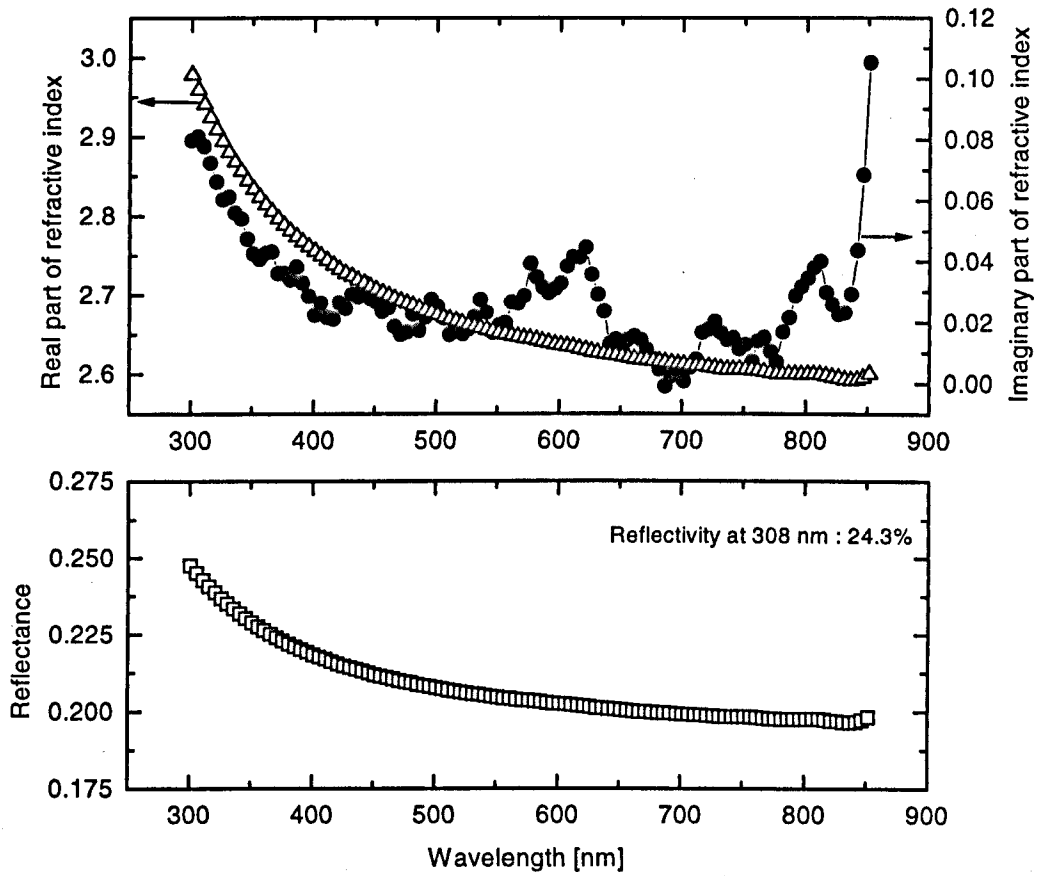
Excimer Laser Interaction with Silicon Carbide:
Determination of Irradiation Parameters

Figure 2.3:1 Top, Ellipsometric data for the real & imaginary part of the refractive index and Bottom, reflectance for epitaxial 4H-SiC, (Courtesy of DERA Malvern).

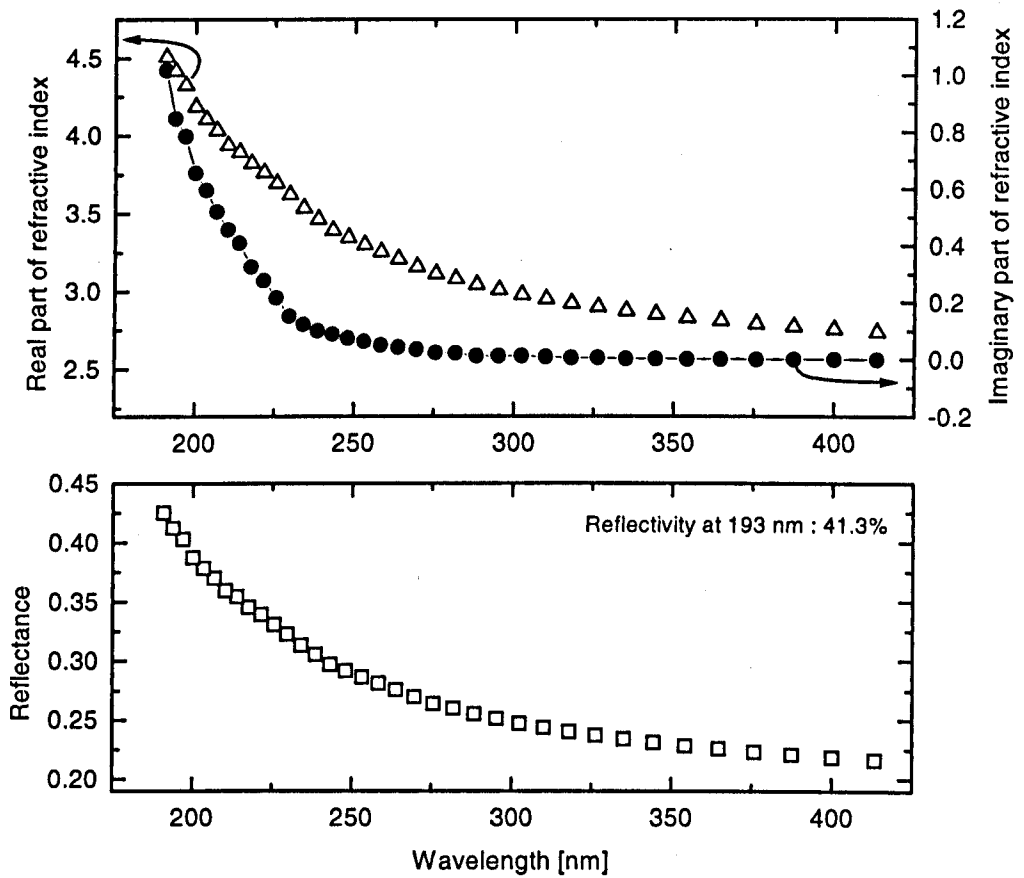
Excimer Laser Interaction with Silicon Carbide:
Determination of Irradiation Parameters

Figure 2.3:2 Top, Real and imaginary part of the refractive index and Bottom, reflectance of Silicon Carbide. Data taken from Zollner et-al [16]. (Courtesy of DERA Malvern).

Excimer Laser Interaction with Silicon Carbide:
Determination of Irradiation Parameters

Wavelength (nm)	Absorption Depth (Palik Ref 14)	Absorption Depth (Elipsometry)	Reflectivity %
193	10.8 nm	14 nm	41
308	2.6 μm	3.5 μm	24

Table 2.3:1 Absorption depth and reflectivity data at 193 and 308nm. The published data is taken from Palik [Ref 14], Experimental absorption measurements were carried out using elipsometric and laser ablated etch depth measurements.

2.4 Experimental Procedure

2.4.1 Introduction

Ablation and desorption experiments have been studied in great depth over the last few decades. However, very few papers at the present time exist on excimer laser ablation of Silicon Carbide [3,5,17]. Laser ablation and desorption can result from photo-chemical and photo-thermal processes at the surface and near-surface causing molecules, atoms, ions, and even clusters to be expelled from the surface. Ablation can be thought of as a sputtering process where continued irradiation leads to a surface being structurally or compositionally modified on mesoscopic length scales. The removal rates are material and wavelength dependent, typically nm per pulse with a non-linear dependence on fluence. However, the fundamental physical mechanisms of laser ablation have not been clearly identified and differing views can be found in the literature [18]. The formation of weakly to moderately ionised ablation plumes above the surface, expanding gas plumes associated with laser ablation adds to the complications of plasma surface



interactions [19], gas dynamics and photo induced chemistry. In comparison, laser induced desorption appears to be a more subtle material removal process on a microscopic level. Species are removed from the surface leaving little compositional and structural changes on the mesoscopic scale.

However, ablation and desorption are not entirely different phenomena. Ablation need not involve catastrophic volumetric material removal and the difference between the two phenomena close to some threshold becomes less distinct. In fact it is important not to confuse a physical threshold with a detection threshold. When energy densities are used such that a material reaches or comes very close to the melt-evaporation/solid-sublimation temperature, a more subtle ejection of material in the gas phase can occur. As an example, ablation/desorption measurements were carried out by Brannon *et-al* using a quartz micro-balance to investigate the ablation rates close to threshold [20]. Briefly, their findings illustrated an Arrhenius increase on the material removal rate, particularly at longer wavelengths where previous experimental evidence suggested a sharp onset of ejected species occurred. However, acknowledging their observations, the intention for this work is to obtain a laser fluence 'window' using Beer's Law in order to carry out sub damage annealing experiments, rather than carrying out a microscopic studies of the exact onset of the material removal processes.

2.4.2 Sample Information

Both epitaxial and bulk Silicon Carbide samples have been used for these experiments the properties of which are listed below. Epitaxial material was chosen because of it's suitability for electronic devices, particularly field effect transistors (FET), where the channel mobility can be controlled via controlling the dopant concentrations in the epitaxial region. N-type bulk material was used to ascertain the processing parameters for subsequent work. Prior to laser irradiation the samples were immersed in acetone and placed in an ultrasonic bath for 30 minutes. The samples were then rinsed in de-ionised water and spun dry.

Excimer Laser Interaction with Silicon Carbide:
Determination of Irradiation Parameters

Polytype	Thickness (μm)	Appearance	Micropipe Defects (cm^{-1})	Dopant	Concentration (cm^{-2})
Bulk 4H-	300	Yellow	30-100	Nitrogen	2.6×10^{17}
Epitaxial	300/3	Brown	NA	Aluminium	$5 \times 10^{18}/2 \times 10^{16}$

Table 2.4:1 Physical Properties of bulk and epitaxial Silicon Carbide

Table 2.4:1 shows some of the relevant parameters for the Silicon Carbide samples. Relevant to this work is the absorption of optical radiation. The colour of Silicon Carbide is mostly determined from absorption for the electric field vector parallel to the 'c' axis. In 'pure' 6H-SiC ($E_g = 2.9 \text{ eV}$) the only absorption band is in the far violet and UV and SiC is therefore transparent in the visible. Nitrogen doped (n-type) material has an extra absorption band at $\sim 2\text{eV}$ (red-orange) and at $2.8\text{-}3.0 \text{ eV}$ (blue) thus eliminating these colours leading to a greenish appearance. In 4H-SiC the absorption band at 2 eV is not present and therefore appears more yellow in appearance. Of course, the colour depends also on the dopant concentrations and crystal quality.

2.5 Experimental Results

2.5.1 ArF Irradiated Epitaxial 4H-SiC: In Vacuum

The majority of this work was undertaken at Exitech, Oxfordshire using a ArF excimer laser model : LPX 25 from Lambda Physik. The pulse duration was of the order of 25 ns. The beam energy was adjusted via a variable double plate quartz attenuator and steered with 3 aluminium mirrors with reflectivities $\sim 90 \%$. The sample chamber was constructed from stainless steel and

Excimer Laser Interaction with Silicon Carbide:
Determination of Irradiation Parameters

fitted with a CCD camera to facilitate sample positioning via a computer controlled x-y stage. A chamber pressure $\sim 10^{-8}$ torr could be achieved via a turbo molecular pump situated directly beneath the sample stage. Argon gas was piped to the system and the volumetric flow rates could be controlled with mass flow controllers. Epitaxial 4H-SiC for these experiments were obtained from CREE research, see Table 2.4:1 for sample specifications.

Scanning Electron Micrographs (SEM's) of laser irradiated material for a number of laser fluence are shown in Figure 2.5:1. At the lower fluence of 2.1 J cm^{-2} , material has been removed leaving a surface vastly different from the higher laser fluence. The presence of globular surface features gives the indication of a melt phase evolving with increasing laser fluence. At the high laser fluence the irregular surface made etch rate measurements very difficult, hence, it was not possible to determine ablation thresholds from etch rate measurements. Surface measurements were carried out on a mechanical profilometer (model: DEKTAK- 1000). Each irradiated site was scanned across the width of the 0.5 mm sites. The measurements revealed raised surface sights with a completely modified topology at the higher fluence and had a somewhat different surface structure at the low fluence range.

Excimer Laser Interaction with Silicon Carbide:
Determination of Irradiation Parameters

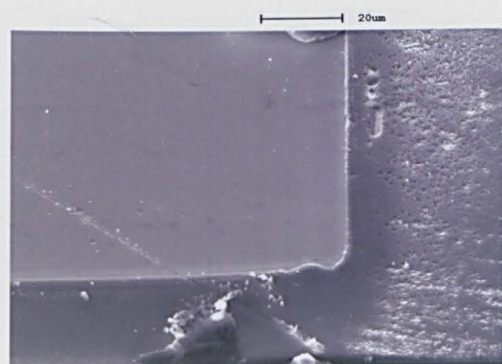
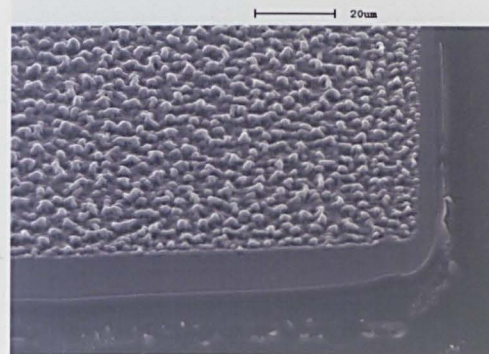
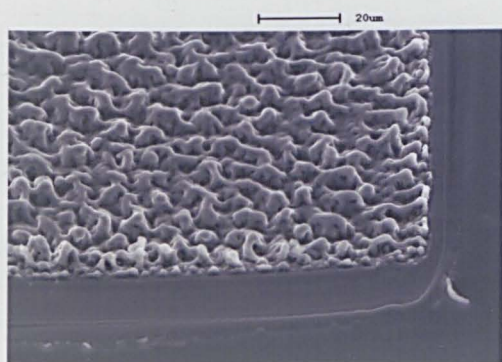
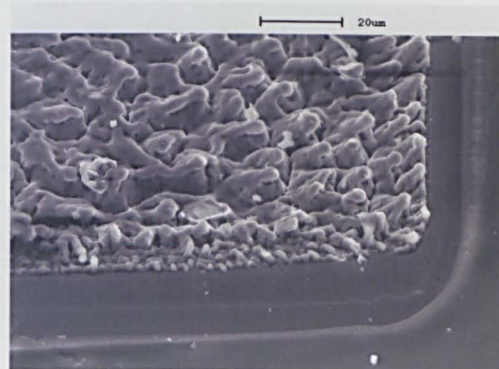
a) 2.1 J cm^{-2} b) 2.8 J cm^{-2} c) 3.4 J cm^{-2} d) 4.0 J cm^{-2}

Figure 2.5:1 Excimer laser irradiated 4H-SiC at a pressure of 500 torr using a repetition rate of 50 Hz with 500 laser pulses.

Excimer Laser Interaction with Silicon Carbide:
Determination of Irradiation Parameters

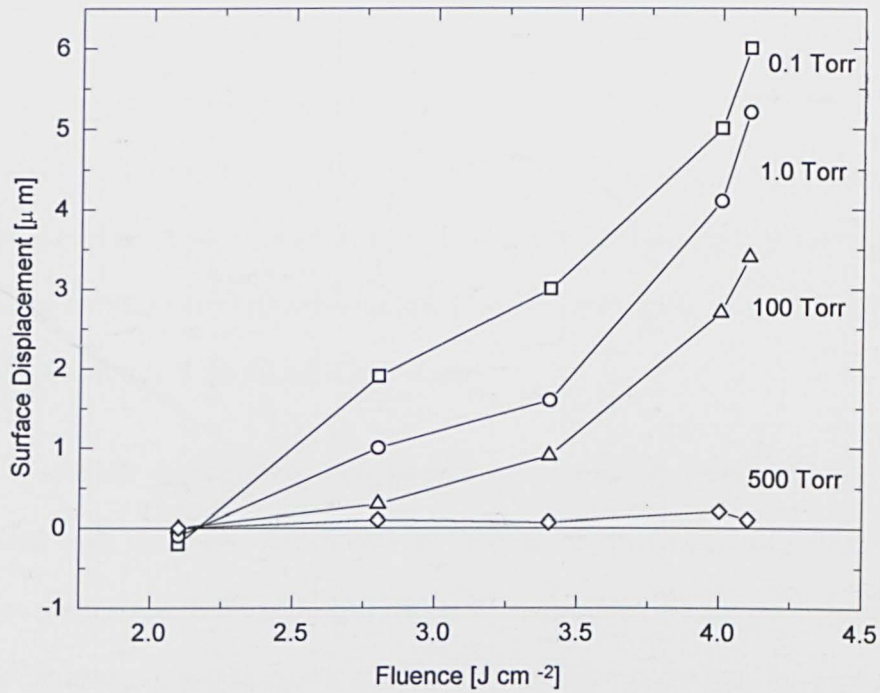
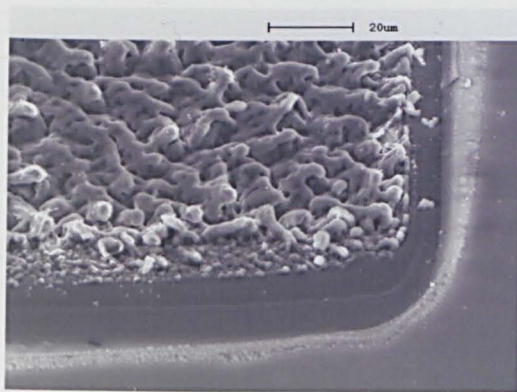
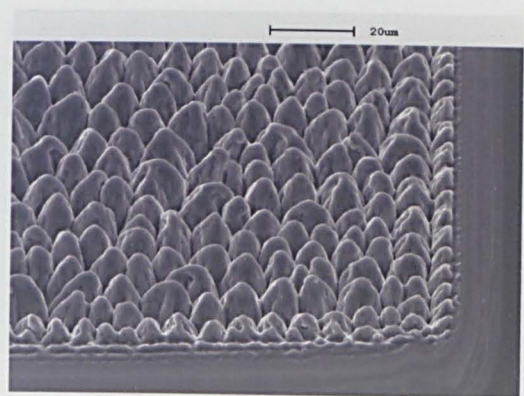


Figure 2.5:2 Surface height measurements at 0.1, 1, 100, and 500 torr
Note; positive values represent raised feature and negative values indicating a depression beneath the surface.



a) 500 torr.



b) 0.1 torr.

Figure 2.5:3 Contrasted surface topology at different pressures for ArF excimer laser irradiated 4H-SiC with 500 pulses at $4.1\ J\ cm^{-2}$.

2.5.2 ArF Irradiated Epitaxial 4H-SiC: In Oxygen

There is a great deal of interest in the interaction of oxygen with semiconducting surfaces. Particularly, the interaction of oxygen with Si to produce dielectric layers for isolation purposes in Metal Oxide Semiconductor (MOS) devices. Oxygen under equilibrium conditions has also been adopted to clean semiconducting surfaces via a sacrificial oxidation process. Similarly, one of the reasons for the interest shown in Silicon Carbide device technology is because of the high quality SiO₂ that forms at the SiO₂/SiC interface.

The role of ambient gases during excimer laser processing has been studied in a variety of combinations over the years. Particularly in the area of reactive etching studies, where the ambient gas plays a role in the etch rate. However, in this work we are more concerned, from a slightly different angle, that is, the transport properties that oxygen may have on any desorbed Silicon Carbide components. There has been some debate in the literature whether or not carbon in the form of gaseous CO is transported away from the Silicon Carbide surface [21]. Recent developments have suggested that under thermal equilibrium, both SiO and CO are transported away. Therefore, irradiation in an oxygen ambient might play a role in the dissociative transport properties. For example, if carbon is preferentially removed in the form of volatile CO this might reduce unwanted graphitic nucleation close to the surface.

In this set of experiments, as-received epitaxial 4H-SiC samples were laser irradiated in an oxygen ambient on the Si face at a static oxygen pressure of 116 torr. As can be seen in Figure 2.5:4 a range of samples were irradiated between 2.0 and 2.6 J cm⁻². What is firstly noticeable is the deposits around the irradiated sites indicating some form of material removal process taking place ^ψ. At a laser fluence of 2.5 and 2.6 J cm⁻², Figure 2.5:4(f) and (g) and Figure 2.5:5, the surface can be seen to become severely damaged. Also the irradiance of the beam appears to be

^ψ Interestingly, the shape of the deposits, referred too as the "rotation effect" has been previously observed by Miotello et-al, Appl. Phys. Lett 61, (23) 2784 (1992).

Excimer Laser Interaction with Silicon Carbide:
Determination of Irradiation Parameters

inhomogeneous, appearing to be somewhat higher at the centre. From optical measurements a surface layer, most probably SiO₂, is evident and appears to grow on the surface before becoming disrupted at the higher laser fluence. The mechanical profile measurements clearly show damage at the higher laser fluence indicating raised features. The raised features can be compared with those in Chapter 2.5, Figure 2.5:1, where Silicon Carbide was irradiated in vacuum. However, irradiation in oxygen produced etch pits thus making it possible to determine the etch rate. By measuring the depth of the etch pits and using equation (2:33) it was then possible to obtain estimates in the threshold fluence using equation 2:33 below

$$X = \frac{1}{\alpha} \ln \left(\frac{F}{F_t} \right) \quad (2:33)$$

where X is the etch rate per pulse and F_t is the threshold laser fluence. From this data it was then possible to determine an estimate of the ablation threshold at 193nm. This data is tabulated in Table 2.5:1 along side data for 308nm. The higher ablation threshold appears to be consistent when the wavelength dependant reflectivity is taken into account. From Figure 2.3:2 it can be seen that the imaginary part of the refractive index, k, is large compared with, k, at 308nm, Figure 2.3:1 Therefore at 193nm only a very shallow volume of Silicon carbide is probed during each pulse at 193nm.

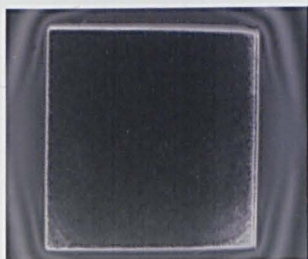
Excimer Laser Interaction with Silicon Carbide:
Determination of Irradiation Parametersa) 2.0 J cm^{-2} b) 2.1 J cm^{-2} c) 2.2 J cm^{-2} d) 2.3 J cm^{-2} e) 2.4 J cm^{-2} f) 2.5 J cm^{-2} g) 2.6 J cm^{-2}

Figure 2.5:4 Epitaxial 4H-SiC Etch sites Irradiated in an Oxygen ambient at a pressure of 116 torr and 1250 laser pulses (50 Hz) at 193nm, (size: $0.5 \times 0.5 \text{ mm}$).

Excimer Laser Interaction with Silicon Carbide:
Determination of Irradiation Parameters

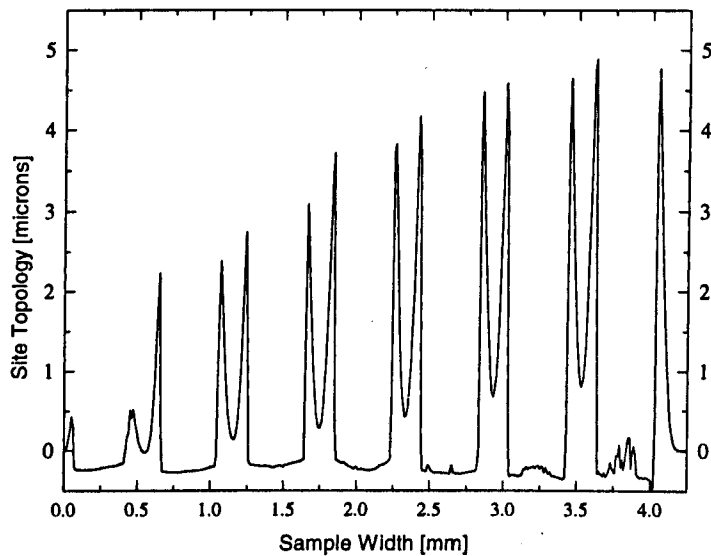


Figure 2.5:5 Surface topology of ArF excimer laser irradiated 4H-SiC (Figure 2.5:4) in the fluence range 2.0 J cm^{-2} to 2.6 J cm^{-2} (left to right respectively) at a pressure of 116 torr, in a Oxygen each site receiving 250 pulses.

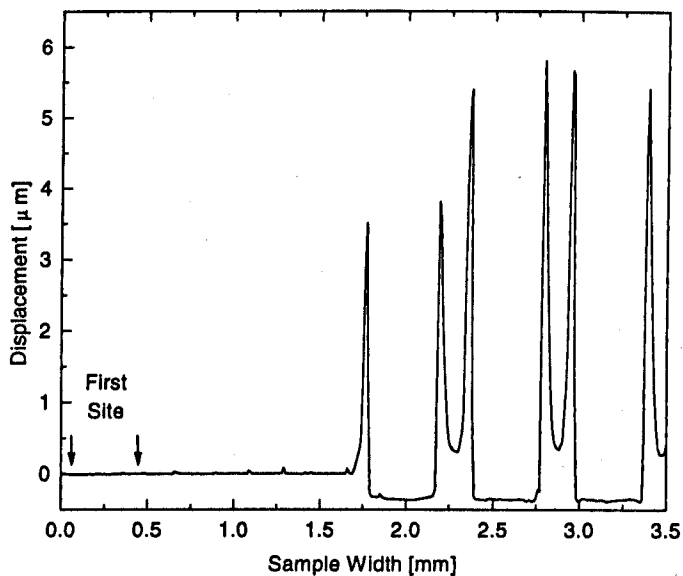


Figure 2.5:6 Surface topology of ArF excimer laser irradiated 4H-SiC with 500 laser pulses, in an oxygen ambient at a pressure of 116 torr, and a laser fluence: 1.2, 1.4, 1.5, 1.6, 1.7, and 1.9 J cm^{-2} . (from left to right).

Excimer Laser Interaction with Silicon Carbide:
Determination of Irradiation Parameters

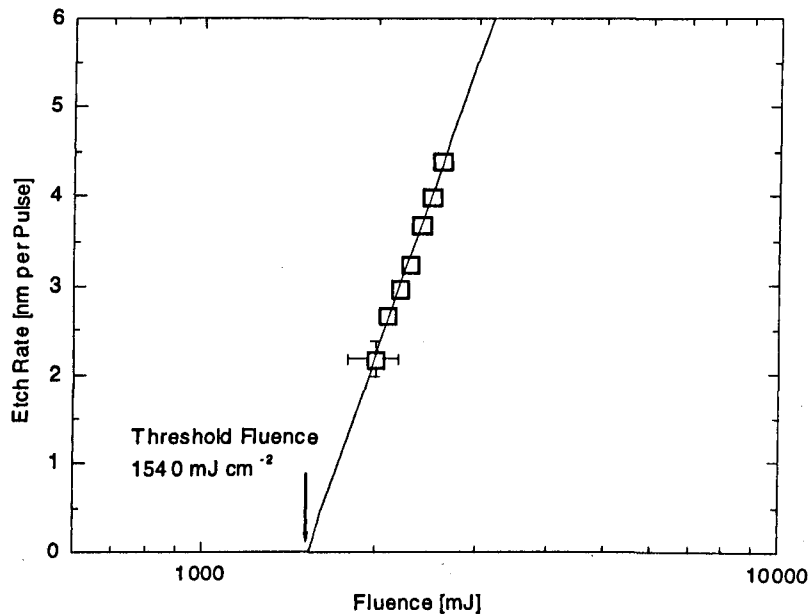


Figure 2.5.7 Etch rate data taken for laser ablated Silicon Carbide at 193nm. Exposed with 1250 laser pulses at a pressure of 116 torr in a Oxygen ambient.

2.5.3 XeCl Irradiated Bulk 4H-SiC: In Argon

Bulk 4H-SiC Silicon Carbide as described previously was irradiated using a Xenon Chloride (XeCl) excimer laser from Lumonics, Model:TE-840-L, having a pulse duration of ~ 25 ns. The sample chamber was flushed with argon and evacuated down to a pressure of $\sim 4 \times 10^{-3}$ torr. In order to increase the laser fluence the image of a 1cm diameter aperture was demagnified using a quartz spherical lens and projected onto the Silicon Carbide surface. The laser fluence was then chosen by inserting the appropriate number of neutral density filters which were positioned before the projection mask, see figure 2.5:9.

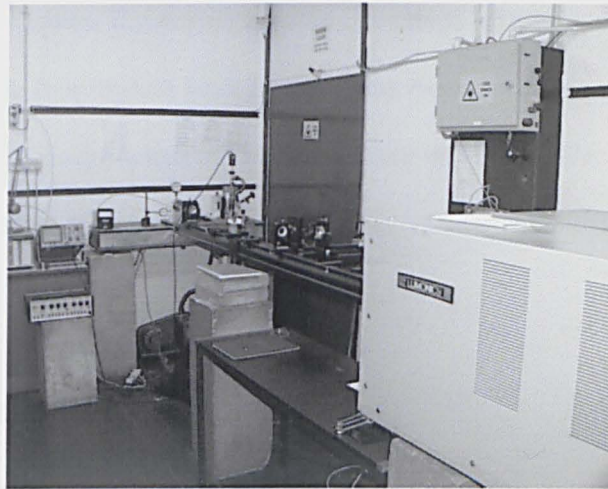
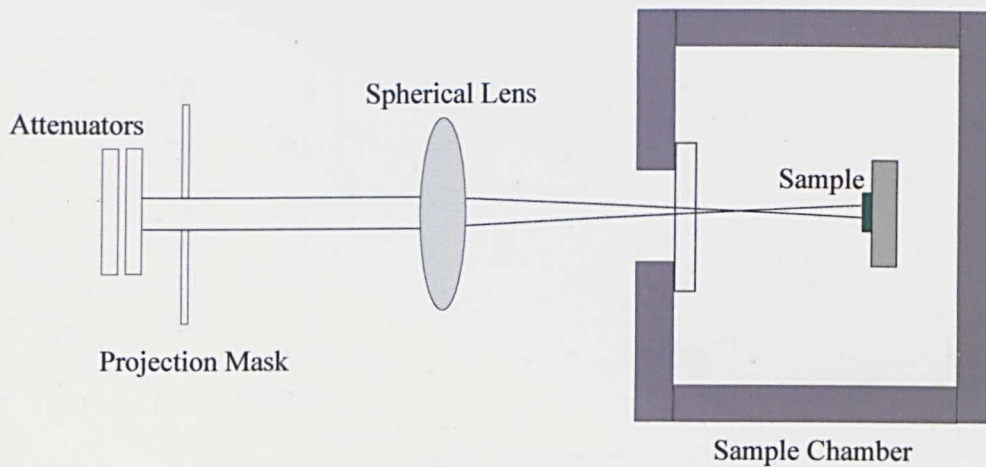
Excimer Laser Interaction with Silicon Carbide:
Determination of Irradiation ParametersFigure 2.5:8 XeCl ($\lambda = 308\text{nm}$) excimer laser, University of Hull.

Figure 2.5:9 Illustration of optical image arrangement and sample chamber.

Each site was irradiated with 150 pulses at a pulse repetition frequency of 1Hz. Figure 2.5:10 illustrates the surface topology measurements which were made using a mechanical profilometer (Dektak). Etch pits can be seen at the four highest fluence, namely, 1.8, 2.3, 2.6

Excimer Laser Interaction with Silicon Carbide:
Determination of Irradiation Parameters

and 2.9 J cm^{-2} . At the lowest fluence of 1.3 J cm^{-2} a raised feature was observed and therefore only the etch pits at the four highest laser fluence were measured. This raised the question of the nature of the surface under the action of laser irradiation and is considered further in Chapter 2.5 and also in the discussion in Chapter 6.

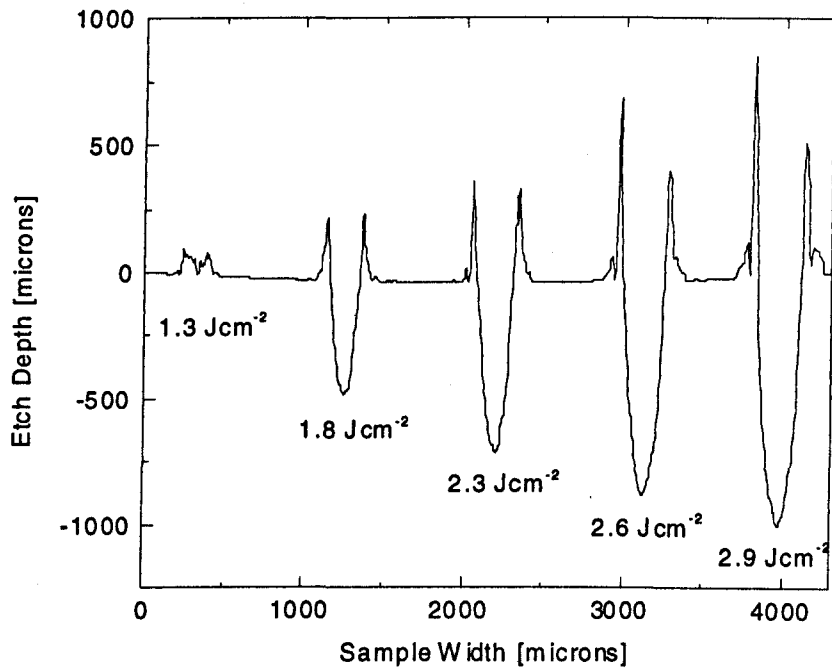


Figure 2.5:10 Excimer laser irradiated 4H-SiC at 308nm with 1250 Pulses at a pressure of 1 atmosphere in an Argon ambient.

Excimer Laser Interaction with Silicon Carbide:
Determination of Irradiation Parameters

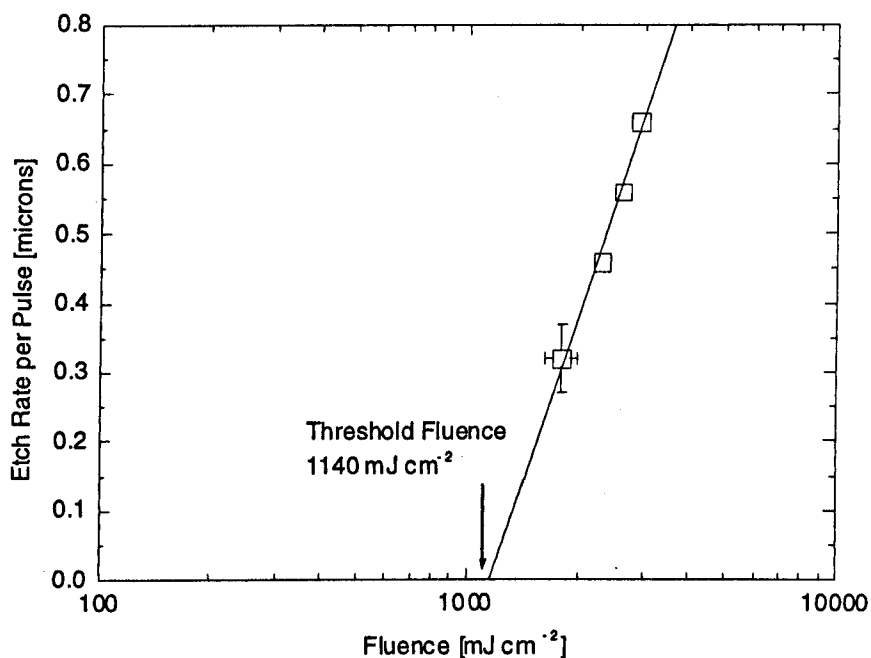


Figure 2.5:11 Etch rate data XeCl (308nm) excimer laser irradiated bulk 4H-SiC at a pressure of 1 atmosphere in argon.

Laser Wavelength	193nm	308nm
Ablation Threshold	1540 +/- 200 mJ cm^{-2}	1140 +/- 160 mJ cm^{-2}
Absorption Depth	12 nm	0.6 μm

Table 2.5:1 Measured ablation thresholds and absorption depths for 4H-SiC using Beer's Law.

2.5.4 Laser Induced Surface Modifications

The main aim of this work is essentially associated with the low value of the diffusion coefficient of nitrogen dopants in Silicon Carbide. In order to select the optimum processing parameters for this work it is important to understand the way in which laser light interacts with Silicon Carbide. The question, does Silicon Carbide melt motivated researchers into carrying

Excimer Laser Interaction with Silicon Carbide:
Determination of Irradiation Parameters

out experimental work in the 1950's. It was subsequently discovered that under equilibrium conditions Silicon Carbide possesses a peritectic point at $2830 \pm 40^\circ\text{C}$ if it is subjected to a pressure of 35atm [22,23]. However, Burdel et-al [2] and more recently, Reitano et-al, [24] have suggested irradiation from nano a second laser pulse can be used to melt amorphous Silicon Carbide.

The concept of melting is an important issue, especially in connection with excimer laser annealing. Dopant diffusivities are greatly enhanced in the melt and can cause dopant redistribution [2,25] and changes in the recrystallisation kinetics [26]. SEM images have illustrated, Figure 2.5:1 and Figure 2.5:3, how the morphology of Silicon Carbide irradiated at 193nm changes with laser fluence and pressure. Between 2.1 and 2.8 J cm^{-2} there would appear to be some mechanistic change in the material removal process. Certainly, there has been a great deal of research in closely related areas to this where the term "phase explosion" [27,28,29] and subsurface heating are often referred too. At 2.1 J cm^{-2} material might be removed via a thermal desorption/evaporation, where as at 2.8 J cm^{-2} and above, a catastrophic mechanism such as ablation might take place.

Excimer Laser Interaction with Silicon Carbide:
Determination of Irradiation Parameters

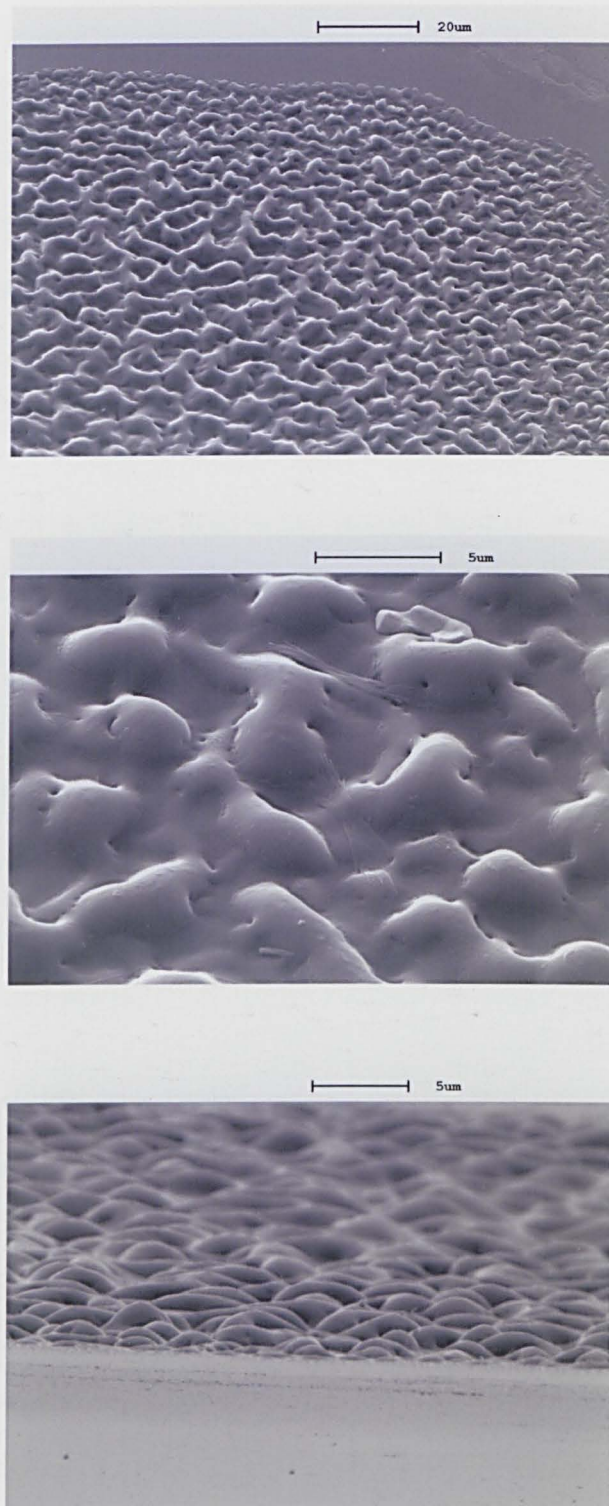


Figure 2.5:12 Surface topology of excimer laser ($\lambda=308$ nm) irradiated 4H-SiC at a laser fluence of 1300 mJ cm^{-2} , with 150 laser pulses, in an argon ambient.

2.6 Conclusion

Preliminary experiments, particularly ablation measurements, have been carried out to establish the experimental conditions necessary for the work in the following chapters. Initially, this was necessary because of the limited information on laser interaction with Silicon Carbide, especially the 4H- polytype. The identification of a process 'window' was crucial for the subsequent chapters, laser annealing experiments (Chapter 5), and to some extent, the Photoluminescence and Positron Annihilation measurements (Chapters 3 and 4) respectively.

Experiments carried out at 193nm at pressures ranging between 0.1 and 500 torr revealed an ablated structure with columnar type features that became ordered with decreasing pressure. The columnar features prevented etch rate measurements to be made directly because they were proud of the surface. Silicon Carbide irradiated in Oxygen at 193nm produced etch pits which allowed the etch rate to be determined, however it is pointed out that the derived ablation threshold would be influenced by the chemical assistance of the Oxygen rich environment. The ablation threshold at 193nm and 308nm were measured as being $1540 \pm 200 \text{ mJ cm}^{-2}$ and $1140 \pm 160 \text{ mJ cm}^{-2}$ respectively.

Elipsometric measurements were carried out and the complex refractive index was used to compare the reflectivity and optical absorption depths with published data.

Finally, the structure of the irradiated material was briefly studied from a qualitative point of view. Scanning electron micrographs revealed melt like features suggesting the material was beginning to dissociate, however no detailed work was carried out in this area.

2.7 References

-
- [1] Cree. Research. Inc., Durham, NC 27713, USA.
- [2] K. K. Burdel, A. S. Akhmanov, V. N. Makarov, A. Yu. Poroikov, V. Suvorov and N. G. Chechenin, *Sov. Tech. Physics. Lett.* **14** (7), 528 (1988).
- [3] R. Reitano, P. Baeri and N. Marino. *Appl Surf. Sci.* **96-98**, 302 (1996).
- [4] G. A. Shafeev, L. Bellard, J. M Themlin, C. Fauquet-Ben Ammar, A. Cros and W. Marine, *Appl. Phys. Lett.* **68**, 773 (1996).
- [5] P. E. Pehrsson, R. Kaplan, *J. Mater. Res.* **4** (6), 1480 (1989).
- [6] W. J. Everson, D. W. Snyder and V. D, *Material Science Forum* **338-342** 837 (2000).
- [7] W.C. Mitchel, J. Brown, D. Buckanan, R. Bertke, K. Malalingham, F. D. Orazio Jr, P. Pirouz, H. Hur, T. Seng, U. B. Rambabdran, and B. Roughani. *Material Science Forum* **338-342**, 841 (2000).
- [8] T. C. Chandler, Jr. M. B. Lari, and T. S. Sudarshan, *Material Science Forum* **338-342**, 845 (2000).
- [9] C. J. McHargue, and J. M. Williams, *Nucl. Instrum. Methods Phys. Res. B* **80/81**, 889 (1993).
- [10] S. K. Iilov, *Diamond and Related Materials.* **4**, 1331 (1995).
- [11] S. V. Baranov, A. G. Vodop'yanov, G. K. Moiseev, and G. N. Kozhevnikov. *J. of Inorganic Materials.* **18**(8), 1097 (1982).
- [12] T. Venkatesan, D. C. Jacobson , J. M. Gibson, B. S. Elman, G. Braunstein, *Phys. Lett.* **53**, 360 (1984).
- [13] Syney Pertowitz, *Optical Characterisation of Semiconductors: Infra red, Raman, and Photoluminescence Spectroscopy*, (London, Academic Press , 1993), p.7
- [14] W. J. Choyke and E. D. Palik, in *Handbook of Optical Constants*, edited by E. D. Palik (Academic, New York , 1985), p.587.
- [15] S. G. Sridhara, R. P. Devaty, and W. J. Choyke, *J. Appl. Phys.* **84**, 2963 (1998).
- [16] S. Zollner, J. G. Chen, E. Duda, T. Wetteroth, S. R. Wilson and J.N. Hilfiker, *J. Appl. Phys.* **85**, (12) 8353 (1999).
- [17] G. Nicolas, M. Autric. *Appl. Sur. Sci.* **96-98**, 296 (1996).
- [18] *Laser Processing and Chemistry*, D. Bauerle (Berlin, London Springer 2000).
- [19] Y. F. Lu, M. H. Hong. and T.S. Low, *Appl. Phys.* **85** (5), 2899 (1999).
- [20] S. Kuper, J. Brannon and K. Brannon, *Appl. Phys.* **A56**, 43 (1993).

Excimer Laser Interaction with Silicon Carbide:
Determination of Irradiation Parameters

- [21] *Properties of Silicon Carbide* (Edited by G. L. Harris), pp. 131-149
- [22] J. Smiltens, Proceedings of the Conference on Silicon Carbide, Boston, Massachusetts, p3, (1959).
- [23] R. I. Scace and G. A. Slack, Proceedings of the Conference on Silicon Carbide, Boston, Massachusetts, p24, (1959).
- [24] P. Baeri, C. Spinella and R. Reitano. *Int. J. of Thermophysics*. **20** (4), 1211 (1999).
- [25] K. K. Burdel, P. V. Varamkin, V. N. Makarov, A. V. Suvorov, and N. G. Chechenin. *Sov. Phys. Solid State*. **30** (2), 364 (1988).
- [26] E. N. Arutyunov, S. Yu. Karpov, Yu. V. Koval'chuk, V. E. Myachin, Yu. V. Pogorel'skii, V. B. Smirnitskii, and I. A. Sokolov *Sov. Tech. Phys. Lett.* **11**, 38 (1985).
- [27] M. M. Martynuk. *Sov. Phys. Tech. Phys.* **21**, 430 (1976).
- [28] M. M. Martynuk. *Sov. Phys. Tech. Phys.* **19**, 793 (1974).
- [29] M. M. Martynuk. *Rus. J. Phys. Sov. Phys. Chem.* **57**, 494 (1983).

Chapter 3

Photoluminescence Measurements of Excimer Laser Irradiated and Hydrogenated 4H-Silicon Carbide

3.1 Introduction	44
3.2 Radiative Transition in Silicon Carbide	47
3.2.1 Donor Species in Silicon Carbide	49
3.2.2 Acceptors Species in Silicon Carbide	49
3.2.3 Band-Acceptor Transitions. (A_0 peaks)	50
3.2.4 Donor-Acceptor Pair (DAP) Recombination: (B_0 and C_0 peaks)	52
3.3 Experimental Procedure	53
3.4 Experimental Results	55
3.4.1 Photoluminescence Interpretation of As-Received Material	55
3.4.2 Broad Band Photoluminescence Spectra	56
3.4.3 ArF Laser Irradiated 4H-SiC	63
3.4.4 Hydrogen Passivation of Epitaxial 4H-SiC	65
3.4.5 XeCl Laser Irradiated Bulk 4H-SiC.	70
3.5 Conclusion	73
3.6 References	74

Chapter 3

Photoluminescence Measurements of Excimer Laser Irradiated and Hydrogenated 4H-Silicon Carbide

3.1 Introduction

Photoluminescence (PL) spectroscopy is a powerful experimental tool and is routinely made on semiconductor materials to determine dopant concentrations and detect the presence of defects. Most solids maintain their essential properties upon introduction of small amounts of impurities, however, certain semiconductor properties such as conductivity, free carrier mobility and carrier lifetimes can be greatly affected with the introduction of lattice defects and impurities.

Most defect states are located within the bandgap and luminescence generally occurs at sub bandgap wavelengths. Spectroscopic experiments have been previously performed on a plethora of semiconducting materials amongst these is the material Silicon Carbide.

Optical emission studies close to the band edge have proved to be a very useful means for characterising the properties of Silicon Carbide. There have been extensive studies using PL spectroscopy to investigate defect luminescence in as-received Silicon Carbide. Fundamentally, in order to gain a deeper understanding of the various polytypes, and technologically, in order to quantify the amount of damage incurred through techniques such as ion-implantation. Haberstroh, et al, reports on bound exciton emission close to the band edge after doping with Aluminium [1]. Ikeda et al [2] and Patrick [3], have reported the existence of site dependent impurity levels in 4H, 6H, 15R and 6H-Silicon Carbide, and extensive work has been carried out on defect luminescence. However, little work exists on the luminescence studies of laser irradiated Silicon Carbide, especially 4H-material.

To the authors' knowledge, very little work existed at the time on photoluminescence studies of excimer laser irradiated 4H-SiC. In this work, the PL spectra has been measured for as-grown and laser irradiated Silicon Carbide using high intensity radiation ($\sim 50\text{MW cm}^{-2}$) from an ArF (193nm) and a XeCl (308nm) lasers. Essentially, the reason for this work stems from the difficulties associated with the low degree of atomic diffusion [4] and activation [5] of Nitrogen dopants in Silicon Carbide. PL measurements are used here to measure any spectroscopic changes that might occur subsequent to exposure from these lasers. The presence of new bands, shifts in existing bands and changes in intensity will therefore indicate that modifications to the material have taken place.

The PL experiments have therefore been carried in order to-

- 1) Characterise the as-received Silicon Carbide before irradiation takes place.
- 2) Measure any spectroscopic changes that might take place subsequent to laser irradiation.

Any changes in the PL spectra that might be observed (point 2) can then be further investigated (Positron annihilation measurements, Chapter 4) to identify the nature of these changes. In this way it is intended to correlate luminescence bands with possible defect bands and see if these defects can be utilised to enhance the atomic diffusion.

Atomic diffusion is complex, where many competing mechanisms take place. Fickian diffusion was first described in 1855 where a concentration gradient serves as the driving force for atomic diffusion to take place. The introduction of vacancy defects might therefore modify the chemical potential, which in turn could possibly influence the diffusion process. However, still today, there is a great deal of debate on the actual diffusion mechanism. It is argued that atomic diffusion without vacancies or interstitials to mediate the process is energetically favourable, the so called, *concerted exchange mechanism* [6]. Phenomenological evidence indicates atomic diffusion is enhanced with the creation of vacancy defects and therefore the vacant lattice site

plays an influential role. Recently, the suggestion of a crystal lattice relaxing in the vicinity of a vacant lattice, causing a soliton-like impulse which then acts as a driving force for diffusion has been proposed [7], thus supporting the idea of vacancy mediated diffusion, however, with the crucial difference that in the latter vacancies must be created during, rather than exist prior to the doping. Based on the general acceptance that atomic diffusion is mediated via vacancies, this work sets out to ascertain if it is at all possible to create laser induced vacancy defect structures. The possibility of inducing vacancies with an excimer laser could then open up many new areas of research, one of which might enhance diffusion in materials with low diffusion coefficients like Silicon Carbide.

Semiconductor defects can take on many forms:

- 1) structural or chemical; relating to crystal imperfections or impurities,
- 2) substitutional or interstitial; depending whether or not atoms are located at lattice or interstitial sites,
- 3) simple or complex; depending whether or not the atomic structure consists of single atoms or are molecules,
- 4) shallow or deep; depending if the energy bands are close to the band edge or mid-gap levels,
- 5) donor and/or acceptor impurities and
- 6) iso-electronic; depending whether or not they introduce excess charge into the lattice.

A great deal of interest lies in the defect luminescence in Silicon Carbide. In earlier times, Patrick and Choyke were the first to report on the lattice defects which had been introduced into 3C-SiC by electron and ion bombardment [8]. PL revealed sharp emission lines that were independent of the bombarding species, suggesting the intrinsic nature of the defect. Similar

experiments were carried out on 6H-SiC which revealed three sharp lines corresponding to the three crystallographic inequivalent lattice sites [9]. This type of defect spectra became labelled the D_I and D_{II} spectra corresponding to defects at interstitial and di-interstitial sites respectively. The D_I defect became technologically important since it could be used to construct efficient injection light sources emitting in the green or blue part of the spectrum, [10]. Since then, a great deal of work has been undertaken to identify emission lines due to lattice defects. Defect luminescence close to the band edge in 6H-SiC have been observed and has been shown to be related to silicon, carbon and complex defects [11]. The D_I spectrum has also been observed for epitaxial Silicon Carbide films without any irradiation if the concentration of carbon vacancies is in excess of stoichiometry [12]. Positron-lifetime and Doppler broadening spectroscopic measurements have revealed both silicon and carbon vacancies in electron irradiated n-type material, but no defects could be found under the same conditions in p-type material [13].

Recently, Sorman, et-al, have carried out extensive work on the silicon vacancy, they have reported PL evidence for the neutral silicon vacancy lying at 1438 and 1352 meV and 1366, 1398, and 1433meV in 4H- and 6H- material respectively [14, 15]. The existence of two and three sharp emission lines in 4H- and 6H- silicon carbide respectively is therefore further evidence for inequivalent lattice sites. The observed deep and shallow energy levels associated with ion beam irradiation illustrate some of the possible energy states associated with the intrinsic defects. Wyszomolek et-al, also reported broad emission bands thought to be due to silicon and carbon vacancies in the orange part of the spectrum [16].

3.2 Radiative Transition in Silicon Carbide

Photoluminescence is a powerful non-destructive technique, for material characterisation. PL spectroscopy involves the measurements and interpretation of the spectral distribution of radiative recombination at impurities and defect sites. Usually, electrons and holes are optically excited across the band-gap, E_g , and can become localised or bound at impurity or defects sites

before recombining. The identity of the localised centre can often be determined from the spectral position. Hence, a vast amount of information about the optical and electrical properties of a material can be obtained.

Photoluminescence measurements on Silicon Carbide is no exception. Extensive studies on the broadband luminescence spectra having been carried out many years ago. In 1964, Choyke et al [17], reported a seminal work on the optical characterisation of cubic (3C) Silicon Carbide grown by the Lely technique. However, growth techniques are being continuously improved or new ones are introduced resulting in improved wafer quality. Consequently, the optical properties of the material are modified. Therefore, photoluminescence measurements serve as a very useful diagnostic tool for material characterisation. Dopant concentrations can be determined from the ratio of Free Exciton to Bound Exciton emission (FE/BE) [18] and dopant activation can be determined.

Because of the polytypism in silicon carbide there exist inequivalent lattice sites which are divided into two kinds. Pure cubic structure belongs to the space group C_{6v} and pure cubic structure like 3C belong to T_d . However *cubic-like* and hexagonal-like both belong to the same space group of C_{3v} . Therefore, a labelling scheme based on group theory is not suitable and the conventional notations of cubic-like and hexagonal-like are used in this chapter. Owing to the long unit cells of hexagonal silicon carbide (10.053 Angstroms along the c-axis in 4H-SiC) there exists a number of inequivalent lattice sites [19], e.g. (2H), [3C], {4H}, ({6H}) and [[15R]] having; (h_1) , $[k_1]$, $\{h_1k_1\}$, $(\{h_1k_1k_2\})$ and $[[h_1h_2 k_1k_2k_3]]$ inequivalent hexagonal 'h' and cubic 'k' lattice sites respectively. With reference to 4H-SiC, having two inequivalent lattice sites there is the possibility of two distinct dopant ionisation energies, thus two distinct emission lines. The occurrence of site dependent impurity levels hence plays an important role on the perturbation on the impurity level [2]. A quantitatively a way of identifying the emission peaks is described briefly.

3.2.1 Donor Species in Silicon Carbide

The main two dopants used for producing n-type silicon carbide are the group V dopants Nitrogen and Phosphorous. Nitrogen is probably the more common of the two because it is an intrinsic impurity in the growth processes [20]. It is also a relatively shallow donor which is ideal for particular electronic devices. The ionisation energies for Nitrogen are shown in Table 3.2:1

Polytype	4H [meV]	6H [meV]
H	124 ^[19]	170 ^[21]
K ₁	66 ^[19]	200 ^[21]
K ₂	-	230 ^[21]

Table 3.2:1: Ionisation energies for Nitrogen donors in cubic and hexagonal sites in 4H- and 6H-SiC.

3.2.2 Acceptors Species in Silicon Carbide

Some of the common acceptors from group III of the periodic table, along with their associated ionisation energies are listed below, see Table 3.2:1. The choice of dopant depends on the application and techniques being used. To obtain the desired electrical and optical properties the acceptors with the appropriate ionisation levels have be chosen. Also, if the technique of ion implantation is adopted the mass of the ions have to be taken into account. Three of the more common dopants have been investigated by Suzuki et al [22]. The broad band spectral dependency due to Aluminium (Al), Gallium (Ga) and Boron (B) were investigated and it is these three dopants that are prevalent in the samples used in this work. However there are many other acceptor dopants that can be incorporated. Beryllium, because of the light mass, has

shown some promise due to the high achievable ion range and reduced level of induced crystalline damage during ion implantation [23]. Vanadium has been used in semi-insulating silicon carbide as a mid-gap defect for carrier trapping [24]. There has been little reported evidence of any significant differences in the ionisation energies between polytype or the cubic-like and hexagonal-like environments. However, periodically new ionisation energies do emerge, probably due to novel growth techniques, which makes the assignment of optically active centres rather challenging. Table 3.2 lists some of the more common acceptors with their associated ionisation energies.

Polytype	Al [meV]	B [meV]	Ga [meV]	Va [meV]
4H	$168 + E_x$ ^[22]	$628 + E_x$ ^[22]	$249 + E_x$ ^[22]	800 ^[25]
4H	241.6 ^[26]	627 ^[2]	-	-
6H	249 ^[2]	700 ^[2]	333 ^[2]	660 ^[25]

Table 3.2 Acceptor Ionisation energies for 4H and 6H-SiC Note $E_x = 20$ meV is the exciton binding energy [27].

3.2.3 Band-Acceptor Transitions. (A_0 peaks)

Owing to the long unit cells (10.053 Angstroms along the c-axis in 4H-SiC) there exists a number of inequivalent lattice sites which are dependent on the configuration of surrounding atoms. In particular, 4H-SiC has one hexagonal-like (B atom in the sequence ABC) and one cubic-like site (B atom in the sequence ABA). These inequivalent lattice sites cause site dependent impurity levels, hence, play an important role on the perturbation on the impurity level [2], evidenced in several emission peaks on the lower energy side of the exciton peaks.

The intensity of the free-acceptor transitions can be expressed as a function of electron kinetic energy [28] as

$$I(E_K) = N_A^0 n(E_K) \sigma(E_K) v_{th} \quad (3:1)$$

where, N_A^0 is the concentration of neutral acceptors, $n(E_K)$ is the concentration of free electrons with kinetic energy E_K , and $\sigma(E_K)$ is the cross section for the capture of a free electron by a neutral acceptor and is given as $\sigma(E_K) \approx C_1 E_K^{-1/2}$ and v_{th} is the thermal velocity. The transition cross-section for acceptors is assumed to be the same for all sites because the properties of acceptors in different sites are approximately the same. By expressing $n(E_K)$ and v_{th} as a function of E_K eq(3:1) can be transformed into.

$$I(E_K) = C_1 E_K^{1/2} \exp\left(\frac{-E_K}{kT}\right) \quad (3:2)$$

The photon energy for equation (3:2) for a transition between a free electron and a neutral acceptor is given by

$$E_{F-A} = E_G - E_A + \frac{1}{2} kT \pm nE_p \quad (3:3)$$

where, E_G , is the band gap energy, E_A is the acceptor energy and k is Boltzman's constant. Here the term, $\frac{1}{2} kT$, arises from thermal activated filling, T , is the temperature in Kelvin and the term $\pm nE_p$ is the simultaneous absorption or emission of $n = 0, 1, 2, \dots$ phonons of energy, E_p . Because of the inequivalent lattice sites, Table 3.2:1 there exists a number of ionisation energies, E_A^i , hence equation (3:1) can be transformed to

$$I(E_K) = C_1 \sum_i E_{ki}^{1/2} \exp\left(\frac{-E_{ki}}{kT}\right) \quad (3:4)$$

where, $E_{ki} = E_{hv} - E_G + E_A^i$, and E_{hv} is the energy of the emitted light.

3.2.4 Donor-Acceptor Pair (DAP) Recombination: (B₀ and C₀ peaks)

The energy relation for D-A pair transitions can be written :-

$$E_{D-A} = E_G - (E_D + E_A) - E_C \pm nE_p \quad (3:5)$$

E_D and E_A , are the donor and acceptor ionisation energies respectively, and E_C is the Coulomb attraction between the electron and hole written as

$$E_C = \frac{e^2}{4\pi\epsilon\mathfrak{R}} \quad (3:6)$$

where, e , is the electronic charge, ϵ is the dielectric constant and \mathfrak{R} is the electron hole separation.

For the case of weak excitation and for $N_A \gg N_D$, $a_A^3 N_A \ll 1$ and $a_D^3 N_D \ll 1$ the dependence of luminescence intensity on the pair distance, \mathfrak{R} , can be approximated as

$$I(\mathfrak{R}) \propto \mathfrak{R}^{-6} \exp\left[-\frac{4}{3}\pi N_A \mathfrak{R}^3\right] \quad (3:7)$$

where a_A and a_D are the hole and the electron Bohr radii respectively. Whence for example the Bohr orbit for nitrogen a donor at an hexagonal site is 8-15 Angstroms and those of cubic sites are ~ 6-10 Angstroms.

A very simple schematic illustration of the recombination channels is shown in Figure 3.2:1. The band gap energies for 4H and 6H-SiC are shown on the right hand side in this figure. Note that in SiC the n-type dopants, eg. Nitrogen would have energy levels that are generally shallower in terms of energy than, say, p-type dopants, such as Boron.

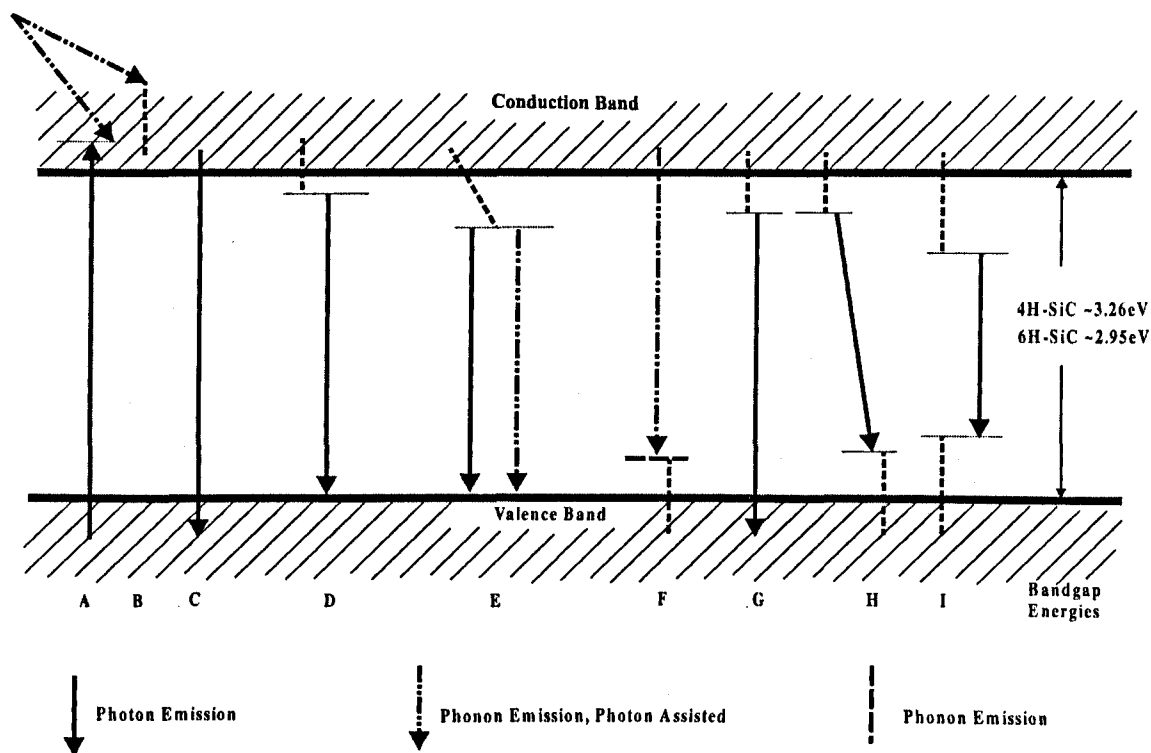


Figure 3.2:1: Schematic visualisation of some of the possible transitions leading to photo emission in Silicon Carbide.

A and B: Phonon assisted Intraband transitions, C: Intraband Transition, D: Recombination via excitons, E: Recombination via bound excitons, F and G: Conduction band to neutral acceptor and neutral donor to valence band, H: Donor level to acceptor level, and I: Recombination via impurity states.

3.3 Experimental Procedure

Photoluminescence measurements were carried out using two systems, The first system, see figure 3.3:2, consisted of a cryostat that could be filled with either liquid nitrogen or helium. The samples were wrapped in aluminium foil, with the intention to prevent strain being induced

into the samples, and attached to a cold finger. An argon ion Ar^+ laser (333.6, 351.1 and 363.8 nm), with the strongest excitation line at 351.1 nm was used to excite the material with above band gap excitation. The luminescent signal was steered with plane mirrors and collected using a quartz spherical lenses. The luminescence was dispersed with a Czerny-Turner type spectrometer utilizing a echellette grating with 1200 grooves/mm blazed at 500nm and having a reciprocal linear dispersion $\sim 8.3 \text{ \AA/mm}$. The signal was detected using a photomultiplier tube (PMT) and was amplified with a lock-in amplifier at a frequency $\sim 300 \text{ Hz}$.

The same Ar^+ laser previously described was used as the excitation source for the other system, but in this case was not in free space, but delivered down the centre of a quartz bifurcated fibre optic cable. The luminescent signal being guided along six separate fibres positioned coaxially around excitation cable. The spectrometer, fitted with a CCD array (Ocean Optics, Model 2000) had a spectral resolution $\sim 2\text{nm}$.



Figure 3.3:1: Photoluminescence spectroscopy laboratory, Ar^+ laser pictured in the foreground and the liquid helium/nitrogen cryostat in the center.

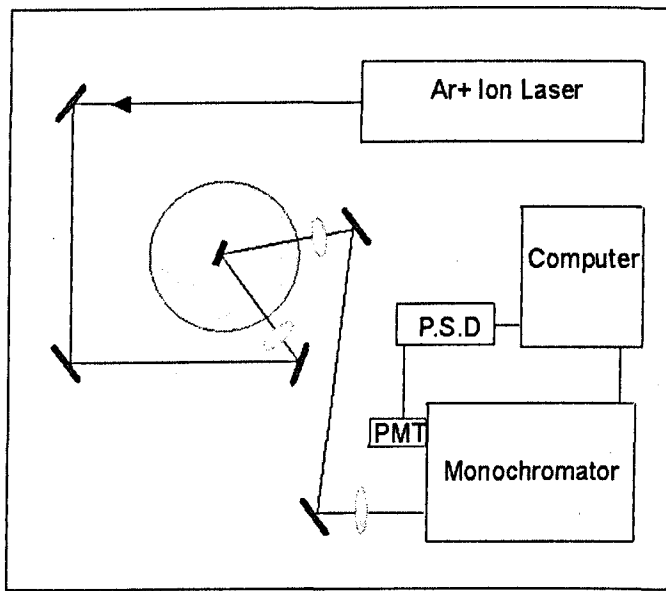


Figure 3.3:2: Schematic drawing of the photoluminescence setup.

The cryostat described in the second system (Ocean Optics) had a larger cryostat which allowed the measurement of larger samples, whereas the cold finger shown above could only accommodate samples $\sim 10 \times 10$ mm. The OceanOptic system also allowed the sample to be translated in the x-y plane beneath the bi-furcated fibre thus enabling photoluminescence measurements too be mapped across the sample when necessary.

3.4 Experimental Results

3.4.1 Photoluminescence Interpretation of As-Received Material

In order to compare the Silicon Carbide after subjection to excimer laser irradiation, PL measurements were made on as-received material. The sample numbers, shown in , are listed in

the order they were received. The quality of the samples were noticeably higher with the later samples. Sample #4 for example contained far fewer micropipe defects than sample #1.

Sample	Growth	Doping [cm^{-3}]	Thickness [μm]
#1	Epitaxial p-type	$2 \times 10^{16}/5 \times 10^{18}$	3/330
#2	Bulk n-type	3×10^{17}	345
#3	Sub/Ion-Implanted	$2 \times 10^{17}/1 \times 10^{21}$	300/~0.240
#4	Bulk p-type.	2×10^{17}	440

Table 3.4:1: 4H-Silicon Carbide sample specifications.

3.4.2 Broad Band Photoluminescence Spectra

As discussed in Chapter 3.2, the broad band spectra of Silicon Carbide consists of Free-Acceptor transitions, labelled A_0 , and site dependent Donor-Acceptor transitions, labelled B_0 and C_0 , for hexagonal-like and cubic-like sites respectively. Phonon replicas have been observed in the literature with numerous guises, typifying the types and quality of wafers. Although there were no observable phonons in the broadband spectra in these results, the energies of 'typical' phonon replicas for nitrogen and aluminium species in 4H-silicon carbide are presented so that free-acceptor and donor-acceptor bands can be identified with more certainty, see Table 3.4:2

Phonon Replica	Nitrogen [meV]	Aluminium [meV]
TA	46.3	46.2
LA	79.4	77.5
TO	94.4	94.5
LO	102.8	103.2

Table 3.4:2: Phonon replicas of the nitrogen bound exciton complex and the aluminium bound exciton complex in 4H-Silicon Carbide [17].

Figure 3.4:2 show PL spectra of as-grown epitaxial material from wafer #1, normalized to the maximum intensity in each. The striking difference in the two spectra are the two bands at 2.53 and 2.59eV seen in Figure 3.4:2. The spectra were measured on different samples, but diced from the same wafer and illustrate some inhomogeneities in the wafer quality. These samples were purchased at the beginning of this work (1996) when micropipe defects, were to some extent, abundant and problematic. The nature of the emission bands are not clear, however the excitation wavelength of 351 nm has an absorption depth, α^{-1} , that will certainly probe the substrate-epitaxial interface [29]. Therefore if the band is defect related [30,31] it is not certain whether the origin of the emission centre is sub surface or not. It is probably worth pointing out here that there are also the same number of inequivalent lattice sites in 4H-Silicon Carbide as there are bands seen here in the PL spectra. However, there are obviously other influencing factors which might be also give rise to these bands. The bands at the higher energy could also be related. Using the equation (3:5) and values of the Nitrogen donor and aluminium acceptor ionisation energies puts the band at 2.8eV in the energy range for DAP emission. The intensity of the band at 2.703 eV in Figure 3.4:2 is also higher probably indicative of differences in dopant concentrations between samples.

The PL spectra of as grown n-type 4H-Silicon Carbide can be seen in Figure 3.4:3. As can be seen the emission is dominated at lower energies compared to the latter p-type material, thus the recombination processes emanate at different recombination centres. Although the sample is predominately n-type, the sample contains boron. Boron is a deep centre, see Table 3.2, consequently the DAP emission should have a peak energy that is typically $\sim 2.388\text{eV}$ This appears to be in close agreement with the observed peak in Figure 3.4:3. However, the PL spectra is dominated by the emission at lower energies and appeared yellow in colour. This is in agreement with that observed in most n-type 4H-SiC, where, the absence of an absorption band at $\sim 2\text{eV}$ thus, the samples appear more yellow in colour.

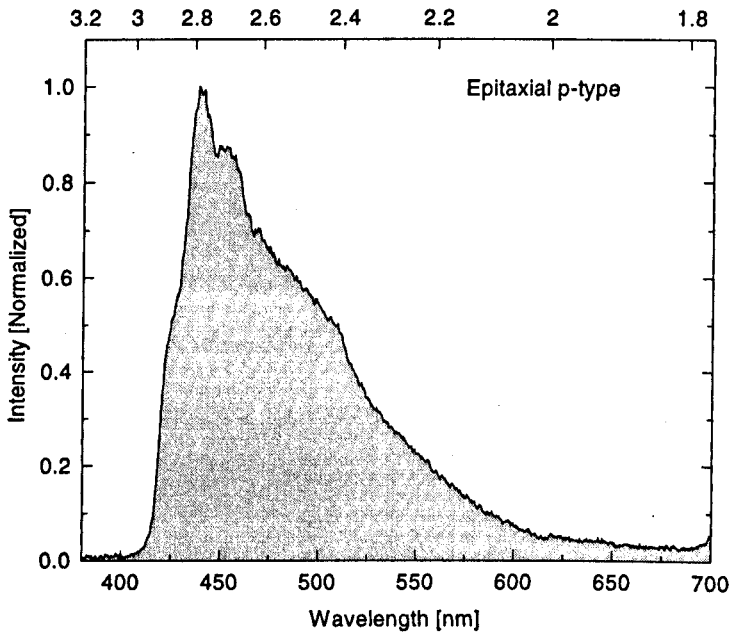


Figure 3.4:1: Photoluminescence spectra of epitaxial p-type 4H-SiC taken at 77K; Wafer #1

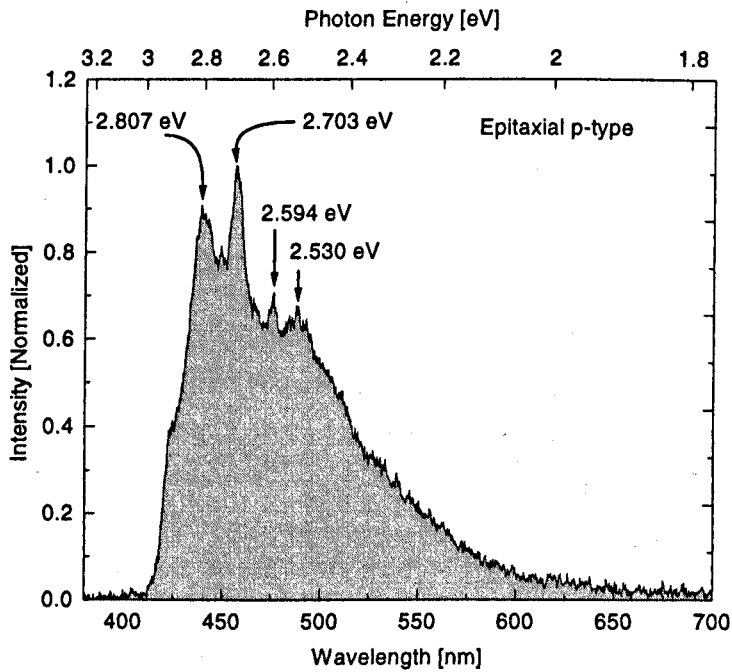


Figure 3.4:2: Photoluminescence spectra of epitaxial p-type 4H-SiC taken at 77K; Wafer #1.

Figure 3.4:4, Sample #4, was bought about one year later when growth techniques had been much improved. There were less micropipe defects and impurities in this sample of SiC and as a consequence the material was much more transparent than in earlier samples. The PL spectra resembled very typically the p-type nature with a relatively sharp feature at 3.005 eV and a less pronounced peak at 3.033 eV. The assignment of such peaks is extremely difficult because of the sophisticated crystal structure. A 'pure crystal' generally consists of a single polytype, thus having unique ionisation energies. If, however, small islands of varying polytypes coexist within a sample the PL spectrum, might, depending on the amount of inhomogenities, emit at an energy that is characteristic of the native polytype. This therefore, complicates the identification and true assignment of the ionisation energies, consequently it is difficult to ascertain the centre that is responsible for particular emission band. If one considers the ionisation energies of different dopant species in Table 3.2, Gallium and Aluminium have the same ionisation energy (249 meV) for both the 4H- and 6H-polytypes. Therefore it is important establish what type of dopants exist in the crystal when assigning a type of dopant with a particular ionisation energy. Referring to Figure 3.4:4, Figure 3.4:5 Figure 3.4:6 and Figure 3.4:7 illustrates the sample inhomogeneity of the bulk n-type sample #2. The majority of the sample was yellow-green in colour, Figure 3.4:6, the orange sample, was taken from the edge of the wafer.

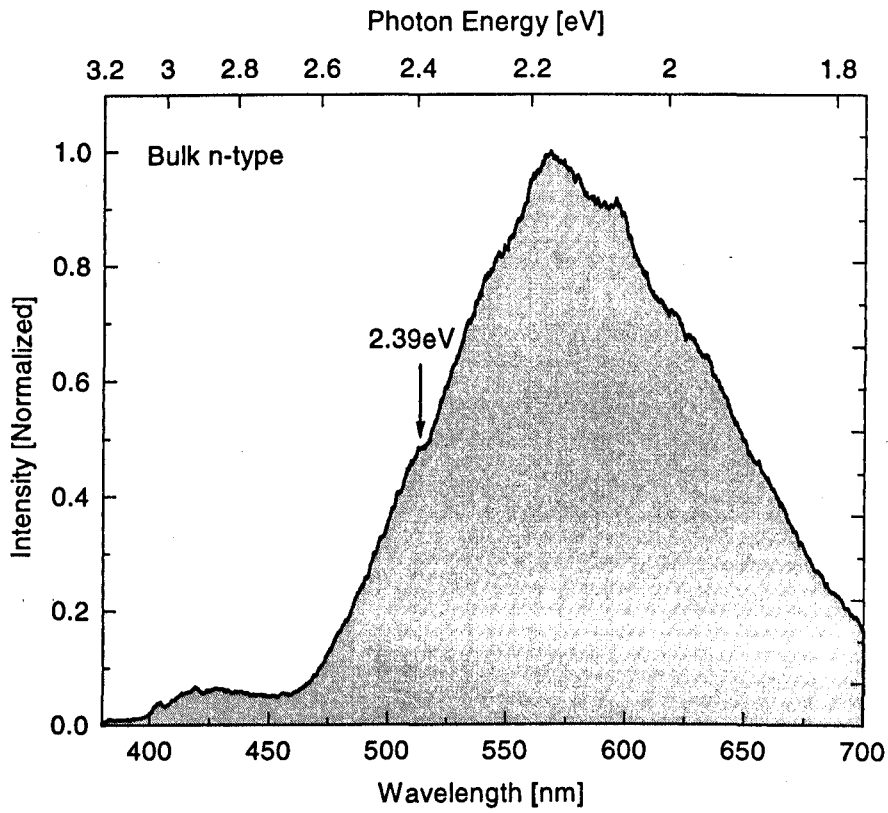


Figure 3.4:3: Photoluminescence spectra of bulk n-type 4H-SiC taken at 77K; Wafer #2.

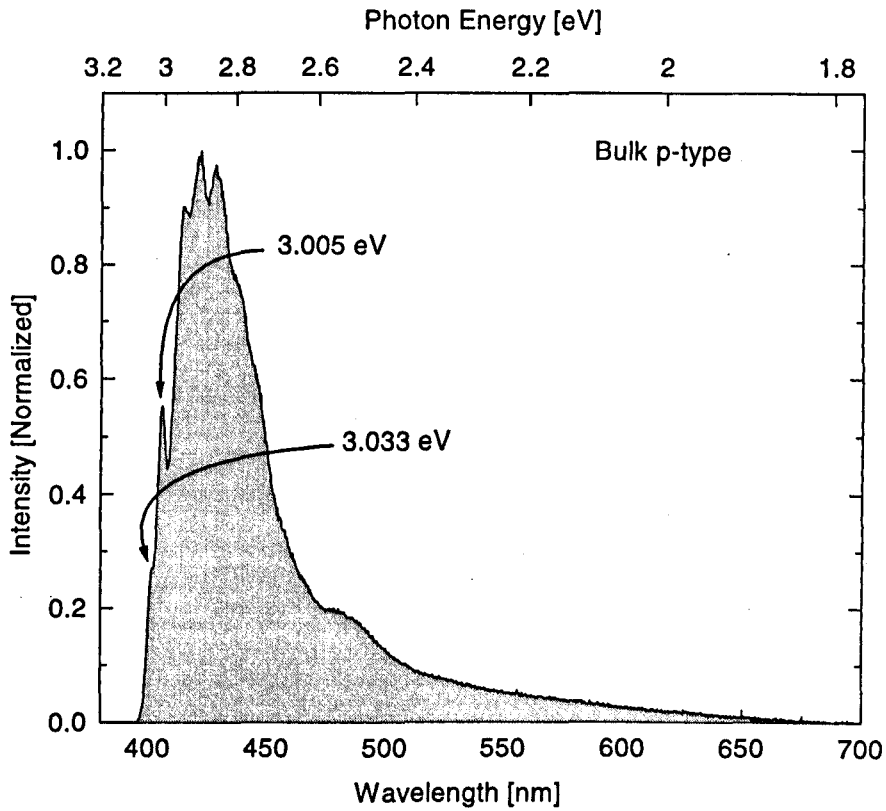


Figure 3.4:4: Photoluminescence spectra of bulk p-type 4H-SiC taken at 77K; Wafer #4.

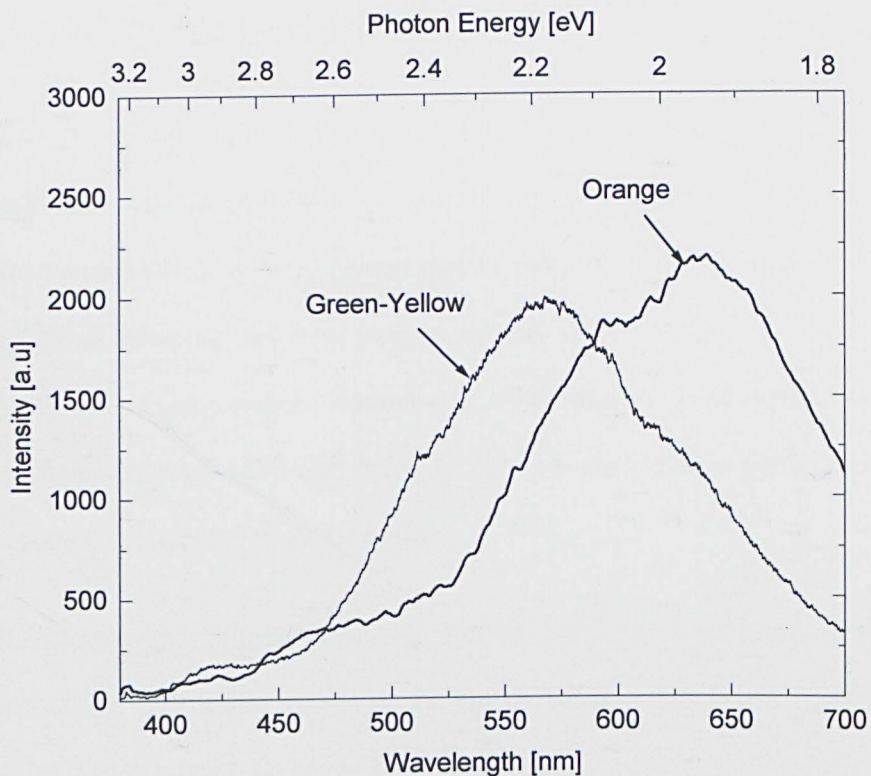


Figure 3.4:5: Photoluminescence spectra of two separate samples from the same wafer illustrating inhomogeneous growth around the wafer edge in 4H-SiC ; Wafer #2.

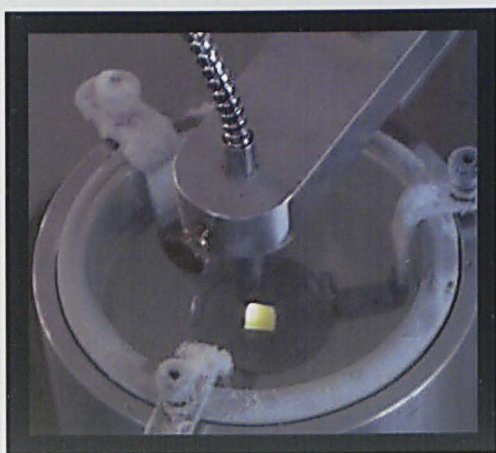


Figure 3.4:6: High quality as-grown n-type 4H-SiC The sample is from the same wafer as that seen in Figure 3.4:3.

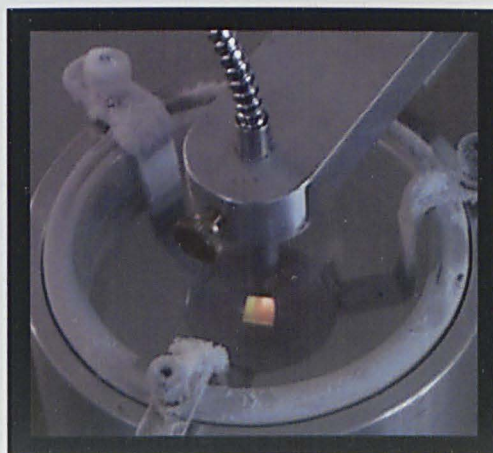


Figure 3.4:7: As-grown n-type 4H-SiC Carbide illustrating non-uniform emission towards the wafer edge, both spectra shown above.

3.4.3 ArF Laser Irradiated 4H-SiC

The main thrust of the work in this section is to investigate the possibility of inducing vacancy type defects at sub-threshold fluences. Because silicon has a higher vapour pressure than Silicon Carbide the intention is to drive silicon species away from the near surface. Hence, there is the possibility of inducing radiative centres around silicon vacancies. However, there is the possibility of inducing carbon vacancies or some other form of defect complex. Therefore, photoluminescence spectroscopic measurements are used here to identify any changes in the luminescence spectra that might take place.

The PL spectrum for the epitaxial sample with the previously identified emission bands at 2.594 eV and 2.530 eV were measured at liquid helium and liquid nitrogen temperatures. Figure 3.4:8 shows that both bands were quenched at 4.2 K along with the broad peak at 2.703 eV. A small peak, however, emerged at 4.2 K at 2.976 eV. Because the bands were quenched at the lower temperature suggests that some phonon assisted emission process took place at the higher temperature.

In Chapter 2, estimates were made to establish the damage threshold fluence at 193 nm. Figure 3.4:9 shows an epitaxial sample irradiated below this threshold at four different laser fluence. At 1.1 J cm^{-2} the intensity can be seen to be slightly higher at 2.807 eV compared with the as-received material. The peaks in this region are thought to be DAP related, in this particular case Nitrogen-Aluminium. Quite clearly, the overall intensity decreased with increasing laser fluence indicating some sort of modification to the optical properties. The reduction in overall intensity clearly indicates the sensitivity of PL measurements. A broad band appeared at $\sim 2.5 \text{ eV}$ which was evident at all the laser fluence, probably indicative of the induced optical modification / damage onset. Incidentally, when these samples were irradiated very subtle colour changes were observed, a silvery/grey speckled appearance was evident over the irradiated site.

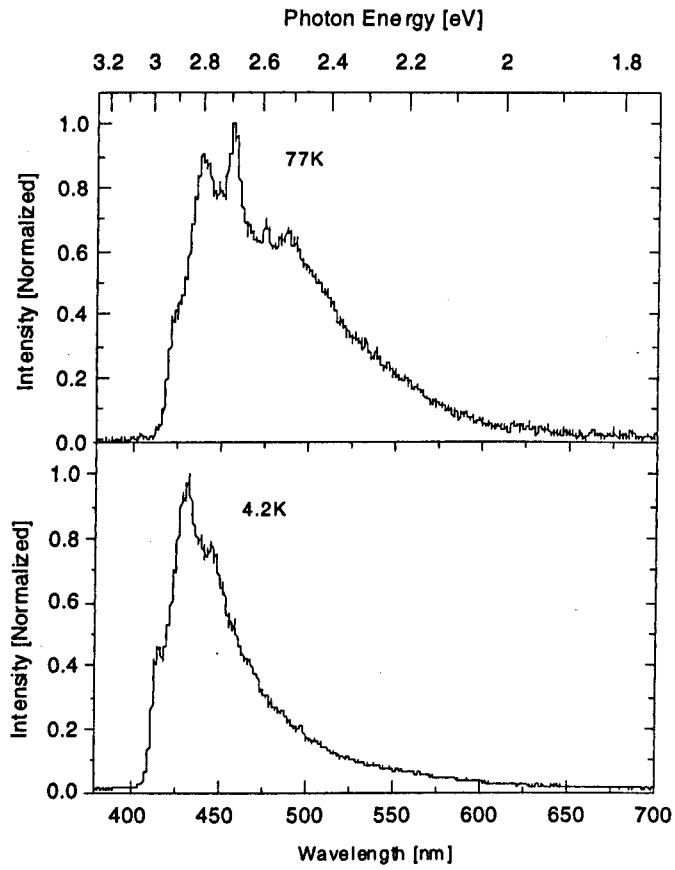


Figure 3.4:8: Photoluminescence spectra of epitaxial 4H-Silicon Carbide at 4.2 and 77K.

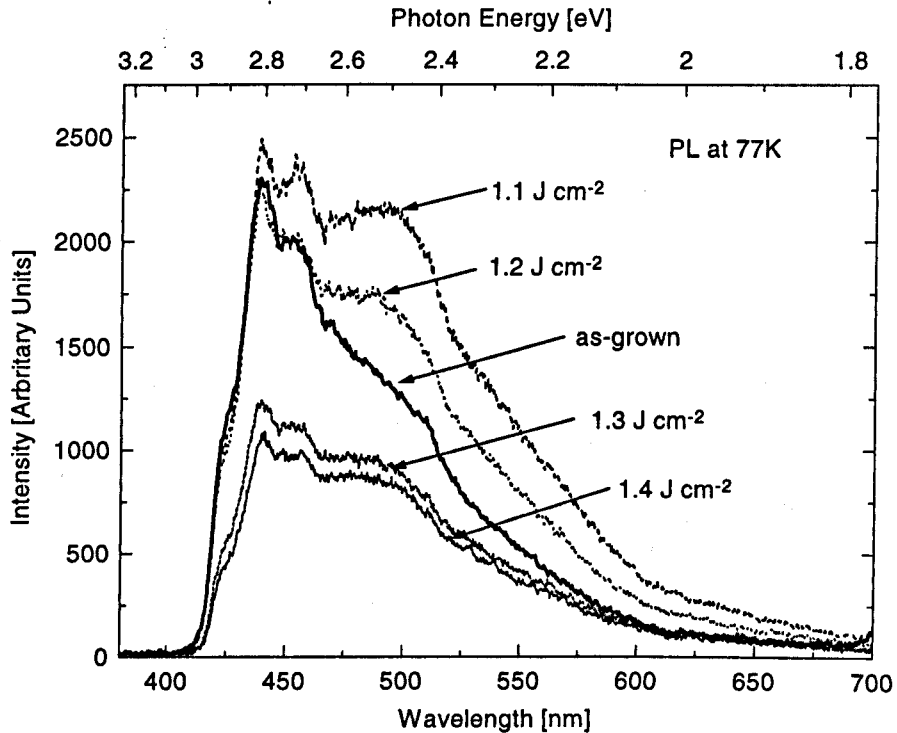


Figure 3.4.9: Photoluminescence spectra of excimer laser ($\lambda=193$ nm) irradiated Silicon Carbide at a pressure of 4×10^{-6} Torr at 50 pulses.

3.4.4 Hydrogen Passivation of Epitaxial 4H-SiC

Hydrogen passivation and hydrogenation is widely used to passivate electrically active centres [32]. Hydrogen can be incorporated unintentionally by contamination, and can be a severe problem during for example wet etching or during growth [33, 34]. Alternatively, hydrogen can be intentionally incorporated during growth or by post growth techniques such as electron cyclotron resonance (ECR) plasma or RF hydrogen generated plasma. In the literature, hydrogenation of silicon carbide has been achieved intentionally by heating at elevated temperature and pressure in H_2 investigate the effects of passivation of nitrogen donors and aluminium and boron acceptors in 6H-SiC [35]. Hydrogen has been implanted and plasma treated to measure the stability with time [36]. It has been found that passivation is most

noticeable for acceptor dopants and to a lesser extent it has also been seen with donor species or deep-level centres. Passivation carried out using hydrogen plasmas can however create defects and as has been to some extent verified by passivation using an He plasmas.

Throughout the literature there exist detailed calculations on atomic displacement energies for the production of simple defect and complex defects. Typical values for the displacement energies for silicon and carbon vacancies, V_{Si} , V_C , are in the range $\sim 4.0 - 8.0$ eV [37]. However displacement energy thresholds as high as 22 eV have been calculated [38]. A low bias potential, 30 V, was set to reduce the possibility of damage occurring via hydrogen sputtering. Although the incident ion energy is greater than the predicted displacement energy the production of either silicon or carbon vacancies is possible, however, the creation of defects are not expected because of the small cross section for violent collisions. As a check, but not specifically adapted for such low incident energies, TRIM calculations were made to obtain estimate of the ion range and number of induced vacancies [39]. At 30 eV the results suggested that the maximum depth of hydrogen was 6 angstroms and no vacancies were produced. Therefore, an implantation mechanism would infer the incorporated hydrogen is a surface feature. A similar hydrogen treatment using ECR plasma at 500 W for 30 minutes at 300 C have been carried out [36]. Secondary ion mass (SIM) spectroscopic measurements indicate penetration depths ~ 50 nm which is probably more realistic compared with TRIM calculations using the low acceleration potential.

In this work, hydrogenation was carried out to investigate the nature of the laser induced band at ~ 2.5 eV. Samples were exposed to a hydrogen plasma for differing time intervals and power densities. The laser irradiated silicon carbide samples were placed in an evacuated chamber ($\sim 2 \times 10^{-5}$ torr) and back flushed with H_2 . The samples were placed between two electrodes that were spaced by 100mm and an acceleration potential of ~ 30 V was applied. An r.f supply (13.65Mhz) set at 100Watts was applied to the H_2 gas and the pressure inside the sample chamber was allowed to increase to achieve a hydrogen discharge. After the relevant hydrogen

dosage the samples were removed and PL measurements were taken and recorded. It was interesting to note that the silvery/grey discolouring that had occurred subsequent to excimer laser irradiation was no longer visible to the naked eye after a single exposure of 30 minutes at 10 Watts.

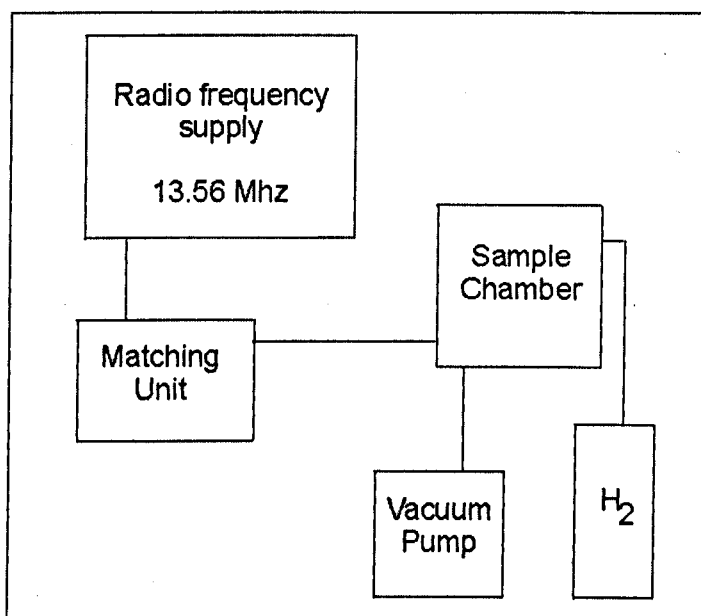


Figure 3.4:10: Schematic drawing of hydrogen passivation system.

Figure 3.4:11, Figure 3.4:12 and Figures 3.4:13 illustrate the changes in the PL spectra with hydrogenation for epitaxial samples laser irradiated at 1.1, 1.3 and 1.5 J cm⁻². There are very little differences between all three figures. The emission band at 2.5 eV is evident at all three laser fluence, probably due to defects of some sort. In all three spectra the intensity of this band decreases with increasing hydrogen dosage. The process was reversed, Figure 3.4:11 using an XeCl laser at a fluence of 1.0 J cm⁻². One week after the hydrogenation and photoluminescence measurements had been taken, the sample shown in Figure 3.4:11 was evacuated down to a pressure of 2×10^{-4} torr and irradiated with 50 overlapping pulses at 308 nm. The photoluminescence spectra was retaken within the space of two days and the photoluminescence spectra returned back close to the original spectra after laser irradiating at 193 nm. These results

indicated the effects of hydrogenation was reversed to some extent. The stability of the hydrogen was measured for the sample shown in Figures 3.4:13. The sample had been untouched for close to six weeks and stored in a standard sample box. The photoluminescence showed that the spectra had shifted slightly over this time again indicating a shift towards the originally irradiated spectra at 193 nm.

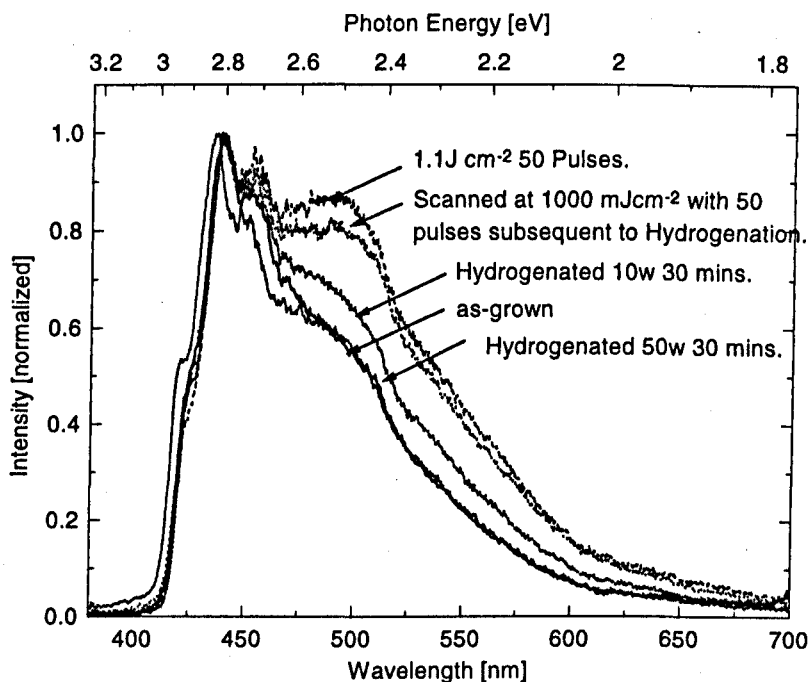


Figure 3.4:11: Photoluminescence of 4H-SiC excimer laser irradiated at 1.1 J cm^{-2} and hydrogenated in an r.f excited hydrogen plasma.

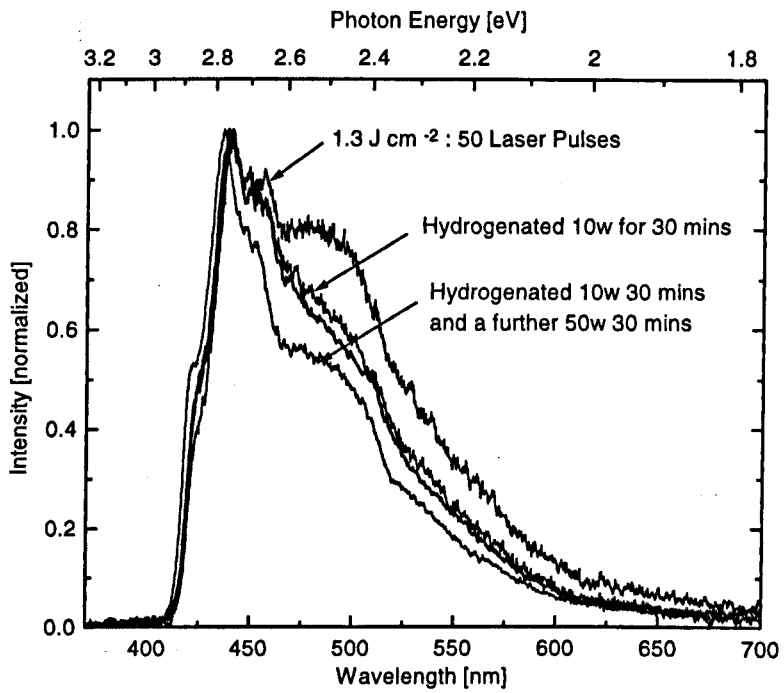
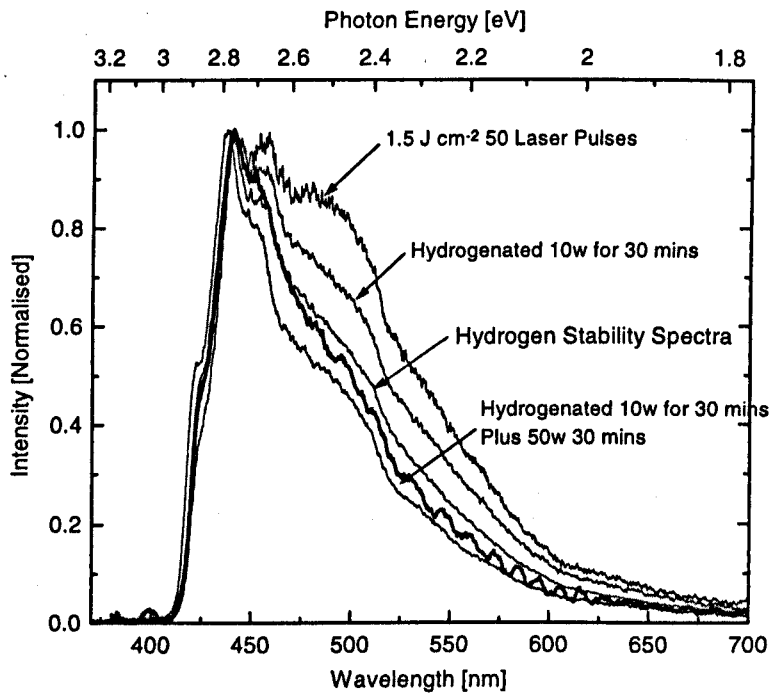


Figure 3.4:12: Photoluminescence of 4H-SiC excimer laser irradiated at 1.3 J cm^{-2} and hydrogenated in an r.f excited hydrogen plasma.



Figures 3.4:13: Photoluminescence of 4H-SiC excimer laser irradiated at 1.5 J cm^{-2} and hydrogenated in r.f excited hydrogen plasma.

3.4.5 XeCl Laser Irradiated Bulk 4H-SiC

Bulk Silicon Carbide, sample #2, was irradiated using a XeCl ($\lambda = 308$ nm) excimer laser at a range of laser fluence. The experiments were carried out to observe any spectroscopic changes for a range of fluence either side of the damage threshold, and also to elucidate the laser induced band at ~ 2.5 eV which was discussed in Chapter 3.4:3. Two sets of experiments were conducted, one using p-type material, sample #1, at below damage threshold at 0.8 and 1.0 J cm^{-2} . The second, using n-type material, sample #2, at above and below damage threshold at a laser fluence of, 1.1, 1.2, 1.3, 1.4, and 1.8 J cm^{-2} with 10 laser pulses at a repetition rate of 1 Hz.

The photoluminescence spectra for the p-type sample irradiated below threshold is shown in Figure 3.4:14. At 0.8 J cm^{-2} with 10 pulses two very distinct broad peaks can be seen at 2.546 and 2.476 eV. The two peaks can be compared although they are not identical, with those of the as-received epitaxial material shown in Figure 3.4:2. The combination of 10 laser pulses at 0.8 J cm^{-2} appears to have optically activated some emission centre. Coincidentally, the bands induced with the 308 nm radiation do lie within the same spectral region as the broad band induced at 193 nm at 1.1, 1.3, and 1.5 J cm^{-2} .

It could be argued that the spatial origins of the bands in the as-received epitaxial material, Figure 3.4:2, and those induced with the 308 nm radiation are the same, since the penetration depth at 308 nm would be sufficient to reach the substrate/epitaxial interface. However, the induced bands at 193 nm, although at similar emission energies, the penetration depth is a few nm and would therefore the EM radiation at 193 nm would not be of sufficient intensity to influence centres at the interface. In terms of the nature of the emission band, because of the similar emission bands energies the origin of the emission could be related to the same species, but it is not possible to say in detail due to the lack of experimental data on the composition of the irradiated sites.

The photoluminescence data shown in Figure 3.4:15 and Figure 3.4:16, spans the laser fluence where the ablation threshold. On visual inspection, the irradiated sites showed a distinct structural change between 1.2 and 1.4 J cm⁻². The surface became roughened and appeared to be highly disrupted. This was also evident in the PL spectra where a large shift in the peak emission occurred. The emission at centred at ~2.5 eV and above, induced by excimer irradiation at 1.4, 1.6 and 1.8 J cm⁻² bares spectral similarities to that of porous Silicon Carbide. The broad band spectrum is typical of porous Silicon Carbide with intense emission often above the band gap [40, 41, 42]. It as been suggested that the origins of the above band gap emission in cubic (3C-SiC) is due quantum confinement effects and increased emission intensity with increased surface area [43].

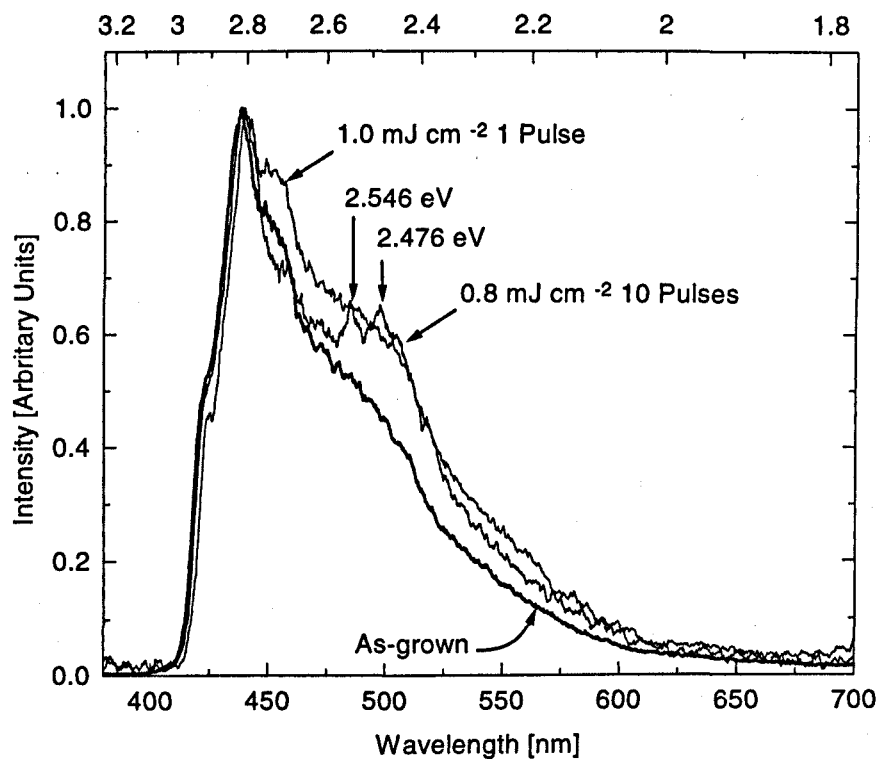


Figure 3.4:14: Photoluminescence spectra of p-type SiC at 77 K, laser irradiated at 308 nm below the damage threshold, sample #1.

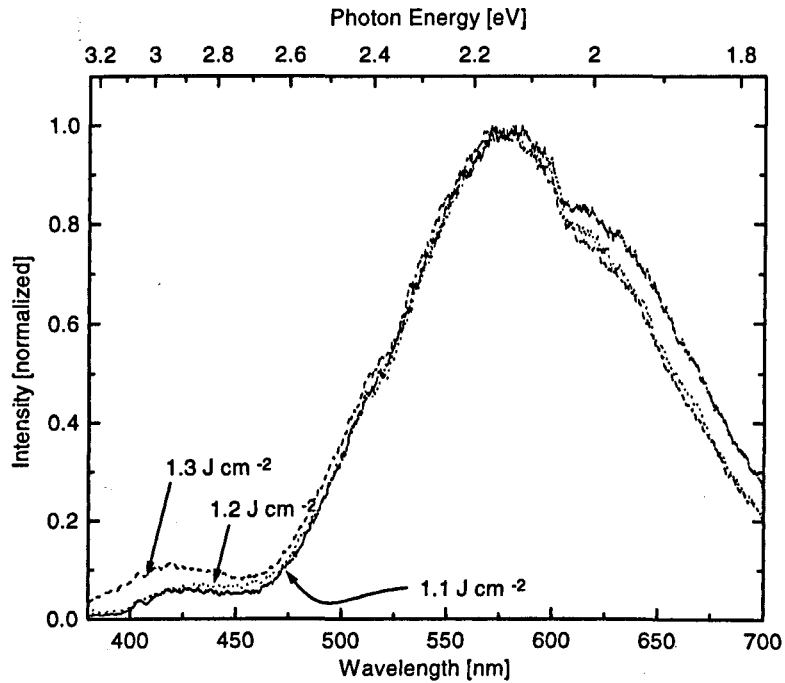


Figure 3.4:15: Photoluminescence spectra of XeCl laser irradiated n-type Silicon Carbide vs. laser fluence, sample #2.

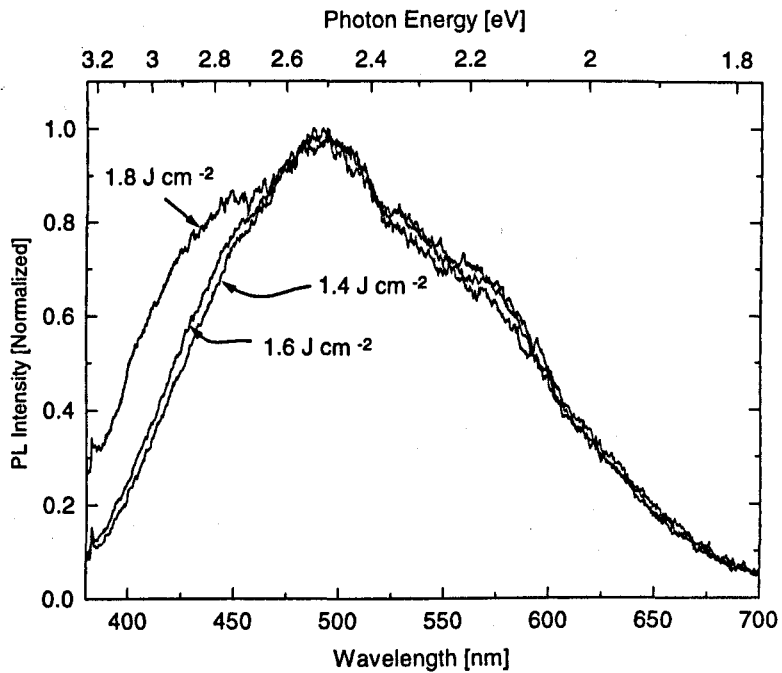


Figure 3.4:16: Photoluminescence spectra of XeCl laser irradiated n-type Silicon Carbide vs. laser fluence, illustrating laser induced damage, sample #2.

3.5 Conclusion

It has been shown in p-type Silicon Carbide, at a sub-ablation threshold the emergence of a laser induced emission band when irradiated at 193nm using an ArF laser. The luminescent intensity is seen to decrease with increasing laser fluence indicating the possibility of a damage mechanism is taking place. This intensity of the band can be recovered when passivated with molecular hydrogen such that the spectra returns near to the as grown spectra. With the intention of trying to remove the hydrogen and hence de-passivate the treated surface using light at 308nm from a XeCl laser, the defect band can be seen to re-emerge. It was noted that the spectral position of the aforementioned laser induced band is energetically similar to an emission measured in as-received epitaxial material with a relatively high density of micropipe defects ($\sim 100 \text{ cm}^{-2}$).

Photoluminescence measurements carried out at 308nm on n-type Silicon Carbide showed a large blue shift in the spectra when irradiated above the ablation threshold. The broadband photoluminescence intensity of the highly disrupted material now peaked $\sim 2.5 \text{ eV}$ and is typical of porous Silicon Carbide.

The results demonstrate the presence of a laser induced band and therefore the need for further investigation. In Chapter 4, further work is carried out in order to elucidate the nature of this emission at $\sim 2.5 \text{ eV}$ by the use of Positron Annihilation measurements.

3.6 References

-
- [1] Ch. Haberstroh, R. Helbig, and R.A. Stein, *J. Applied Physics*, **76** (1), 509 (1994).
- [2] M. Ikeda, H. Matsunami and T. Tanaka, *Physical Review B*, **22** (6), 2842 (1979).
- [3] L. Patrick, *Physical Review*, **127** (6), 1878 (1962).
- [4] J. A. Edmond, H. J. Kim, and R. F. Davis, *Mater. Res. Soc.*, **40**, 645 (1993).
- [5] S. Ahmed, C. J. Barbero, and T. W. Sigmon, *Appl. Phys. Lett.* **66** (6), 712 (1995).
- [6] K. C. Pandey, *Physical Review Letters*, **57** (18), 2287 (1986).
- [7] F. Razul, P.h.D Thesis, Hull, Chapter 7, *Non-Linear Soliton like Excitations In A Solid* (1999).
- [8] W. J. Choyke and L. Patrick, *Physical Review. B* **4**, 1843 (1971).
- [9] L. Patrick and W. J. Choyke, *Physical Review B*, **5** (8), 3253 (1972).
- [10] V. M. Gusev, K. D. Demakov, M. G. Kosaganova, M. B. Reifman and V. G. Stolyarova, *Soviet Physics. Semiconductor*. **9**, 820 (1975).
- [11] N. T. Son, E. Sorman, W. M. Chen, M. Singh, C. Hallin, O. Kordina, B. Mornemar, and E. Janzen. *J. Appl. Phys.* **79**, 3784 (1996).
- [12] Yu. A. Vodakov, G. A. Lomakina, E. N. Mokhov, V. G. Oding, M. G. Ramm and V. I. Sokolov. *Sov. Phys. Semicond.* **20** (8), 900 (1986).
- [13] S. Dannefaer, D. Craigen, and D. Kerr. *Physical Review B*. **51** (3), 1928 (1994).
- [14] E. Sorman, W. M. Chen, N. T. Son, C. Hallin, J. L. Lindstrom, B. Monemar and E. Janzen, *Material Science Forum*, **264-268**, 473 (1998).
- [15] E. Sorman, N. T. Son, W. M. Chen, O. Kordina, C. Hallin, and E. Janzen. *Physical Review B*, **61** (4), 2613 (2000).
- [16] A. Wyszomolek, J. M. Baranowski and M. Kaminska, *Acta. Physica. Polonica A*, **88** (5), 957 (1995).
- [17] W. J. Choyke, D. R. Hamilton, L. Patrick, *Physical Review A*, **133**, 1163 (1964).
- [18] A. Henry, O.Kordina, C. Hallin, C. Hemmingsson, and E. Janzen. *Appl. Phys. Lett.* **65**, (19) 2457 (1994).
- [19] M. Ikeda, H. Matsunami, *Physica. Status. Solidi*, **58**, 657 (1980).
- [20] D. Schulz, K. Irmscher, J. Dolle, W. Eiserbeck, T. Muller, H. J. Rost, D. Siche, G. Wagner, and J. Wollweber. *International Conference o Silicon Carbide and Related Materials*, (1999) p.87.
- [21] L. Patrick, D. R. Hamilton, J. W. Choyke. *Phys. Rev.* **132**, 2023 (1963).
- [22] A. Suuki, H. Matsunami and T. Tanaka, *J. Electrochemical. Society, Solid State Science and Technology*, **124** (2), 241 (1977).

-
- [23] T. Henkel, Y. Tanaka, N. Kobayashi, S. Nishizawa and S. Hishita, Conference Proceedings, *Silicon Carbide and Related Materials 1999*, Raleigh N. C. pp953-956.
- [24] N. T. Son, E. Sorman, W. M. Chen, O. Kordina, B. Monemar, and E. Janzen. *Appl. Phys. Lett.* **65** (21), 2687 (1994).
- [25] J. R. Jenny, J. Skowronski, W. C. Mitchel, H. M. Hobgood, R. C. Glass, G. Augustine, and R. H. Hopkins, *Appl. Phys. Lett.* **68**, 1963 (1996).
- [26] Institute of Physics Conference Series, **142**, Silicon Carbide and Related Material, (1995) p493.
- [27] G. B. Dubrovskii, V. I. Sankin, *Sov. Phys. Solid. State.* **17**, 1847 (1975).
- [28] K. Colbow, *Physical Review* **141**, 742 (1966).
- [29] S. G. Sridhara, R. P. Devaty, and W. J. Choyke. *J. Appl. Phys.* **84**, 2963 (1998).
- [30] J. W. Steeds, F. Carosella, G. A. Evans, M.M Ismail, L. R. Danks, W. Voegeli, *Silicon Carbide And Related Materials, ECSCRM2000*, *Mat. Sci. Forum.* **353**, 381-384 (2000).
- [31] L. Masarotto, J. M. Bluet, M. Berenguer, P. Girard, G. Guillot, *Silicon Carbide And Related Materials, ECSCRM2000*, *Mat. Sci. Forum.* **353**, 393-396
- [32] S. J. Pearton, J. W. Corbett and M. Stavola, *Hydrogen in Crystalline Semiconductors* (Springer, Berlin, 1982).
- [33] D. J. Larkin, S. G. Sridhara, R. P. Deavaty and W. J. Choyke, *J. Electron. Mater.* **24**, 298 (1995).
- [34] A. Schoner, K. Rottner, N. Dordell, M. Linnarsson, C. Peppermuller and R. Helbig, *Diamond and Related Materials.* **6**, 1293 (1997).
- [35] F. Gendron, L. M. Porter, C. Porte, and E. Brringeruier, *Appl. Phys. Lett.* **67**, 1253 (1995).
- [36] J. M. Zavada, R. G. Wilson, F. Ren, S. J. Pearton, and R. F. Davis, *Solid State Elecron.* **41**, 677 (1997).
- [37] J. Bernholc, S. A. Kajihara, C. Wang, and A. Antonelli. *Mater. Sci. and Eng.* **B11**, 265. (1992).
- [38] A. Barry, B. Lehmann, D. Fritsch, and D. Brauning, *IEEE Trans. Nucl. Sci.* **38**, 1111 (1991).
- [39] (TRIM: Transport of Ions in Matter), described in J. F. Ziegler, J. P. Biersack, and U. Littmark, *The Stopping and Range of Ions in Solids* (Pergamon, New York, 1985).
- [40] A. M. Danishevskii, V. B. Shamun, E. G. Guk, and A. Yu. Rogachev. *Semiconductors* **31**, (4) 354 (1997).
- [41] A. O. Konstantinov, A. Henry, C. I. Harris, and E. Janzen. *Appl. Phys. Lett.* **66**, (6) 2250. (1995).
- [42] J. N. Wang, Z. M. Chen, P. Woo, W. K. Ge, Y. Q. Wang, and M. B. E. Yu. *Appl. Phys. Lett.* **74**, (7). 923 (1999).
- [43] L. S. Liao, X. M. bao, Z. F. Yang, and N. B. Min. *Appl. Phys Lett.* **66** (18), 2382 (1995).

Chapter 4

Positron Annihilation Studies of Excimer Laser Irradiated 4H-Silicon Carbide

4.1 Introduction	76
4.2 Positron Annihilation Spectroscopy	76
4.3 The Momentum Distribution Technique: Doppler Broadening	78
4.3.1 Interpretation of S and W Parameters	80
4.3.2 Positron Implantation and Diffusion	81
4.4 Experimental Procedure	83
4.5 Experimental Results	85
4.5.1 XeCl Laser Irradiated 4H-SiC	86
4.5.2 ArF Laser Irradiated Epitaxial 4H-SiC	88
4.6 Conclusion	93
4.7 References	94

Chapter 4

Positron Annihilation Studies of Excimer Laser Irradiated 4H-Silicon Carbide

4.1 Introduction

Lattice defects strongly influence or even determine some of the electrical and optical properties of semiconductors and are thus of great technological importance. In this chapter, the general thrust is to investigate using Positron Annihilation Spectroscopy (PAS) the microscopic modifications that occur to Silicon Carbide when subjected to radiation from an excimer laser.

The positron annihilation measurements were carried out at the using a variable energy positron beam source at the University of Bath. This work is a continuation to the photoluminescence measurements in Chapter 3, more specifically, the nature of the laser induced emission band which was not identified. There is a strong possibility that the radiative recombination is due to some kind of vacancy related defects and therefore PAS was adopted to help elucidate the origin of the transition. To the authors' knowledge at the time of writing this thesis there were no research papers on positron studies of excimer laser irradiated 4H-SiC.

4.2 Positron Annihilation Spectroscopy

In 1927 Paul Adrien Maurice Dirac predicted the existence of the antiparticle of the electron [1]. The first indications of an unknown particle came from the work by Anderson in 1932, where he was able to photograph cosmic rays from within a bubble chamber. This particle was later identified as the positron, and was the first reported antiparticle in the subject of physics.

Positron Annihilation Studies of Excimer Laser Irradiated 4H-SiC.

Positron Annihilation Spectroscopy (PAS), as the name suggests, is the spectroscopy of photons emerging from the annihilation of electrons with positrons. The technique is non-destructive, and does not require any special sample preparation as compared with some other defect characterization techniques. Some of the early attempts to use the technique of positron annihilation spectroscopy were hindered by the poor quality of the available material. However, in recent years, the production of high quality material has reduced the types of defects and their concentrations. Thus, the improvements in growth techniques have played an important part in the advancement of PAS. The technique is now well established for the study of electronic and defect properties in metals and semiconductors [2,3,4]. PAS has proven to be very sensitive tool for in the detection of open volume defects [5,6]. Positrons diffusing through a semiconductor may be captured at trapping sites. Once captured the positron wavefunction can become localized until it meets it's fate and annihilates with an electron in the immediate surroundings with the production of two gamma photons. Since the local electron density and the electron momentum distribution is different to the crystal environment in a defect free lattice the annihilation radiation can be utilized to obtain information about the localized site. Hence, the character and the concentration of the trapping centres can be established.

Positron techniques can be classified into two principle groups which are distinguished by the sensitivity of positrons to the electron density a) *positron life time measurements*, and to the electron momentum distribution in the sample b) *Doppler-broadening spectroscopy and angular correlation of annihilation radiation*. Since the electron density and electron momentum distribution in defects capable of trapping positrons differ from the *perfect* site, these techniques present a tool to study the type and number of these crystal defects. Since the early 1980s, as a result of the rapid progress in variable-energy positron beam techniques PAS has emerged as a very successful means of detecting low concentrations of defects. For example, in bulk crystalline materials the technique can detect defect concentrations as low as

Positron Annihilation Studies of Excimer Laser Irradiated 4H-SiC.

$1 \times 10^{15} \text{ cm}^{-3}$ which put the technique at the front of other conventional techniques in terms of defect resolution.

Pure Silicon Carbide is a highly stoichiometric compound and intrinsic defects are very low. Up to temperatures of 2000 K no indications of thermal vacancy formation have been detected using PAS [7]. Within the literature, positron lifetime measurements have been carried out to investigate the defect structures in 4H- and 6H-SiC [8,9]. Radiation damage induced by ion implantation has been studied by mono-energetic positron beam techniques in 6H-material [10,11]. Using similar techniques, investigations have been undertaken on ion-implantation induced defects and their annealing properties for N_2^+ or Al^+ implanted 3C-SiC [12,13,14] and 6H-SiC [15]. Silicon Carbide is a relatively difficult material to produce, necessitating a wide range of growth techniques in order to achieve the desired material properties. The difficulties arise due to the high stability of lattice defects and the relatively high temperature needed for recrystallization. Slow positron beam experiments have been previously carried out on chemical vapour deposited Silicon Carbide thin films to study the variation in the Doppler broadening S parameter, where it was found that the positrons are very sensitive to the growth conditions.

In this Chapter, a set of Doppler broadening experiments have been undertaken to quantify the structural modifications that occur subsequent to laser irradiation. A condensed description of the physics involved in Doppler broadening is described below.

4.3 The Momentum Distribution Technique: Doppler Broadening

The kinematics of the emerging photons are determined by the initial energy and momentum of the electron-positron pair participating in the annihilation. Having entered a material the positron rapidly thermalizes within about the first 1-10 pico-seconds, initially by inelastic collisions with core electrons, and ultimately by electron hole creation, plasmon and phonon

Positron Annihilation Studies of Excimer Laser Irradiated 4H-SiC.

excitations. Annihilation during the slowing down process, known as 'annihilation-in-flight', is possible, but is usually very small (<1%) and is generally neglected. From thereon, much of the positrons life time ($\sim 2 \times 10^{-10}$ s) is spent freely diffusing through the crystal lattice, with a deBroglie wavelength ~ 60 Angstroms. The probability of the positron annihilating with a electron with a given momentum state is determined by the overlap of the of the positron wavefunction. A defect site with a missing atom or electron provides a local energy minimum, i.e. a trapping site, for a positron. Consequently, positrons are strongly attracted to open volume defects such as vacancies and voids and can become trapped at impurity sites due to a distorting he local potential. The annihilation energy of a positron-electron pair produces photons with a total energy of $2m_0c^2$ less the electron binding energy, $\approx 2m_0c^2$, where m_0 denotes the electron rest mass energy.

As a result of momentum conservation during the annihilation event, the momentum of the electron-positron pair, p , is transferred to the annihilation photon pair. Therefore the relative motion and the Doppler shift will be a suitable signature of the electronic environment around the annihilation site. For non-relativistic electrons, the doppler shift of the annihilation gamma ray photons is given by:

$$\delta E = \frac{1}{2} cp_z \quad (4:1)$$

where p_z is the momentum component in the propagation direction and, c , the speed of light.

Since numerous annihilation events take place, the Doppler shift of the individual gamma ray photons results in a broadened annihilation photon peak. The common method of characterizing the electron momentum from the annihilation peak is to use the parameters, S , (sharpness) and, W , (wings).

4.3.1 Interpretation of S and W Parameters

The S and W parameters used in electron momentum distribution measurements used to characterize the electron momentum are somewhat qualitative, but are extremely sensitive to changes. The S parameter is defined as the ratio of the counts (i.e., area) in a central region of the photon peak to the total number of counts (area) in the complete peak. 'W' is defined in an analogous way, the number of counts in a defined wing area to the total counts.

$$S, W = \frac{\sum_I \int_{-\infty}^{\infty} \int_{-\infty}^{\infty} dp_x dp_y d(P)}{\sum_{\text{total}} \int_{-\infty}^{\infty} \int_{-\infty}^{\infty} dp_x dp_y d(P)} \quad (4:2)$$

where \sum_I is the appropriate energy window for S and W, and \sum_{total} is taken over the full annihilation peak. The S and W parameters have a simple relationship to the Doppler broadening, for example, if the positron encounters an open volume defect such as a mono – or multi vacancy lattice site, the positron quickly becomes trapped ($\sim 10 \times 10^{-15}$ sec). If the positron becomes trapped due to a vacant lattice site the overlap of the positron wavefunction is predominately with the valence electrons which results in a narrow, hence, increased S parameter. Alternatively, if the positron becomes trapped at an impurity site, or somewhere in the bulk, the positron wavefunction extends to the core electrons resulting in a greater shift in annihilation photon energy, hence the spectrum is broadened, thus resulting in a reduced S parameter. Succinctly, a high S value indicates positrons trapped at vacancies and a low S parameter indicates that a large fraction are trapped somewhere within the bulk. The S parameter increases when the line shape becomes narrower, while the W parameter increases as the line shape broadens.

The use of simple parameters such as S and W yield information about open volume defects and the internal electric fields. However the absolute meaning of the S and W parameters have little

Positron Annihilation Studies of Excimer Laser Irradiated 4H-SiC.

meaning since they depend on the definition of the windows chosen for the central and wing regions and on the response of individual photon-detection systems. It is the general relative change in these parameters that carry the information and therefore the S and W parameters are usually normalized

$$S_{\text{norm}} = \frac{S}{S_{\text{bulk}}} \quad (4:3)$$

where S_{bulk} is the value of S taken from a defect free sample.

4.3.2 Positron Implantation and Diffusion

Until the recent advances in the production of low energy positron beams most studies used positrons from radioactive sources with a large spread in the energy distribution. This energy spread precluded the use of positrons as a depth-resolved probe for defects. Now, with a variable-energy positron beam, a depth resolved distribution of defects can be derived. A quantitative interpretation requires a good understanding of the position dependent implantation profile. Positron beams are generally used to study defects in the top few microns of a material which corresponds to acceleration potentials of $\leq 50\text{keV}$. For such energies Monte-Carlo simulations can be used to estimate the stopping profiles [16]. The resulting implantation profile for a homogeneous, semi-infinite material can be approximated using the Makhovian distribution [16] given by

$$P(z) = \frac{mz^{m-1}}{z_0^m} \exp\left[-\frac{z^m}{z_0^m}\right] \quad (4:4)$$

where 'z' denotes the depth into the material from the surface and 'm' is known as the shape parameter, and z_0 , is related to the mean implantation depth, \bar{z} by

Positron Annihilation Studies of Excimer Laser Irradiated 4H-SiC.

$$z_0 = \frac{\bar{z}}{\Gamma\left(\frac{1}{m} + 1\right)} \quad (4:5)$$

where Γ is the gamma function. In most cases the value of $m = 2.0$ will suffice, in which case the Makovian distribution becomes a simple Gaussian-derivative profile. In many cases the mean positron implantation depth (in Angstroms) can be represented by a simple power law :

$$\bar{z} = \frac{A}{\rho} E^n \quad (4:6)$$

where E is the implantation energy in keV, and ρ is the mass density in g cm^{-3} . The parameters A and 'n' are empirically found, typically taking the values of $n = 1.6$ and $A = 40$ for silicon based systems. However such approximation can only provide estimates in the actual Makhovian profile After implantation the thermalized positrons can diffuse some distance through the crystal before annihilating [17]. Whilst diffusing in a semiconductor material, the positron can encounter charged defect sites and buried electric fields. Because of the complexity, delving into this area would digress somewhat from this work, therefore, a more in depth explanation can be obtained from work already within the literature [18]. However, for analytical purposes, the positron may be considered analogous to a hole in a semiconductor. Its diffusivity D_+ and the mobility μ , can be related to the Einstein equation:

$$eD_+ = k_B T\mu \quad (4:7)$$

where k_B is Boltzmann's constant and e is the elementary charge. The positron diffusivity, put rather simply, relates how quickly a thermalized positron reaches a trapping site. The positron diffusion length, L_+ , during it's bulk lifetime τ_b , in a defect free material is given as:

$$L_+ = \sqrt{D_+ \tau_b} = \sqrt{D_+ \lambda_b^{-1}} \quad (4:8)$$

Positron Annihilation Studies of Excimer Laser Irradiated 4H-SiC.

where λ_b is the positron annihilation rate. A typical room temperature positron bulk lifetime for SiC is 144 ± 2 pico seconds taken from ref [19] and a diffusivity of $2.7 \times 10^{-4} \text{ m}^2 \text{ s}^{-1}$. This yields a positron diffusion length $L_+ \approx 197 \text{ nm}$. If there is an open-volume defect in the lattice, the positron wave function can condense into the potential minimum with high efficiency. In material with a uniform defect distribution an effective diffusion length $L_{+ \text{eff}}$ is given as:

$$L_{+ \text{eff}} = \sqrt{\frac{D_+}{\lambda_b + \kappa_t}} \quad (4:9)$$

where κ_t is the trapping rate into defects given by :

$$\kappa_t = v_t \eta_t \quad (4:10)$$

where v_t represents a specific trapping for a type of defect present within the lattice of atomic density η_t .

4.4 Experimental Procedure

The energy broadening spectra reported in this chapter were carried out using the low positron beam shown in the photograph of Figure 4.4:1, and illustrated in the schematic drawing shown in Figure 4.4:2. The Helmholtz coils are suspended on a non-magnetic framework and can be adjusted to collimate the beam when necessary. The positron source was a typical ^{22}Na β^+ emitter with a half life of $\tau_{1/2} = 2.6$ years. Sodium sources are used because of the relatively long life time in comparison to some of the other sources and because of their high branching ratio with a yield of about 90%. Another advantage of the sodium radio-isotope is the almost simultaneous emission of 1.27 MeV gamma ray which can be utilized for positron lifetime measurements. The positrons emitted have a broad energy distribution with a mean energy distribution of $\sim 500 \text{ keV}$. Positrons with these sorts of energy are too energetic for

Positron Annihilation Studies of Excimer Laser Irradiated 4H-SiC.

practical surface profiling experiments since they would penetrate far too deeply into the sample ($\sim 10\text{-}100\ \mu\text{m}$). In this work, the energy of positrons were moderated to $\sim 30\ \text{eV}$ using a pure, 99.5 % polycrystalline tungsten thin foil ($\sim 7\ \mu\text{m}$ thick) which was positioned directly in front of the sodium source. The tungsten has a negative positron work function and an efficiency $\sim 4 \times 10^{-4}$ which results in the preferential emergence of slow positrons. The versatility of Silicon Carbide as was briefly mentioned in the introduction as having the potential application as a field assisted moderator [20,21,22,23], and incidentally, it is the only semiconductor known so far with a negative positron work function.

The positron beam was transported by a solenoid magnetic field generated by six copper wound coils which produce a uniform axial field of 0.01 Tesla (100 Gauss) that is large enough to confine a positron with a transverse kinetic energy of 1eV to a gyration radiation of 0.25mm. The mono-energetic positron beam is then accelerated down the flight tube at a potential of up \sim to 30 eV where they enter the sample and suffer their various fates. After annihilation, some of the gamma ray photons are emitted from the sample surface and are detected using a liquid to nitrogen cooled Ge crystal detector. The gamma ray photons impinge onto a nitrogen cooled Ge

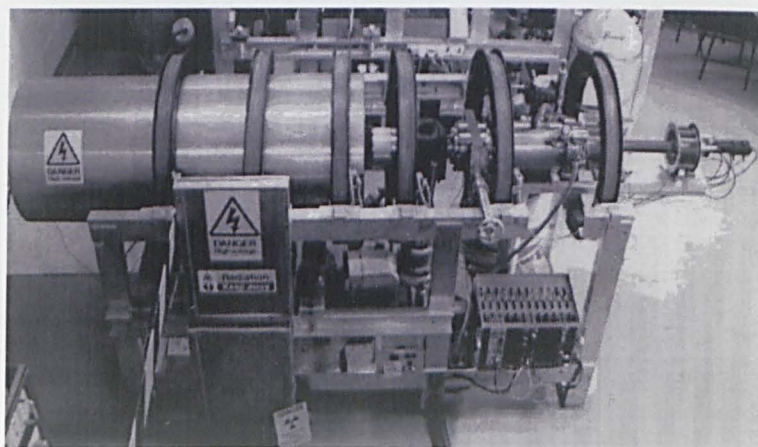


Figure 4.4:1 Photograph of the University of Bath's slow positron beam [24], Courtesy of F. Malik.

Positron Annihilation Studies of Excimer Laser Irradiated 4H-SiC.

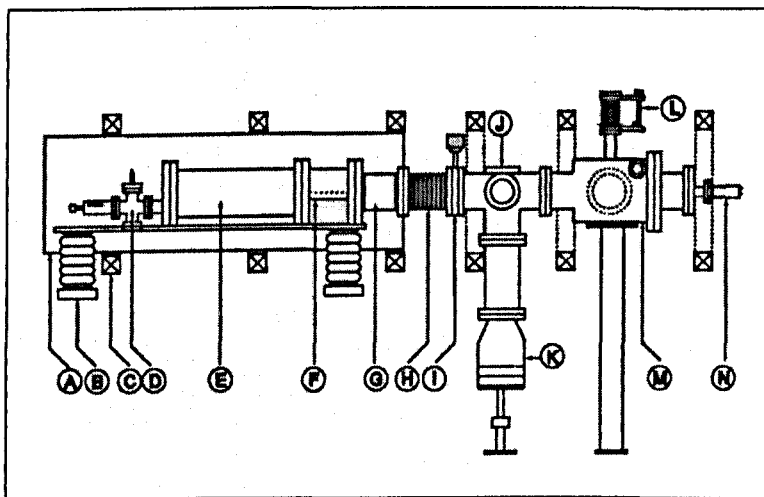


Figure 4.4:2 Schematic drawing of the University of Bath's slow positron beam: A:-grounded shield, B:-stand off insulators, C:-Helmoltz coils, D:-source/moderator, E:- $E \times B$ plates, F:-lead shield, G:-accelerator, H:-bellows, I:-gate, J:-guiding coils, K:-turbo molecular pump, L:-sample manipulator, M:-sample chamber, N:-CEAMA/CCD camera.

crystal detector where the kinetic energy is converted in to electrical energy via the photoelectric effect . A process of electron avalanche results in a detected voltage peak which is proportional to the energy of the original gamma ray photon.

4.5 Experimental Results

The PAS (Doppler broadening) measurements were carried out using the equipment described above. Positron beam energies ranged between 0.5 and 30 keV. The samples were mounted on thin tungsten wires to minimize the any detectable annihilation photons that might emerge from

Positron Annihilation Studies of Excimer Laser Irradiated 4H-SiC.

material other than the sample under investigation. The Doppler broadening S parameter was then measured and used to characterize the effects subsequent to excimer laser irradiation.

4.5.1 XeCl Laser Irradiated 4H-SiC

For this series of experiments bulk Silicon Carbide, (sample 2#, chapter 3) was irradiated with a range of laser fluence between 1.1 and 1.8 J cm⁻² using 10 laser pulses. The samples chamber was flushed with argon in an attempt to remove most of the oxygen and other unwanted ambient gases from within the sample chamber. The chamber was then pumped down to a pressure of $\sim 4 \times 10^{-5}$ torr using an oil diffusion pump.

Figure 4.5:2 shows results of the normalized S parameter for the laser irradiated and an as-grown sample for reference. As can be seen at a laser fluence of 1.3 J cm⁻² and below the spectra are very similar i.e. with only small changes in the normalised S Parameter.

An attempt to correlate the value of S_{norm} to the concentration has been given by Anwand *et-al*, Ref [26]. Their detailed investigations of Doppler broadening and positron lifetime measurements coupled with theoretical calculations showed that the dominant defect formed subsequent to Ge ion-implantation was the silicon-carbon di-vacancy. Combining these results with other cited positron studies [5,10,25], Anwand *et-al*, arrived at a scaling curve that correlates S/S_{bulk} for positrons trapped in an agglomerate of silicon-carbon di-vacancies with the number of di-vacancies in the agglomerate. For the purpose of discussion the results of Anwand *et-al* have been reproduced and are illustrated in Figure 4.5:1. At a laser fluence of 1.3 J cm⁻² and below the normalized S parameter is ~ 1.04 . With reference to Figure 4.5:1, the number of silicon-carbon di-vacancies is between zero and one.

Positron Annihilation Studies of Excimer Laser Irradiated 4H-SiC.

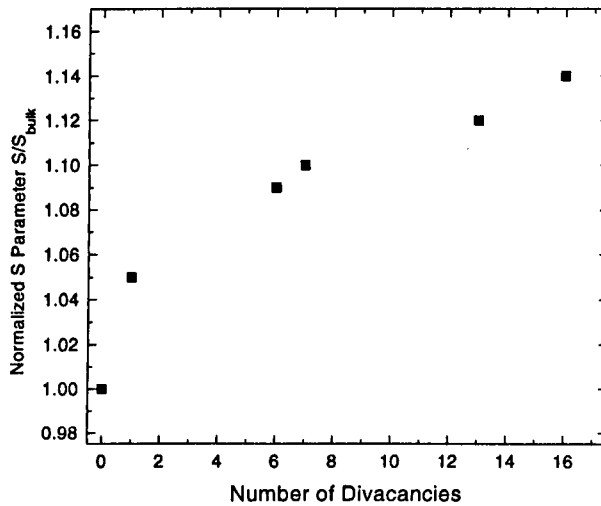


Figure 4.5:1 Normalized S parameter vs. number of agglomerated Silicon Carbide di-vacancies, after reference [26].

The situation is, however, rather different at a laser fluence of 1.3 J cm^{-2} and above where it can be seen there is a large increase in the normalized S parameter. According to Figure 4.5:1 above, a laser fluence of 1.4 J cm^{-2} related to a normalized S parameter between 1.08 - 1.10. This indicates the existence of positron trapping sites and corresponds to about six to eight di-vacancies. Such a high value is suggestive of a decrease in the structural integrity of the material induced by the laser.

Once having obtained the Doppler broadening data it is instructive to determine the concentration of defects and their spatial dependence. Two software packages that are commercially available are VEPFIT [27] and POSTRAP-4 [28]. The former was used to fit the experimental data for an unirradiated (as-received) Silicon Carbide sample, this package assumes a single layer (bulk) structure in order to determine a value for the positron diffusion length. This was calculated and corresponded to a value $\sim 100 \text{ nm}$, hence, using published bulk

Positron Annihilation Studies of Excimer Laser Irradiated 4H-SiC.

lifetime values, equation (4:8) was used to obtain a value for the positron diffusion coefficient. Using this data, POSTRAP-4, could then be used by dividing the sub-surface region into a number of 'slabs' until an acceptable fit to the S(E) data is obtained.

Figure 4.5:3 and Figure 4.5:4 illustrates the plot calculated after using VEPFIT and POSTRAP-4, for the two highest laser fluence irradiated at 308 nm. The results show a buried layer of defects at about 50 nm beneath the surface and consisting of a modified layer ~70 nm thick. The defect layer tends to extend further into the sample when the laser fluence is increased. At a laser fluence of 1.4 J cm^{-2} it was possible to fit the data with three slabs where as at the higher fluence of 1.8 J cm^{-2} four slabs had to be used in order to obtain a similar fit to the data, see Figure 4.5:4.

4.5.2 ArF Laser Irradiated Epitaxial 4H-SiC

For this set of experiments, epitaxial 4H-SiC was irradiated using a ArF laser at 193 nm in vacuum conditions similar as those explained above. A higher vacuum was achieved in this case due to a turbo molecular pump fitted on the system. The samples received 50 laser pulses at a pressure of $\sim 2 \times 10^{-6}$ torr. The thickness of the epitaxial layer was $\sim 3 \mu\text{m}$ which was greater than both the optical absorption and positron implantation depth. Therefore, any defects that may exist at the substrate/epitaxial interface should not confuse the positron results. The data for the samples irradiated at 193 nm is shown in Figure 4.5:5. There is very little correlation of the data with laser fluence, however, the data does indicate that most of the trapping, hence defect structure occurs close to the surface in comparison to the 308nm data. This is in some agreement with the shallow absorption depth ($\sim 10 \text{ nm}$) at 193 nm.

Positron Annihilation Studies of Excimer Laser Irradiated 4H-SiC.

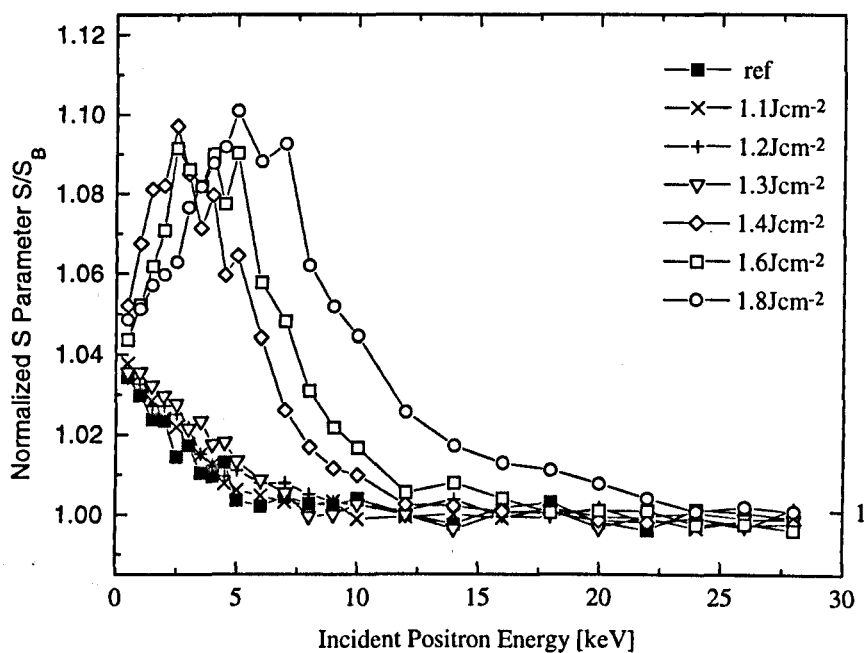


Figure 4.5:2 Positron annihilation Doppler broadening spectra of bulk 4H-SiC laser irradiated using a XeCl excimer laser at 1.1, 1.2, 1.3, 1.4, 1.6 and 1.8 J cm⁻² with 10 pulses at a 1Hz repetition rate.

Positron Annihilation Studies of Excimer Laser Irradiated 4H-SiC.

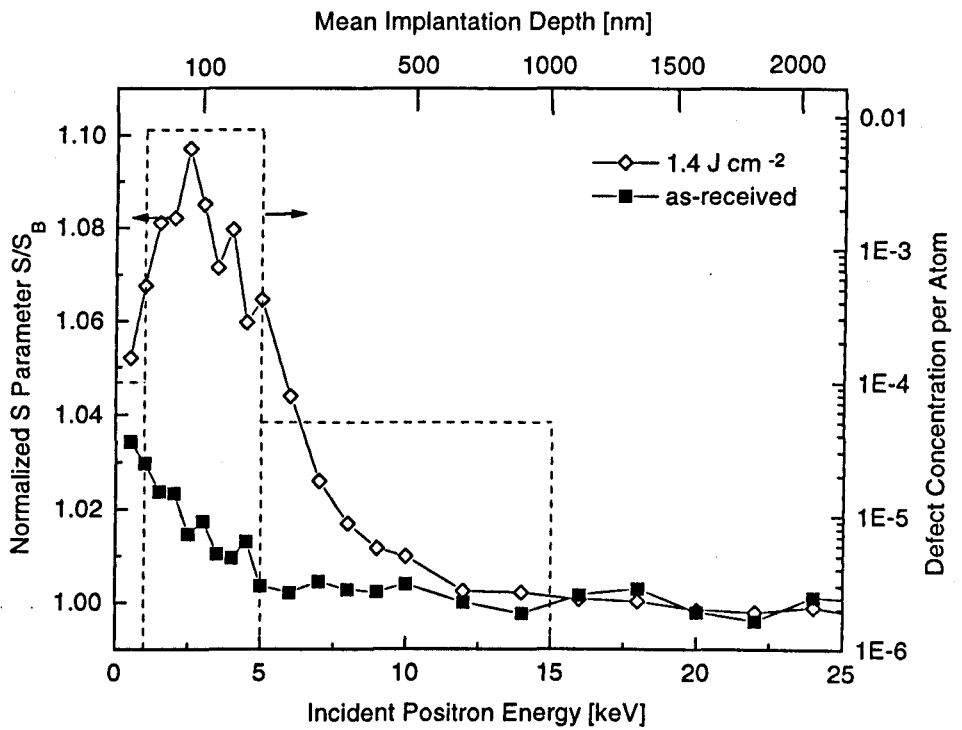


Figure 4.5.3 Positron annihilation Doppler broadening spectra of bulk 4H-SiC laser irradiated using a XeCl excimer laser at 1.4 J cm^{-2} with 10 pulses at a 1Hz repetition rate and contrasted against calculated defect concentration.

Positron Annihilation Studies of Excimer Laser Irradiated 4H-SiC.

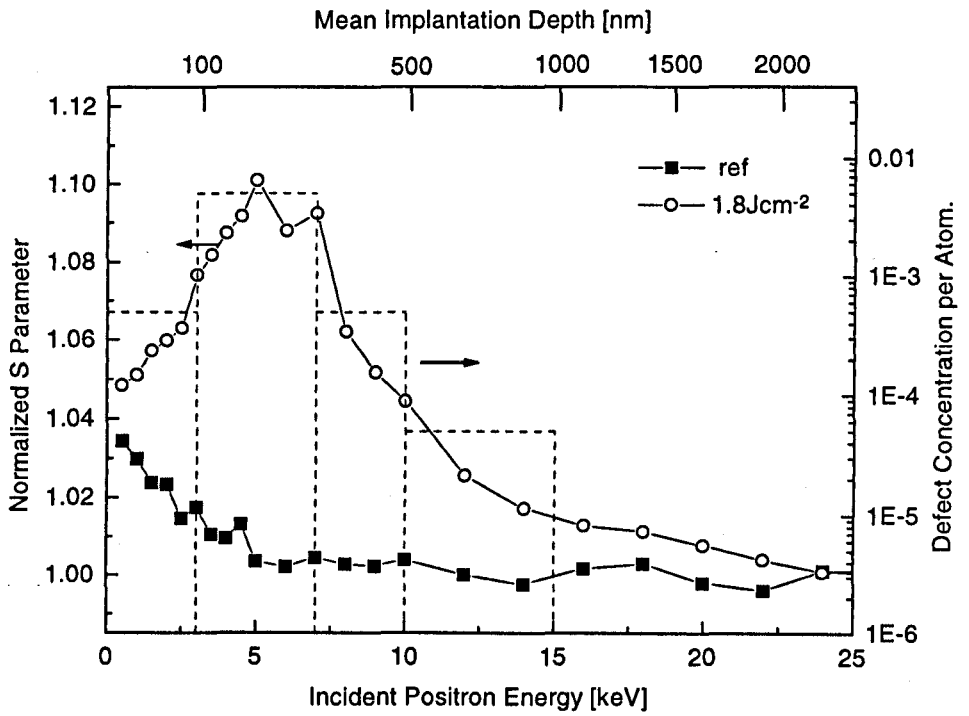


Figure 4.5:4 Positron annihilation Doppler broadening spectra of bulk 4H-SiC laser irradiated using a XeCl excimer laser at 1.8 J cm^{-2} with 10 pulses at a 1Hz repetition rate and contrasted against calculated defect concentration

Positron Annihilation Studies of Excimer Laser Irradiated 4H-SiC.

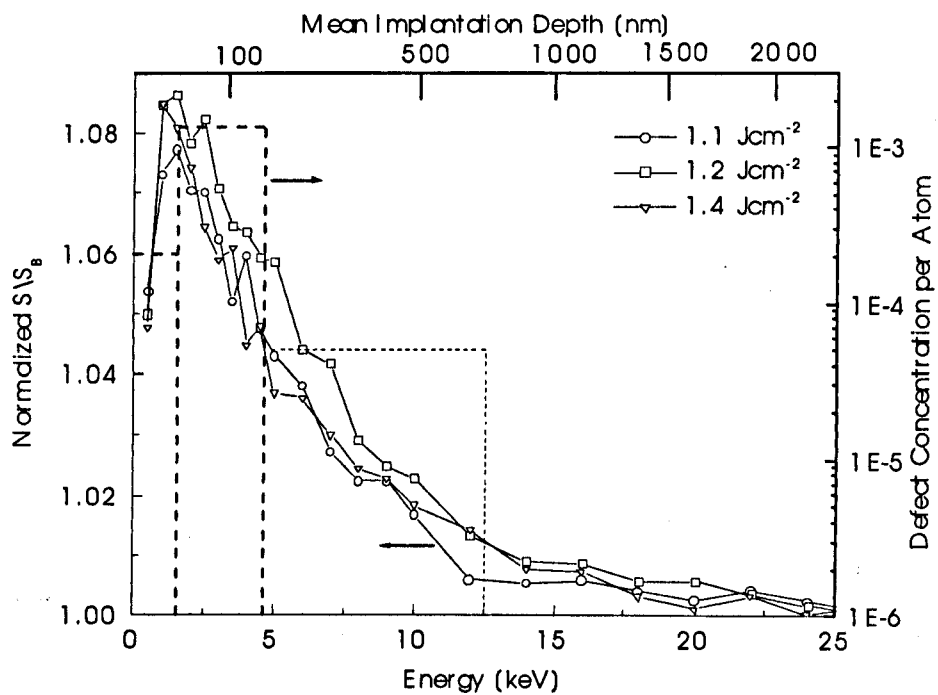


Figure 4.5:5 Positron annihilation Doppler broadening spectra of bulk laser irradiated 4H-SiC, using an ArF excimer laser at 1.1, 1.2 and 1.4 J cm⁻² with 10 pulses at a 1Hz repetition.

4.6 Conclusion

Laser induced damage is seen to occur beneath the surface and shows a wavelength dependency. The depth the damage extends is seen to be greater when irradiated at 308nm when compared with 193nm. Therefore, it is argued that the extent of damage is influenced by the optical absorption depth, a point highlighted in Chapter 2, equation 2:31, and Table 2.3:1.

The increased normalized S parameter corresponding to an increase in the defect concentration is in close agreement to what would be the onset of the ablation/desorption threshold. An increase in the laser fluence will induce a corresponding increase in the surface temperature which could lead to a damage/recovery process to take place close to the surface and therefore cause preferential damage on cooling.

Positron Annihilation experiments on laser irradiated Silicon Carbide has served as a useful diagnostic tool for the detection of defects. It is difficult from the measurements alone to determine the exact mechanisms that might take place subsequent to laser irradiation. However, this will be covered in more depth by combining the previous Photoluminescence work, Chapter 3 and the following Infrared experiments, Chapter 5.

4.7 References

-
- [1] Dirac P. A. M. Proc. Roy. Soc. **117**, 610 (1928).
- [2] G. Pensl, and R. Helbig, in *Advances in Solid State Physics*, edited by U. Rossler **30**, 133 (1990).
- [3] G. Pensl, and W. J. Choyke, *Physica B* **185**, 264 (1993).
- [4] *Positrons in Solid-State Physics. Proceedings of the International School of Physics "Enrico Fermi" Course LXXXIII, Varenna, 1982*, edited by W. Bradt and A. Dupasquier (North Holland, Amsterdam, 1983).
- [5] G. Brauer, W. Anwand, P. G. Coleman, J. Stormer, F. Plazaola, J. M. Cambell, Y. Pacaud, W. Skorupa. *J. Phys. Cond. Mat* **10**, 1147 (1997).
- [6] T. Ohshima, A. Uedono, K. Abe, H. Itoh, Y. Aoki, M. Yoshikawa, *Appl. Phys. A* **67**, 407 (1998).
- [7] M. Foster, W. Claudy, H. Hermes, M. Koch, K. Maier, J. Major, H. Stoll, and H. E. Schaefer. *Mater. Sci. Forum* **105-110**, 1005 (1992).
- [8] A. A. Rempel, and H. E. Schaefer. *Appl. Phys. A* **61**, 51 (1995).
- [9] W. Puff, M. Boumerzoug, J. Brown, P. Mascher, D. Macdonald, P. J. Simpson, A. J. Balogh, H. Hahn, W. Chang, and M. Rose. *Appl. Phys. A* **61**, 55 (1995).
- [10] G Brauer, W. Anwand, P. G. Coleman, A. P. Knights, F. Plazaola, Y. Pacaud, W. Skorupa, J. Stormer, and P. Willutzki. *Physica Review B*. **54**, 3084 (1996).
- [11] A. Uedono, T. Oshima, H. Itoh, R. Suzuki, T. Ohdaira, S. Tangawa, Y. Aoki, M. Yoshikawa, I. Nashiyama, and T. Mikado. *Jpn. J. Appl. Phys.* **37**, 2322 (1998).
- [12] A. Uedono, H. Itoh, T. Oshima, Y. Aoki, M. Yoshikawa, I. Nashiyama, H. Okumura, S. Yoshida, T. Moriya, T. Kawano and S. Tanigawa. *Jpn. J. Appl. Phys.* **35**, 5986 (1996).
- [13] H. Itoh, A. Uedono, T. Okumura and S. Yoshida. *Appl. Physics A*. **65**, 315 (1997).
- [14] H. Itoh, T. Ohsh, Y. Aoki, K. Abe, M. Yoshikawa, I. Nashiyama, H. Okumura, S. Yoshida, A. Uedono and S. Tanigawa. *J. Appl. Phys.* **82**, 5339 (1997).
- [15] A. Kawasuso, H. Itoh, S. Okada, and H. Okumura. *J. Appl. Phys.* **80**, 5639 (1996).
- [16] S. Valkealahti and R. m. Nieman. *Appl. Phys. A*. **32**, 95 (1983).
- [17] T. McMullen, *Positron Annihilation*, Eds., P. C. Jain, R. M. Singru, and K. P. Gopinathan, World Scientific, Singapore, (1985) p. 657.
- [18] M. J Puska, and R. M. Nieminen, *Reviews of Modern Physics*, **66**, 841 (1994).
- [19] S. Dannefaer, W. Puff, and D. Kerr. *Physical Review B* **55** (4), 2182 (1997).
- [20] W. Bauer-Kugelman, G. Kogel, P. Sperr, W. Triftshauser. *Mater. Sci. Forum.* **255-257**, 662 (1997).

Positron Annihilation Studies of Excimer Laser Irradiated 4H-SiC.

-
- [21] C. D. Beling, R. I. Simpson, M. Charlton, F. M. Jakobsen, T. C. Griffith, P. Moriarty, S. Fung. *Appl. Phys A* **42**, 111 (1987).
- [22] G. Brauer, W. Anwand, E. M. Nicht, P. G. Coleman, N. Wagner, H. With, W. Skorupa. *Appl. Surf. Sci.* **116**, 19 (1997).
- [23] J. Stormer, A. Goodyear, W. Anwand, G. Brauer, P. G. Coleman, W. Triftshauser. *J. Phys. Cond. Mat.* **8**, L89 (1996).
- [24] N. B. Chilton, P. G. Coleman, *Meas. Sci. Technol.* **6**, 53 (1995).
- [25] G. Brauer, W. Anwand, E. M. Nicht, J. Kuriplach, M. Sob, N. Wagner, P. G. Coleman, M. J. Puska, and T. Korhonen. *Phys. Rev. B* **54**, 2512 (1996).
- [26] W. Anwand, G. Brauer, P. G. Coleman, W. Skorupa, *MRS Symp Proc.* (1997)
- [27] A. Van. Veen, H. Schut, J. E. de Vries, R. A. Hakvoort, M. R. Ijpa, *Positron Beams for Solids and Surfaces*, in P. J. Schultz, G. R. Massoumi, P. J. Simpson (Eds), *AIP Conf. Proc. No 218*, New York, 1990, p. 171.
- [28] G. C. Aers, *Positron Beams for Solids and Surfaces*, in P. J. Schultz, G. R. Massoumi, P. J. Simpson (Eds), *AIP Conf. Proc. No 218*, New York, 1990, p. 162.

Chapter 5

Excimer Laser Annealing of Ion-Implanted 4H- and 6H-Silicon Carbide

5.1 Introduction.	96
5.2 Lattice Recovery.	98
5.2.1 Ion-Implantation Damage.	98
5.2.2 Pulsed Laser Annealing.	100
Thermal Model	101
Plasma Model	102
5.3 Infrared Reflectivity in Silicon Carbide: The Reststrahlen Band.	104
5.3.1 The Lorentz-Drude Model.	105
5.4 Experimental Procedure.	107
5.4.1 Infrared Measurements.	107
5.4.2 XeCl Excimer Laser Annealing.	108
5.5 Experimental Results:	110
5.5.1 Reflectivity of As-received and Ion-Implanted 4H-SiC	110
5.5.2 Near Normal Reflectivity of Laser Irradiated 4H-SiC	116
5.5.3 Spatial Dispersion Effects of Laser Irradiated 6H-SiC	123
5.5.4 Lorentz-Drude Interpretation of Laser Annealed 4H-SiC	133
5.5.5 Dopant Activation.	143
5.5.6 Structural Modifications of XeCl Laser Annealed 4H-SiC	148
5.6 Conclusion	151
5.7 References.	153

Chapter 5

Excimer Laser Annealing of Ion-Implanted 4H- and 6H-Silicon Carbide

5.1 Introduction.

In Chapters 3 and 4, photoluminescence and positron annihilation techniques were used to measure the presence of any defects that were created subsequent to laser irradiation. In this chapter we take an alternative approach and adopt excimer laser annealing to investigate the feasibility of removing ion implantation damage with the aim of activating implanted nitrogen dopants. Ion implantation doping is an attractive route for elaborating, with a high degree of control, sub-micron p-n junctions for device purposes. One of the associated problems concerning the latter is associated with the high temperatures required in the activation process. At a typical anneal temperature ~ 1700 °C there are several major problems. First, Silicon Carbide begins to decompose at these temperatures [1, 2], and second, masking material used in self-aligned processing for device fabrication cannot with stand these sorts of temperatures [3]. Additionally, there are also problems associated with increased surface roughness and step migration. With respect to the decomposition problems, the surface layer begins to loose silicon and can become enriched with carbon and the surface stoichiometry is severely disrupted, hence, destroying the semiconducting properties [4, 5]. Therefore, there is a need to approach the problem in a way that sufficient energy can be imparted to an ion-implanted crystal without

Excimer Laser Annealing of Ion-Implanted 4H- and 6H-Silicon Carbide

inducing detrimental modification, either to the host/or masking materials. One such approach is to reduce the thermal budget via non-equilibrium techniques. Rapid thermal processing and laser annealing have the advantage of much shorter thermal cycles. The material is at an elevated temperature for a shorter time interval therefore the possibility of the material decomposing is reduced. It has been reported that the p-n junction profile, created using ion implantation was severely disturbed after laser annealing which caused dopants to be swept to the surface [6]. Therefore not only is thermal degradation a severe problem associated with the annealing and activation of Silicon Carbide, but the influence on the internal structure has to be considered if laser annealing is to become a feasible solution.

There are a plethora of measurement techniques available to quantify the effects of annealing. In this work, we adopt infrared reflection spectroscopy to investigate the effects prior and subsequent to excimer laser processing. Fourier Transform infrared (FTIR) reflection spectroscopy is a very powerful non-destructive technique for characterising the surface and subsurface modifications. The infrared measurements have been carried out to investigate the near-surface region of as-received, as-implanted and excimer laser annealed Silicon Carbide. Infrared measurements have been taken in the range, $400 - 7800 \text{ cm}^{-1}$ to assess the effects that excimer laser annealing has on a damaged Silicon Carbide crystal. The ease of the infrared measurements, combined with a minimal amount of required sample preparation, enabled a quick turn-round time, highlighting infrared reflection spectroscopy as a rather efficient measurement technique.

5.2 Lattice Recovery.

5.2.1 Ion-Implantation Damage.

Ion implantation doping is a preferred technique for the selective incorporation of dopant species. It is recognized as the technique that gives precise vertical and lateral incorporation of dopants for making p-n junctions when fabricating Silicon Carbide devices [7]. This is especially true in the case of Silicon Carbide where the thermal diffusion coefficient for nitrogen dopants is extremely small, rendering ion implantation doping the only technologically recognised technique [8, 9]. Two serious problems that accompanies ion-implantation is the damage to the lattice which is imparted by the energetic dopant atoms [10,11,12] and also, the difficulty associated with the electrical activation of the dopant species [13,14], both these drawbacks are recognised within the Silicon Carbide community has being non-trivial. The former is particularly problematic at high implantation doses carried out at room temperature [15,16,17]. Ion beam induced damage from the crystalline phase towards the amorphous phases are of great technological importance in connection with the latter. The degree of lattice damage and the recovery process are dependent on the ion mass, ion flux and the implantation temperature. The current understanding of ion beam-induced damage and recovery processes have recently been reviewed and summarised [18, 19]. In general, the atomic disorder increases sigmoidally with ion fluence (i.e at high ion fluence the damage is so severe that amorphisation takes place and the level of damage no longer increases linearly, but saturates). Also the rate of disordering decreases with irradiation temperature due to a competitive process between damage recovery and damage accumulation. The study of ion-beam irradiation effects and induced defect accumulation in Silicon Carbide has received a great deal of attention, and a fundamental understanding of defect formation and recovery processes are important for the fabrication of electronic devices. Whilst intensive research efforts are currently being

Excimer Laser Annealing of Ion-Implanted 4H- and 6H-Silicon Carbide

undertaken in the understanding of ion-implantation induced defect formation, this work concentrates in parallel with the latter on aspects concerning lattice recovery.

One of the advantages that Silicon Carbide has to offer is the stability at high temperatures and in high radiation environments. Unfortunately, the very nature of the thermal stability that makes Silicon Carbide such a promising high temperature device material becomes a disadvantage at the post implantation annealing stage. As a consequence, any lattice defects or defect complexes present are also extremely stable, hence, are very difficult to anneal-out. However, the surge in demand for high temperature electronics has provided encouragement and driven research activity in this area [20]. Post-implantation annealing at high temperatures to remove such defects has been conducted using various energetic sources outlined in the introduction. We therefore discuss briefly some of the alternative methods that have been investigated within the Silicon Carbide community and then move onto the method that is adopted in this thesis, that being, pulsed excimer laser annealing at 308 nm.

There are of course alternative ways of annealing and selectively activating implanted material and some of the various ways are listed below. One such process is Ion-beam-Induced Epitaxial Crystallization (IBIEC). The latter has been carried out on amorphous layers on top of single crystalline silicon carbide substrates to induce epitaxial growth [21, 22]. Rapid thermal annealing has been utilized for activation purposes with some degree of success, however, the technique is still far from maturity. Thermal annealing and rapid thermal annealing of Silicon Carbide are especially problematic for the removal of ion-implantation induced damage and activation due to the aforementioned decomposition problems.

5.2.2 Pulsed Laser Annealing.

The successful application of high intensity laser pulses in the restoration of disturbed semiconductors has given rise to new technological advancements and opened up novel routes in material processing. Because of the advent of energetic sources such as excimer lamps and ion beams e.t.c, laser annealing can be more precisely referred to as 'pulsed laser' annealing, with the addition of an identifier associated with the source it self, i.e. 'pulsed lamp', or 'pulsed ion beam' annealing. Annealing⁹, however, goes back many years and is particularly relevant to metals having developed stress during processing. In this work, we are concerned with annealing silicon carbide that has been disturbed by nitrogen ion-implantation. The severity of the disordering in the Silicon Carbide is dependent on the implantation dose, which was in the range 1×10^{14} - 3×10^{15} cm⁻². In the context of this thesis, we refer to annealing when we are concerned with the re-ordering of the lattice atoms in an attempt to remove any unwanted crystal imperfections such as dislocations, interstitial and antisite defects. Thus, in an actual material, when impurity species have been introduced for doping purposes, the intention is to reduce any internal stresses and remove unwanted defects whilst improving the translational symmetry of the crystal lattice.

Some of the earliest work on pulsed laser annealing was undertaken on ion beam disrupted semiconductors [23, 24]. Pulsed laser annealing became very promising when it was found that the electrical conductance subsequent to laser annealing was higher in comparison to more conventional thermal anneals. One of the most significant differences between thermal and pulse laser annealing is in the duration of the excitation cycle. Typically, furnace anneals can be ~ hours, whilst in pulsed laser annealing it is nano-seconds. In a similar manner, the duration and energy density of a laser pulse delineates two different models that can be used in

⁹ The word anneal stems from an Old English word, '*onaelan*' meaning 'aelan': to burn, 'al': from fire.

Excimer Laser Annealing of Ion-Implanted 4H- and 6H-Silicon Carbide

explaining the annealing phenomena. Namely, the ‘thermal’ model (melting) and the ‘plasma’ model (long-lived, ~100ns, electron-hole plasma).

Thermal Model

The absorption and reflection of optical radiation are the key moments in laser annealing. In a “semiconducting” mechanism, i.e., when the photon energy is greater than the bandgap energy, $h\nu > E_g$, the equilibrium density of free carriers is low, and the non-radiative transition time is short and fundamental absorption takes place. The efficiency of the energy transfer process is described by the reflection coefficient, equation (2:29) and the absorption coefficient, equation (2:31), which depend on several factors including the optical wavelength and the structure of the material. As a result of the optical absorption, the light pulse is absorbed practically instantaneously to the electron subsystem, by heating of free carriers, generation of non-equilibrium electron-hole pairs, and heating of these pairs. The main channel for the relaxation of hot carriers occurs through electron-phonon interactions. The phonon relaxation times are typically pico seconds and effectively the energy of the photon is transferred almost instantaneously to the lattice where it was absorbed. The lattice is therefore in thermal equilibrium with the pulse and the lattice temperature essentially follows the laser pulse. This results in a very rapid heating of the surface (10^{10} K s^{-1}) having little effect below the skin depth. Therefore the conditions become favourable for local thermal annealing at temperatures less than the melt temperature, $T < T_m$ in the case of solid state crystallisation or, $T > T_m$ for liquid phase epitaxial regrowth, the latter predominates when the laser fluence is high enough such that $T > T_m$. The thermal mechanism accounts well for most experimental results on laser annealing, however there are some results that cannot be accounted for. This generated much debate and the search for other possible mechanisms to explain similar experimental findings, therefore a brief explanation of one such model is discussed below.

Plasma Model

Under the action of very high powered lasers, (typically > Giga Watts), with pulse duration's of nano and pico second or shorter, electron-hole plasmas can be produced. In some of the very first experiments using nanosecond lasers it was found that certain features did not agree with a thermal model. E.g., Silicon can be re-crystallised over the duration of a typical nano second pulse and during this time the reflection coefficient has been reported to be less than that of molten silicon. A plasma model developed by Van Vechten [25] was proposed based on the observed differences in reflectivity and annealing dependencies on ionising radiation when compared with thermal annealing. Briefly, the action of a relatively short laser pulse (10^{-8} – 10^{-7} sec) with a photon energy higher than the bandgap energy of the semiconductor in question, $E_{hv} > E_g$, a dense ($\sim 10^{21}$ cm⁻³), long-lived electron-hole plasma (~ 100 ns) is generated. According to the thermal model the presence of an electron hole plasma can weaken the covalent bonds such that they can no longer stabilise the phonon modes. In the limit when the crystal can no longer stabilise the phonon modes (remain in the solid state), the structure could in essence be referred to as a 'liquid'. However, the liquid state generated through the 'plasma' mechanism is different from that of a thermally generated liquid in equilibrium, i.e. the 'thermal' mechanism. In the former, the energy is imparted as electronic excitations, whereas in the latter it is thought to occur via kinetic vibrations of lattice atoms at the melting point. In the case of the plasma model, the annealing process can be regarded as a second-order phase transition which can result in a reversible phase transition to a covalently-bound phase without the catastrophic influence of strong thermal gradients. An alternative plasma model can be described as follows: a dense-electron-hole plasma can neutralize Coulomb defect capture centres in a disordered layer, caused by implantation damage, thus stimulating the diffusion of defects and impurities. Thus, referring back to Chapter 3, the diffusion coefficients of vacancies and other defects can rise by several orders of magnitude.

Excimer Laser Annealing of Ion-Implanted 4H- and 6H-Silicon Carbide

The hypothesis of various laser annealing models, and especially that of a long lived plasma has brought about a great deal of objections and criticisms from many specialists. The brief discussion on just two mechanisms associated with pulsed laser annealing as been included only to illustrate the complexities that are involved. Complete explanations are far from being completely understood. In both laser models, the thermal and plasma models involve the interaction of a photon with matter and a deeper understanding could be obtained with the application of quantum electro dynamics, however, this thesis, fortunately, is more concerned with the practicalities of the annealing process and the brief background was introduced in preparation for the discussion in Chapter 6.

Although there is great deal of interest in laser annealing on the materials Si and GaAs, very little work existed at this time on laser annealing of Silicon Carbide. In the time since the experimental work described in this thesis was completed two relevant papers were published on recrystallisation of 6H-SiC [26,27]. The authors investigated the possibility of recrystallising ion-implanted material and also the suppression of implantation damage by simultaneously annealing during implantation. Unlike this work the authors used a large number of pulses, typically 100's of thousands.

Also pertinent to this work was that carried out by Ohyama *et-al* [28] who used a Free Electron Laser (FEL) in order to anneal and activate implanted material and that of Makarov *et-al* [29] using a CO₂ laser. The work is particularly appropriate when pieced together from the point of view of achieving activation and recrystallisation by annealing in the infrared. Both workers, be it some time apart, used the idea of residual ray absorption in the infrared to directly excite the crystal lattice on 3C- and 6H-SiC.

5.3 Infrared Reflectivity in Silicon Carbide: The Reststrahlen Band.

Reflectivity is a very important effect and can provide a wealth of information on the optical properties of a solid. Many solids possess strong absorption in the infrared part of the electromagnetic spectrum which is in turn associated with high reflection. Nearly a century ago Rubens and Nichols discovered in alkali halides a band of almost total reflection [30]. The band of high reflection, the so called Reststrahlen band, (a German term having the meaning, *residual* or *remaining* rays), spans the region between the transverse optical (TO) and longitudinal optical (LO) phonons modes with a reflectivity very close to 100%. In the case of Silicon Carbide, the phonon modes (TO $\sim 797 \text{ cm}^{-1}$ and LO $\sim 987 \text{ cm}^{-1}$) are so distinct, the reflectivity spectra have been used in classical examples of dispersion analysis for the determination of optical constants.

The mid and far infra red spectra of doped semiconductors are often dominated by free carrier optical absorption. Because of the direct dependence of the absorption on carrier density it is possible to determine the bulk carrier densities using transmission and reflection spectroscopy [31]. If the bulk is stratified, i.e. the carrier concentration varies with depth, the optical properties will also change with depth. The thickness of can still however be however be determined with reasonable confidence via multi layer optical models [32]. Polarized infrared reflection spectroscopy has been used to study the crystallographic structural modifications subsequent to ion beam bombardment. [33,34] In this work we utilise the reflectivity spectra in the Reststrahlen region to investigate the effects of excimer laser annealing of Silicon Carbide.

5.3.1 The Lorentz-Drude Model.

The Lorentz-Drude model can be used to account for much of the optical-phonon structure in polar semiconductors. In this thesis I adopt the model to extract information from the reflectivity spectra to obtain information on the crystal quality before and after excimer laser annealing.

In Chapter 2 equation (2:25), it was stated the complex refractive index was shown to be related to the dielectric function. In the case of normal incidence the complex refractive index, N , is correlated with the dielectric function by

$$N = n + ik = \sqrt{\epsilon} = \sqrt{(\epsilon_1^2 + \epsilon_2^2)} \quad (5:1)$$

which leads to

$$\epsilon_1 = n^2 - k^2 \quad \text{and} \quad \epsilon_2 = 2nk \quad (5:2)$$

or

$$n = \left[\frac{1}{2} \left(\epsilon_1 + \left(\sqrt{\epsilon_1^2 + \epsilon_2^2} \right) \right) \right]^{\frac{1}{2}} \quad \text{and} \quad k = \left[\frac{1}{2} \left(\sqrt{\epsilon_1^2 + \epsilon_2^2} \right) - \epsilon_1 \right]^{\frac{1}{2}} \quad (5:3)$$

The dielectric function can be used to describe the response of a crystal to an electromagnetic field. This can be calculated using the harmonic oscillator approximation where the response to the electric field is represented by a linear differential equation of motion for harmonic oscillators. This leads to a superposition of the following three terms to the dielectric function:

$$\epsilon(\omega) = (n + ik)^2 = \epsilon_\infty - \frac{\omega_p^2}{\omega^2 + i\omega\gamma} + \frac{s\Omega_o^2}{\Omega_o^2 - \omega^2 - i\omega\Gamma} \quad (5:4)$$

Excimer Laser Annealing of Ion-Implanted 4H- and 6H-Silicon Carbide

where ϵ_∞ is independent of frequency and describes harmonic oscillators with eigenfrequencies much larger than ω . This term represents the contributions of electronic interband transitions to $\epsilon(\omega)$ at infrared frequencies. Secondly, the Drude term, represents the free carriers and describes harmonic oscillators with eigenfrequencies equal to zero. Here ω_p is the plasma frequency and is given as

$$\omega_p^2 = \frac{ne^2}{\epsilon_0 m^*} \quad (5:5)$$

In addition, γ is the damping constant and is given as

$$\gamma = \frac{e}{\mu m^*} \quad (5:6)$$

where μ is the mobility and m^* is the carrier effective mass.

The last term in equation (5:4) describes the phonon contribution to ϵ with eigenfrequencies Ω_0 , where, s , is the oscillator strength and Γ is the phonon damping constant.

Equation (5:4) can be written using the Lyddane-Sachs-Teller relation [35] :

$$\epsilon(\omega) = \epsilon_\infty \frac{\Omega_{LO}^2 - \omega^2}{\Omega_{TO}^2 - \omega^2} \quad (5:7)$$

which gives:

$$\epsilon(\omega) = (n + ik)^2 = \epsilon_\infty - \frac{\omega_p^2}{\omega^2 + i\omega\gamma} + \frac{\epsilon_\infty(\Omega_{LO}^2 - \Omega_{TO}^2)}{\Omega_{TO}^2 - \omega^2 - i\omega\Gamma} \quad (5:8)$$

where Ω_{LO} and Ω_{TO} are the longitudinal and transverse optical phonons respectively.

Excimer Laser Annealing of Ion-Implanted 4H- and 6H-Silicon Carbide

The Lorentz-Drude (L-D) oscillator Model can be regarded as a textbook example concerning the modelling of infrared reflection spectra of bulk and thin film samples. It has been successfully used to analyse experimental results to determine the thickness of epitaxial films on Silicon Carbide substrates [32,36], to infer the carrier concentration, their mobilities and the crystallinity of a material.

With reference to equation (5:8), the phonon damping constant, Γ , the plasma frequency ω_p , and the free carrier damping constant, γ , are of particular interest since they can be taken as a measure of the crystallinity, carrier concentration and mobility respectively. In this work, the phonon damping constant is of especial interest and will be used to gauge crystallinity subsequent to laser annealing. The phonon damping constant is inversely proportional to the phonon lifetime and is an 'ad-hoc' introduced parameter, where, in a perfect crystal reflects the anharmonicity of the potential curve. On one hand the phonon lifetime is limited by coupling processes, opening dissipation channels, and on the other hand, phonons are scattered by defects.. Typical values for high quality material range between 1-3 cm^{-1} in bulk and Chemical vapour Deposited (CVD) material [37,38], about 5 cm^{-1} in Molecular Beam Epitaxy (MBE) [36,39] and by laser polycrystalline layers have been produced for instance by sputtering and laser ablation having constants of several 10 cm^{-1} , [40]. In severe cases when crystalline material has been transformed to an amorphous state by ion implantation the L-D model has described the phonon spectra with very large damping constants of about 200 cm^{-1} [41].

5.4 Experimental Procedure.

5.4.1 Infrared Measurements.

Infrared measurements were conducted at room temperature using a Perkin-Elmer Paragon 1000 FTIR spectrometer, see Figure 5.4:1 below.

Excimer Laser Annealing of Ion-Implanted 4H- and 6H-Silicon Carbide



Figure 5.4:1 Fourier transform infrared spectrometer used in these experiments.

Briefly the beam is split into two, one of the beams has a known optical path length and the length of the other is dependent on the sample being measured. The direct output is an interferogram, which is a plot of the intensity vs. the optical path difference. A Fourier transform of the interferogram produces a spectrum of the light intensity vs. energy (or wavelength). Absolute measurements are obtained by taking a sample spectra and correcting this with the measured background spectrum. The sample beam was normalized to the background beam spectrum using a calibrated reference surface, in this case using a gold reference reflector. In essence, the reflectance spectrum that is obtained from the sample *surface* contains information about optical properties. Any changes that are observed subsequent to laser irradiation can then be used to correlate the laser annealing process parameters.

5.4.2 XeCl Excimer Laser Annealing.

The XeCl excimer laser described in Chapter 2 was also used for this work and therefore the beam characteristics are referred back to this chapter. However the annealing work and beam

Excimer Laser Annealing of Ion-Implanted 4H- and 6H-Silicon Carbide

delivery system were arranged differently and are therefore briefly described. Because Silicon Carbide is reported not to melt under thermal equilibrium conditions a pressure chamber was built to sustain a 35 bar argon over pressure. A 25mm diameter by 10mm thick quartz window with a transmission of ~95% at 308 nm was used as the entrance aperture. The samples were positioned onto their front face first so samples of different thickness would always remain in the image plain. A portion of the Excimer beam was selected using a 10mm ×10mm mask which was imaged onto the target firstly through a spherical lens and then onto a cylindrical lens. Thus the beam could be demagnified and also folded in the horizontal plane to produce an object image of dimensions 250 μm wide by 7 mm high. The chamber was attached to a horizontal translational stage which could then be scanned through the rectangular beam to achieve relatively large area sites for electrical measurements. See Figure below.

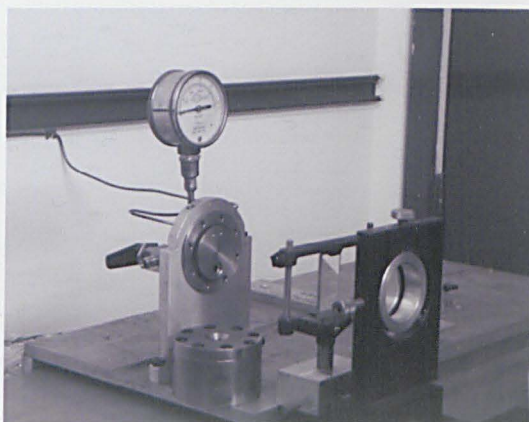


Figure 5.4:2 Pressure chamber (35 bar) and lens arrangement used to carry out the laser annealing experiments.

5.5 Experimental Results:

5.5.1 Reflectivity of As-received and Ion-Implanted 4H-SiC

Infrared experiments have been made on as-grown samples as well as measurements on bulk and epitaxial implanted material. The implanted samples were all implanted with the same dopant, nitrogen, but in some cases at different implantation temperatures and energies. As with the un-implanted material the samples appeared transparent in the visible with a colour depending on the polarity and dopant concentrations. The epitaxial samples appeared darker than the bulk samples and the implanted material became more opaque with increasing implantation dose, see Tables 5.5:1 and 5.5:2 for the un-implanted reference and implanted sample specifications.

Sample Number	Wafer Polarity	Growth Process	Concentration [cm^{-3}]	Orientation
#1	p-type	CVD	1.4×10^{17}	8° off axis
#7	n-type/SiO ₂	Epitaxial	2.0×10^{18}	8° off axis
#9	n-type	Boule	2.0×10^{18}	on axis

Table 5.5:1 As-received SiC sample specifications.

Excimer Laser Annealing of Ion-Implanted 4H- and 6H-Silicon Carbide

Sample Number	Wafer Polarity	Implantation Energy [keV]	Implantation Dose [cm ⁻²]	Implantation Temperature [K]
#2	4H-Epitaxial p-type	20, 40, 60	1×10^{15}	880
#3	4H-Bulk p-type	30, 80, 140	1×10^{14}	RT
#4	4H-Bulk p-type	30, 80, 140	3×10^{14}	RT
#5	4H-Bulk p-type	30, 80, 140	1×10^{15}	RT
#6	4H-Bulk p-type	30, 80, 140	3×10^{15}	RT
#8	6H-Epitaxial p-type	20,50,80,140	2×10^{15}	RT

Table 5.5:2 Ion implanted specifications for 4H and 6H-Silicon Carbide.

The ion implantation was carried out at DERA Malvern, for samples #3, #4, #5 and #6. Sample #4 was capped with ~200 nm of Si₃N₄ to help prevent loss of material during excimer laser annealing. Samples #3, #4 #5 and #6 were implanted at three implantation energies in order to obtain a quasi-square dopant profile using the implant recipe taken from similar work by Kimoto *et-al* [14].

Depth profile calculations of implanted nitrogen ions were made using the software package, TRIM (Transport of atoms in Matter) [42]. The implantation profile for the low dose implant, sample #3, is shown in Figure 5.5:1. The quasi square profile has been achieved by a triple implant. The lower dopant concentration at the surface allows for slight dopant redistribution that can occur whilst laser annealing.

Excimer Laser Annealing of Ion-Implanted 4H- and 6H-Silicon Carbide

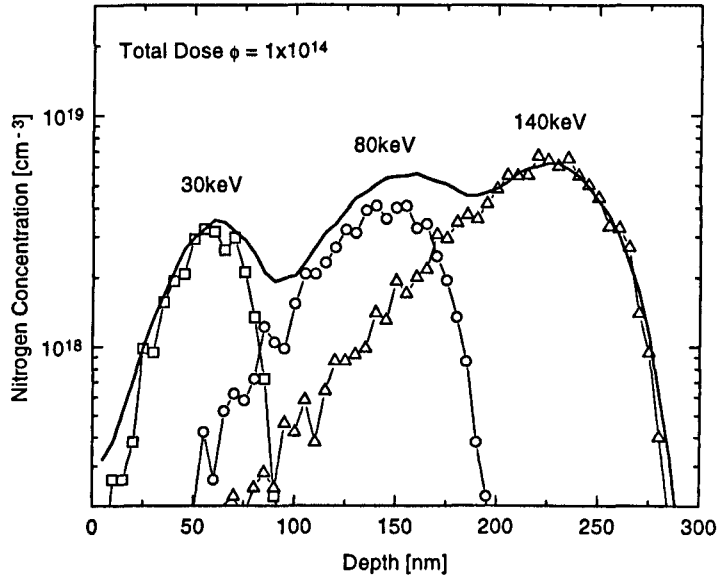


Figure 5.5:1 Simulated depth profile using TRIM (Transport of atoms in Matter) of ion implanted 4H-SiC, sample #3.

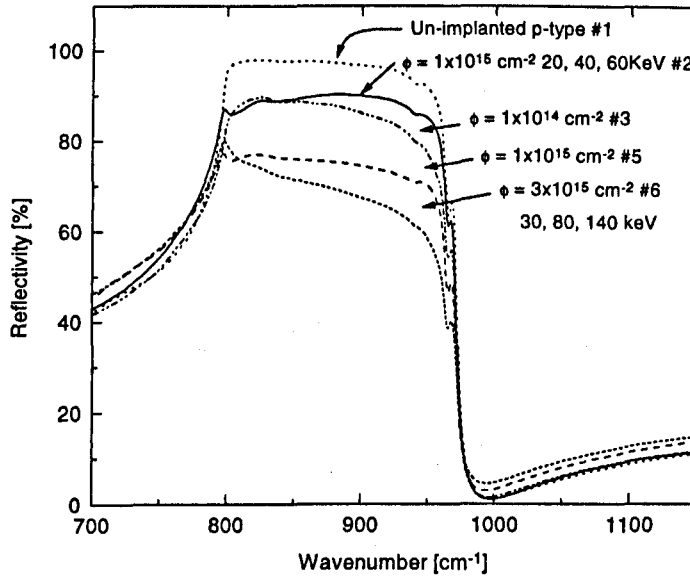


Figure 5.5:2 FTIR reflection spectra for as-grown and ion implanted 4H-SiC for a range of ion doses. Also shown is a sample implanted at a temperature of 880 K, see Table 5.5:2.

Excimer Laser Annealing of Ion-Implanted 4H- and 6H-Silicon Carbide

Figure 5.5:2 shows the infrared reflection spectra at near normal incidence for samples #1,2,3,5, and #6. Sample #1, bulk Silicon Carbide, has the highest reflectivity in the Reststrahlen region which is very close to 100%. The high degree of reflectivity is indicative of a high quality surface. Ion implantation doping causes lattice damage through collision processes [43, 44]. As can be seen in the reflectivity decreases with increasing implantation dose, thus further suggesting an increase in surface damage. Sample #2 was implanted at an elevated temperature of 850K in an attempt to reduce the amount of implantation damage. Increasing the implant temperature is known to reduce such damage in Silicon Carbide [45,46,47] and in many other semiconductors.

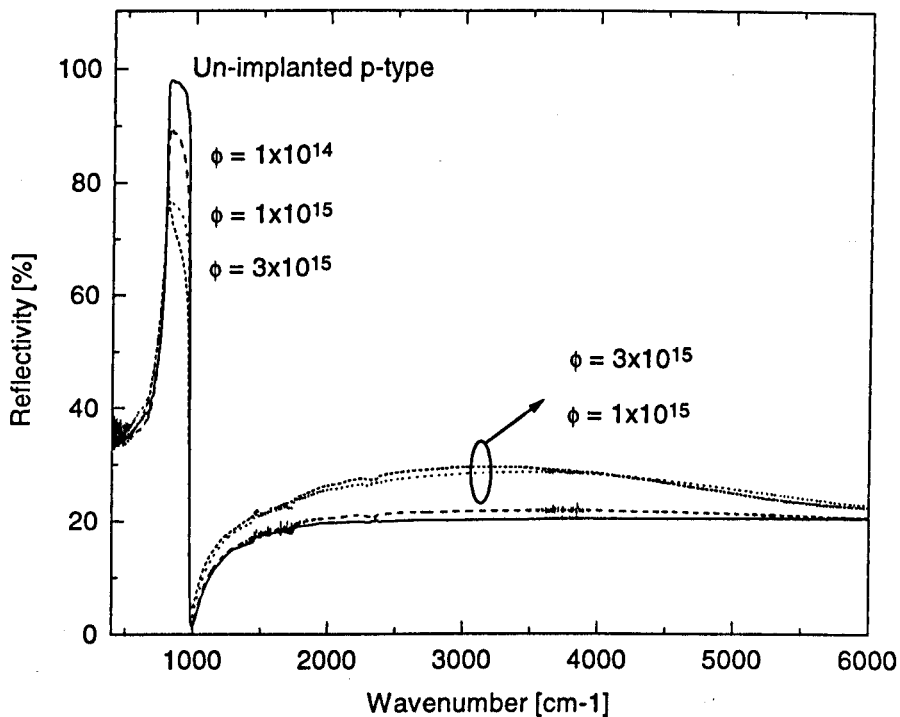


Figure 5.5:3 Broad Band Infrared spectra of ion-implanted 4H-SiC for an un-implanted and three implanted samples, 1×10^{14} , 3×10^{14} , 1×10^{15} , cm^{-2} . Note: oscillations are indicative of layered structures with different optical properties.

Excimer Laser Annealing of Ion-Implanted 4H- and 6H-Silicon Carbide

Although the reflectivity of sample #2 indicates a high surface quality, i.e, reduced damage/improved reflectivity, it is difficult to determine whether this was due partly to the implantation taking place at an elevated temperature and/or at different implantation doses. The same data is shown in Figure 5.5:3, so to illustrate the oscillatory nature at high wavenumbers where a significant change can be seen for the higher implant doses (i.e. 1×10^{15} - 3×10^{15} cm⁻²). Similar effects can be seen for the Si₃N₄ capped Silicon Carbide, Figure 5.5:4. Capping of host material is employed to prevent loss of the host material whilst annealing. Temperatures in the range of 1400 to 1600 °C are required for the activation process to begin, however, at these temperatures the preferential evaporation rate of silicon is high enough to destroy the surface quality [48], [49]. Moreover, the silicon vacancies created by this process can enhance the diffusion rates (analogous to Chapter 3) near the surface. The latter effect has been used to explain the different results on the effects of annealing time [50]. The associated problems with the high vapour pressure of silicon also occur in the encapsulate. Quite recently an aluminium nitride (AlN) capping layer grown by pulsed laser deposition (PLD) was used. Unfortunately a considerable atomic movement occurred and holes can form if there is a variation in film thickness [51].

Excimer Laser Annealing of Ion-Implanted 4H- and 6H-Silicon Carbide

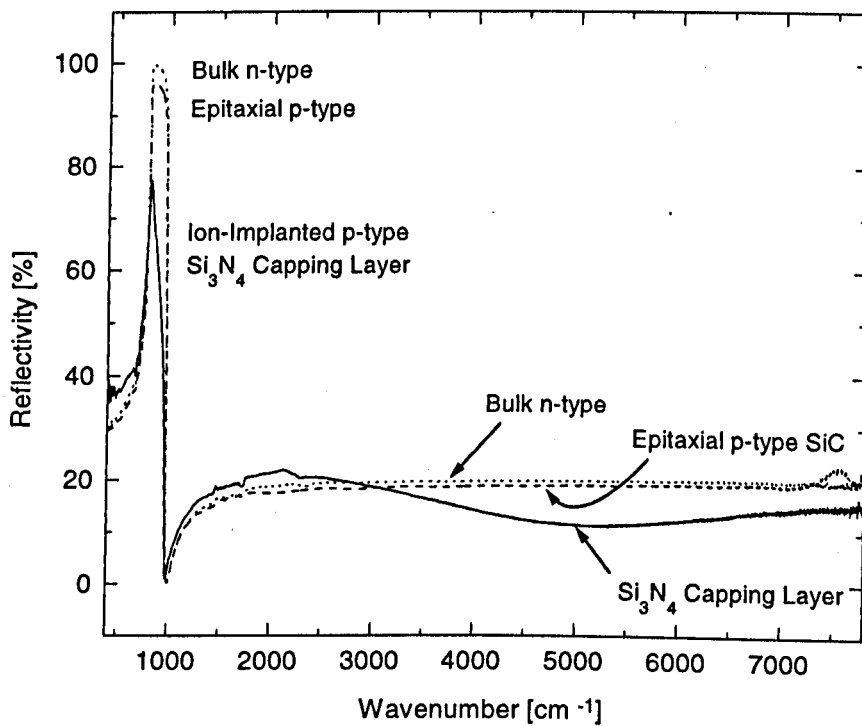


Figure 5.5:4 Infrared reflection spectra for bulk n-type, epitaxial p-type and silicon nitride capped 4H-SiC.

Excimer Laser Annealing of Ion-Implanted 4H- and 6H-Silicon Carbide

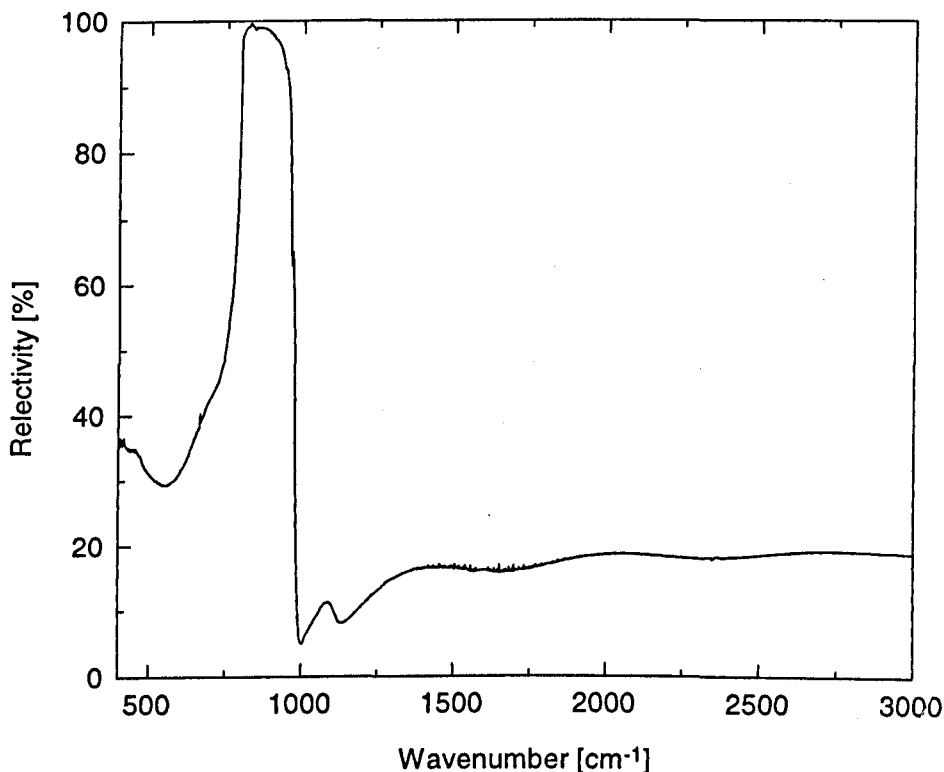


Figure 5.5:5 Infrared reflection spectra of 4H-SiC with a 200nm silicon dioxide layer deposited on top.

During annealing there is the possibility of contamination with ambient gases. Sample #7, was coated with 200nm of SiO₂. The infrared spectra is shown in Figure 5.5:5, with the characteristic oxygen peak at 1090 cm⁻¹.

5.5.2 Near Normal Reflectivity of Laser Irradiated 4H-SiC

In order to investigate the optimum conditions for lattice recovery and activation, Nitrogen implanted 4H-SiC, samples #3, 4 and #5 were irradiated at 308 nm. From each quartered wafer it was possible to irradiate seven 5 × 5 mm sites. The sites were quite large so that electrical measurements could be carried out later to measure level of activation subsequent to the laser

Excimer Laser Annealing of Ion-Implanted 4H- and 6H-Silicon Carbide

annealing. Experimental parameters, laser fluence, pulse number were chosen to try obtain the most information for each of the three samples. The irradiated sites were measured in the infrared at near normal incidence with an incident angle of 16 degrees.

The infrared reflection spectra for the lightly doped sample, #3, is shown in Figure 5.5:6 and Figure 5.5:7. The laser fluence was ranged between 1.0 and 1.3 J cm⁻² using five overlapping laser pulses. The Reststrahlen spectra in Figure 5.5:6, illustrates how the peak reflectivity has been recovered very close to an un-implanted, as-received reference sample. This occurred at 1.0 J cm⁻² using 5 laser pulses. As the laser fluence was increased the reflectivity was seen to decrease such that the highest laser fluence of 1.3 J cm⁻² caused the reflectivity to drop below that of the as-implanted value. Figure 5.5:7 shows a broad band spectra for the same set of results between 1000 and 6000 cm⁻¹. At the highest laser fluence, 1.3 J cm⁻², the reflectivity, when compared with the lower laser fluence, has increased, over this spectral range and outside the Reststrahlen region the reflectivity is seen to maximise at ~3000 cm⁻¹. The 'oscillation' is similar to that seen in the as-implanted material ($\phi = 1 \times 10^{15}$ & 3×10^{15} cm⁻²), samples #5 and #6. Figure 5.5:3, and the Si₃N₄ capped sample, #4. Oscillations of this nature are caused by thin film effects where the optical properties are different between layers. In the case of the Si₃N₄ capped layer, the oscillation is induced due to the different optical properties of dielectric layer, whereas, the thin layer effect in the implanted samples are due to a damaged implanted region affecting the optical resonance. Therefore, it is highly likely that the oscillation induced at 1.3 J cm⁻², has been caused also by some form of surface/subsurface damage.

Very similar results are illustrated in Figure 5.5:8 and Figure 5.5:9, here the heaviest implantation dose, sample #6, was irradiated with ten and fifteen laser pulses between 0.9 and 1.2 J cm⁻². The same trend on peak reflection can be seen as just mentioned, but with a very subtle difference for which the peak reflectivity in the Reststrahlen region occurs at 0.9 J cm⁻². One of the main differences between the lightly and heavily doped samples is the degree of

Excimer Laser Annealing of Ion-Implanted 4H- and 6H-Silicon Carbide

recovery evident in the peak reflectivity. For the low doped sample the maximum reflectivity is ~98% and with the more damaged, heavily dose sample the reflectivity maximum is ~84 %. The lattice recovery dependency on pulse number between these samples, which only covered 5, 10 and 15 pulses, was minimal.

Figure 5.5:10, shows the Reststrahlen spectra as a function of pulse number for sample #4. Here a dependency on pulse number was observed albeit at a somewhat higher laser fluence. This result combined with the recovery/damage dependence on laser fluence suggests that there might be a trade off between the two experimental parameters for the most beneficial result in terms of lattice recovery/activation.

The initial set of experiments in this chapter did not illustrate completely the laser fluence required for maximum lattice recovery. The lowest fluence was 0.9 and 1.0 J cm⁻² for the high and low implantation dose respectively. Investigations were made to establish the maximum reflectivity, hence recovery, over a wider range of laser fluence. Figure 5.5:9 and Figure 5.5:10 illustrates the Reststrahlen reflectivity for a laser irradiated 4H-epitaxial sample, #2. The results suggest that the maximum reflectivity is optimised between 0.9 and 1.0 J cm⁻² which was consistent with our other results. The changes in reflectivity were quite small and to have some degree of confidence, the stability of the spectrometer was measured. The interferometers are always left switched on to ensure temperature instabilities are kept to a minimum. Two scans were taken, one at the beginning of the experiment and another at the end to ensure the small changes in reflectivity were not due to systematic errors. Each set of scans, were taken between 400 and 7800 cm⁻¹, with 64 measurement per scan with a resolution set at 1 cm⁻¹ and were taken ~ 30 minutes apart. From these measurements the trend in results remained unchanged and were repeatable within ±0.5 %. The results therefore indicated an optimum recovery occurring between 0.9 and 1.0 J cm⁻² when irradiated at 308 nm.

Excimer Laser Annealing of Ion-Implanted 4H- and 6H-Silicon Carbide

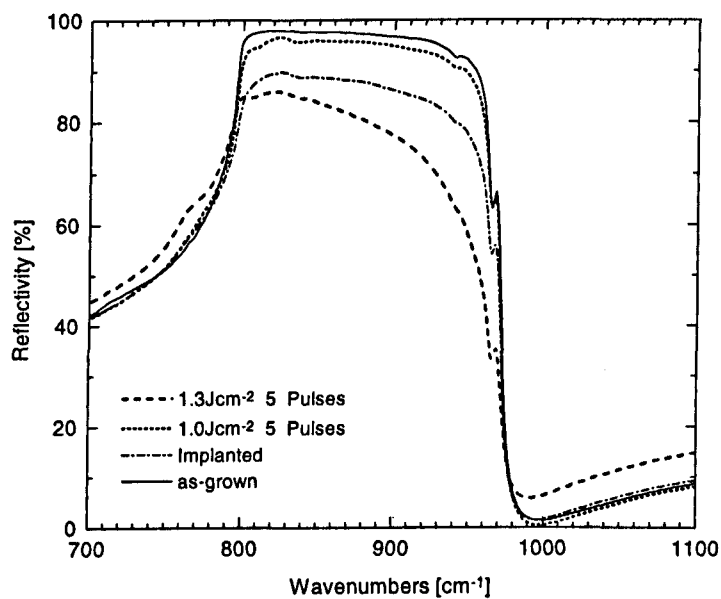


Figure 5.5:6 Infrared reflection spectra in the Reststrahlen region of excimer laser annealed 4H-SiC. Samples were laser annealed at 1.0 and 1.3 J cm⁻² with 5 pulses, sample #3.

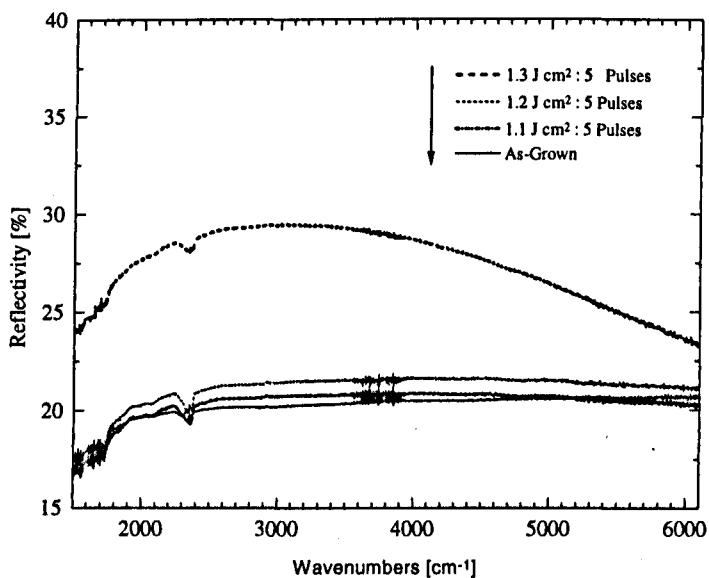


Figure 5.5:7 Infrared reflection spectra of excimer laser annealed 4H-SiC indicating oscillations induced by damage to the surface region, sample #3.

Excimer Laser Annealing of Ion-Implanted 4H- and 6H-Silicon Carbide

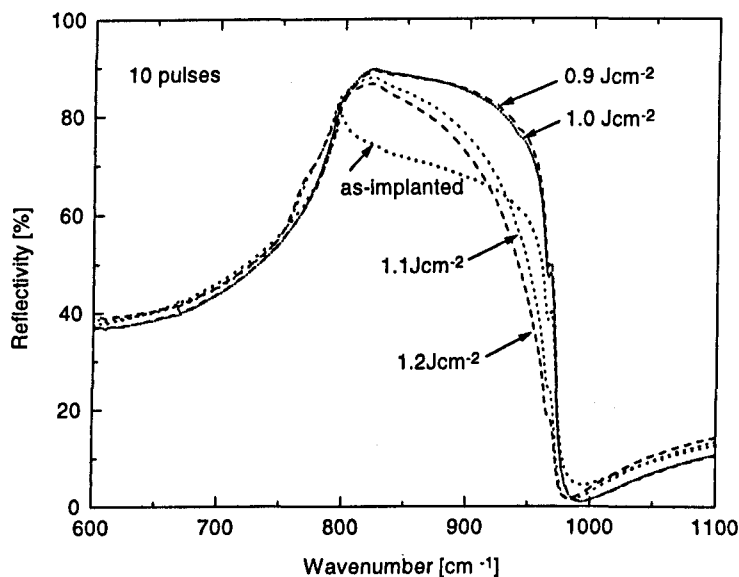


Figure 5.5:8 Infrared reflection spectra of ion implanted and laser annealed 4H-SiC. Laser annealed using 10 laser pulses. The IR measurements were undertaken using unpolarised light. Sample #6.

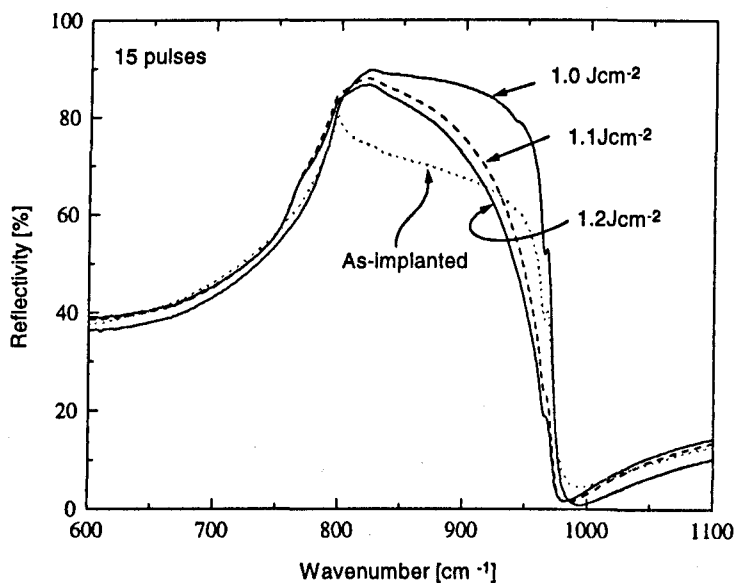


Figure 5.5:9 Reststrahlen reflectivity of ion implanted 4H-SiC laser annealed with 15 pulses, The measurements were made using unpolarised light. Sample #6.

Excimer Laser Annealing of Ion-Implanted 4H- and 6H-Silicon Carbide

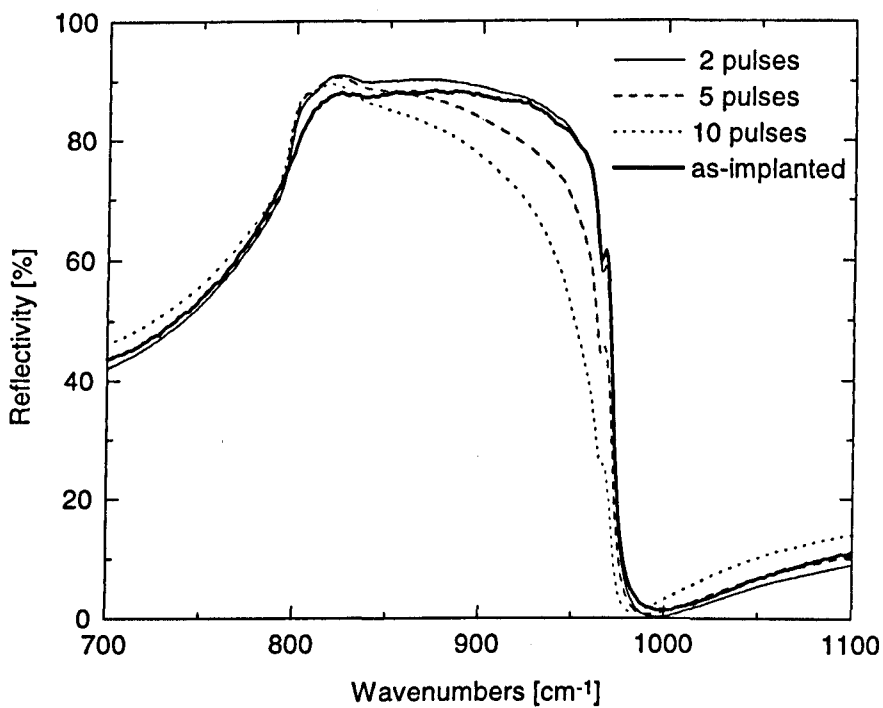


Figure 5.5:10 Reststrahlen reflectivity of ion implanted 4H-SiC, laser annealed at 1.4 J cm^{-2} with 2, 5, and 10 laser pulses. The measurements were carried out using unpolarised light. Sample #4.

Excimer Laser Annealing of Ion-Implanted 4H- and 6H-Silicon Carbide

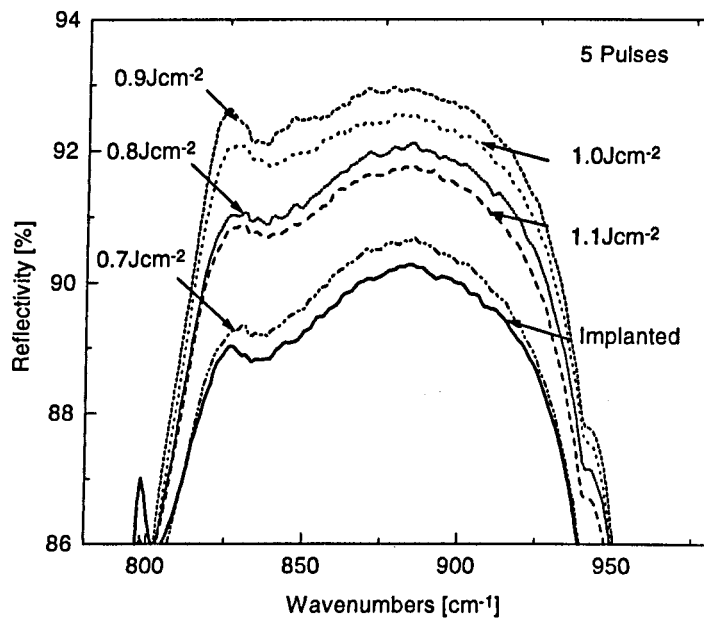


Figure 5.5:11 Infrared reflectivity spectra in the Reststrahlen region of laser annealed and as-implanted epitaxial 4H-SiC.

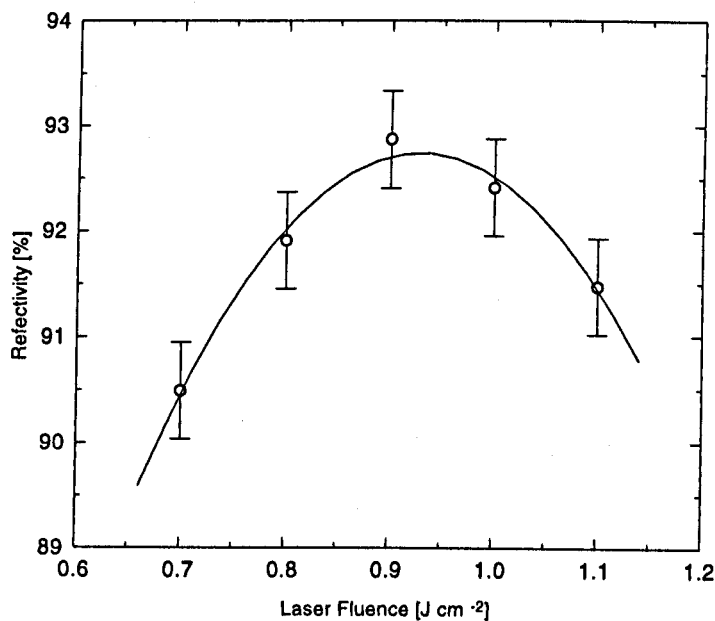


Figure 5.5:12 IR reflectivity measured at an arbitrary point at 870 cm^{-1} for the laser annealed epitaxial 4H-SiC shown above.

5.5.3 Spatial Dispersion Effects of Laser Irradiated 6H-SiC

The hexagonal (α -SiC) form of Silicon Carbide, having a uniaxial crystal (wurtzite structure) possesses infrared active optical modes, which are polarised either parallel to, or normal to the optical axis. We use the established spatial dispersion relationships to investigate the reflectivity dependency on the incident angle of incoming infrared radiation subsequent to excimer laser annealing at 308 nm. By measuring the reflectivity at increasing angles of incidence we note how the so called *Berriman modes* [52] can be used to delineate the TO and LO phonon modes. When infrared radiation is incident at an oblique angle the electric field vector polarised perpendicular to the plane of incidence, (s-polarised), there exist only one excited mode at Ω_{TO} , whereas when the electric field vector is polarised parallel to the plane of incidence (p-polarised) there are two excited modes, Ω_{TO} and Ω_{LO} . Thus, as described previously for 6H-SiC [53], this necessitates two dielectric functions, one parallel, ϵ_{\parallel} , the other perpendicular, ϵ_{\perp} , in order to understand the reflectance spectrum.

$$\epsilon_{\perp}(\omega) = \epsilon_{\perp}^{\infty} + \sum_{j=1}^{\nu} \frac{s_{\perp,j} \Omega_{\perp,j}^2}{\Omega_{\perp,j}^2 - \omega^2 - i\omega\Gamma_{\perp,j}} \quad (5:9)$$

$$\epsilon_{\parallel}(\omega) = \epsilon_{\parallel}^{\infty} + \sum_{k=1}^{\omega} \frac{s_{\parallel,k} \Omega_{\parallel,k}^2}{\Omega_{\parallel,k}^2 - \omega^2 - i\omega\Gamma_{\parallel,k}} \quad (5:10)$$

where ν and ω are the number of active Transverse Optical (TO) phonons according to the selection rules for $E_{\perp c}$ and $E_{\parallel c}$. For calculating the reflectivity of a uniaxial crystal, the Fresnel equation must be solved with $\epsilon_{11} = \epsilon_{22} = \epsilon_{\perp}$, $\epsilon_{33} = \epsilon_{\parallel}$:

$$[\omega^2 \epsilon_{\perp}(\omega) - c^2 k^2] \{ \epsilon_{\perp}(\omega) [\omega^2 \epsilon_{\parallel}(\omega) - c^2 k^2] s_{\perp} + \epsilon_{\parallel}(\omega) [\omega^2 \epsilon_{\perp}(\omega) - c^2 k^2] s_{\parallel} \} = 0 \quad (5:11)$$

Excimer Laser Annealing of Ion-Implanted 4H- and 6H-Silicon Carbide

where k is the wavevector and $s=(s_{\perp}, s_{\parallel})$ its direction with $s_{\perp} = (s_1^2 + s_2^2)^{1/2}$ and $s_{\parallel} = s_3$. The solution of Eq (5:11) corresponds to the ordinary ray (s-polarisation)

$$\epsilon(\omega) = \epsilon_{\perp}(\omega) \quad (5:12)$$

and the extraordinary ray (p-polarisation) as

$$\epsilon(\omega, \theta) = \frac{\epsilon_{\perp}(\omega)\epsilon_{\parallel}(\omega)}{\epsilon_{\perp}(\omega)\sin^2\theta + \epsilon_{\parallel}(\omega)\cos^2\theta} \quad (5:13)$$

where θ is the angle between the optical axis and the direction of propagation. Regarding a single transverse optical mode and without phonon damping ($\Gamma = 0$) and applying the Lyddane-Sachs-Teller relation equation (5:7) $\epsilon(\omega, \theta)$ is given by

$$\epsilon(\omega, \theta) = \frac{(\Omega_{LO,\perp}^2 - \omega^2)(\Omega_{LO,\parallel}^2 - \omega^2)}{(\Omega_{LO,\perp}^2 - \omega^2)(\Omega_{TO,\parallel}^2 - \omega^2)\sin^2\theta/\epsilon_{\infty,\parallel} + (\Omega_{LO,\parallel}^2 - \omega^2)(\Omega_{TO,\perp}^2 - \omega^2)\cos^2\theta/\epsilon_{\infty,\perp}} \quad (5:14)$$

Consequently the directional dependency of the resonant frequencies results in two different Reststrahlen bands in the reflectivity spectrum coinciding with the extraordinary ray (p-polarisation).

Three sites, 10mm \times 5 mm, were laser annealed with the intention of annealing out induced lattice damage and activating the implanted nitrogen. Earlier experiments indicated that a laser fluence between 0.9 and 1.0 J cm⁻² is in the appropriate range for lattice recovery. Therefore two of the sites were irradiated within this range and a third site was irradiated at 1.5 J cm⁻². Although 1.5 J cm⁻² is above experimentally determined damage threshold, this site served quite usefully has a comparative measure on the effects that laser irradiation had on the reflectivity spectrum.

Excimer Laser Annealing of Ion-Implanted 4H- and 6H-Silicon Carbide

Figure 5.5:13 illustrates the calculated reflectivity spectra using equation (5:14) and its dependency on the incident angle, θ , with respect to the c axis. The emergence of the LO mode at around 987 cm^{-1} can be seen with increasing angle, θ . The work so far, undertaken in this chapter, has been concerned with ion-implanted 4H-Silicon Carbide. A slight deviation in that this work looks at excimer laser irradiated 6H-Silicon Carbide. Variable angle infrared reflectivity measurements have been employed to measure the dependency on laser fluence.

In this sub-chapter a quartered 6H-Silicon Carbide wafer, see Table 5.5:2, sample #6 has been irradiated at a laser fluence of 0.9, 1.0, and 1.5 J cm^{-2} .

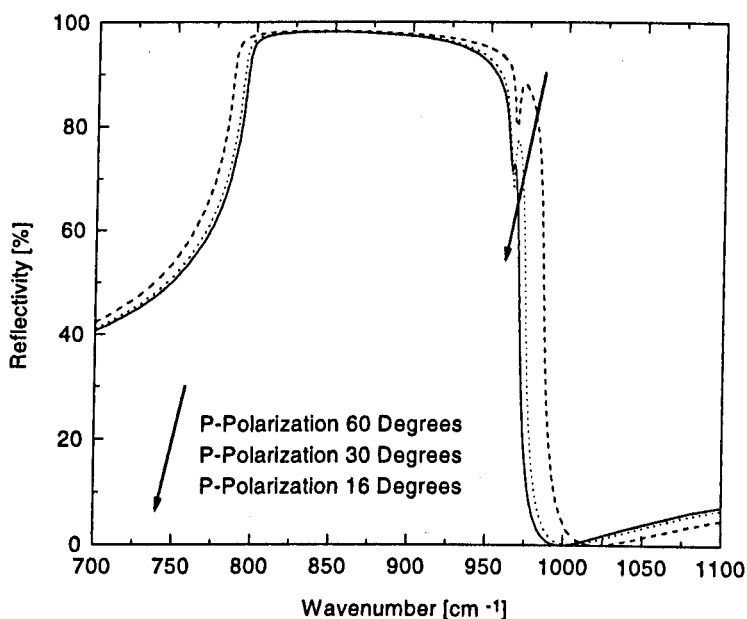


Figure 5.5:13 Calculated infrared spectra at angles of 16, 30 and 60 degrees. Illustrating the angular dependency of longitudinal optical modes due to Berreman coupling.

Excimer Laser Annealing of Ion-Implanted 4H- and 6H-Silicon Carbide



Figure 5.5:14 Nitrogen ion-implanted 6H-SiC quartered wafer laser annealed at 308 nm at 1.5 J cm^{-2} in air (left), and at 1.0 and 0.9 J cm^{-2} (centre and right respectively) at a pressure of 35 bar in argon: sample #6.

Figures 5.5:15 - 5.5:18 illustrate the Reststrahlen reflectivity for angles of incidence of 16, 30, and 60 degrees. Spatial dispersion effects were measured with p-polarised infrared light for an as-grown sample and laser annealed sites at 1.5, 1.0 and 0.9 J cm^{-2} for sites 1, 2, and 3 respectively. The data in Figure 5.5:15 clearly illustrates how the spike in the reflectivity spectrum at around $\sim 966 \text{ cm}^{-1}$ at 16 becomes larger with increasing angles of incidence from the normal indicating that the excitation occurs with the p-polarisation.

Figure 5.5:19 to Figure 5.5:24, show the Reststrahlen reflectivity grouped together for the three irradiated sites and the as-implanted reference site. Both s-polarisation and p-polarisation are shown for the three different angles of incidence. At angles incidence of 16 and 30 degrees the spectra are very similar. A large change can be seen at an angle of incidence of 60 degrees. It is clear from the angular dependency between s- and p-polarisation, particularly at 60 degrees angle of incidence, Figure 5.5:27 and Figure 5.5:24, how the reflection minima close to the LO mode differ between both polarisations. This is of significant importance since any characteristic changes at the reflection minima (plasma edge) subsequent to any induced modification, like for example laser annealing could be masked by the p-polarisation. Shifts in the plasma edge have, in the literature, been employed to infer the electrical properties of a

Excimer Laser Annealing of Ion-Implanted 4H- and 6H-Silicon Carbide

material. The identification of the reflection minima is sharper at angles of incidence of 60 degrees and can be more easily identified. If the damaged site at 1.5 J cm^{-2} is compared at each of the angles of incidence it can be seen that there are little differences between the spectra compared with annealed sites at the lower fluence. More specifically the LO mode at around 968 cm^{-1} is less affected. Because spatial dispersion effects are expected with changes in the angle of incidence, effectively due the crystal anisotropy, the lack of any changes or rather, the less noticeable changes in the reflection spectra are an indication of a reduction in the lattice order at the higher laser fluence.

Excimer Laser Annealing of Ion-Implanted 4H- and 6H-Silicon Carbide

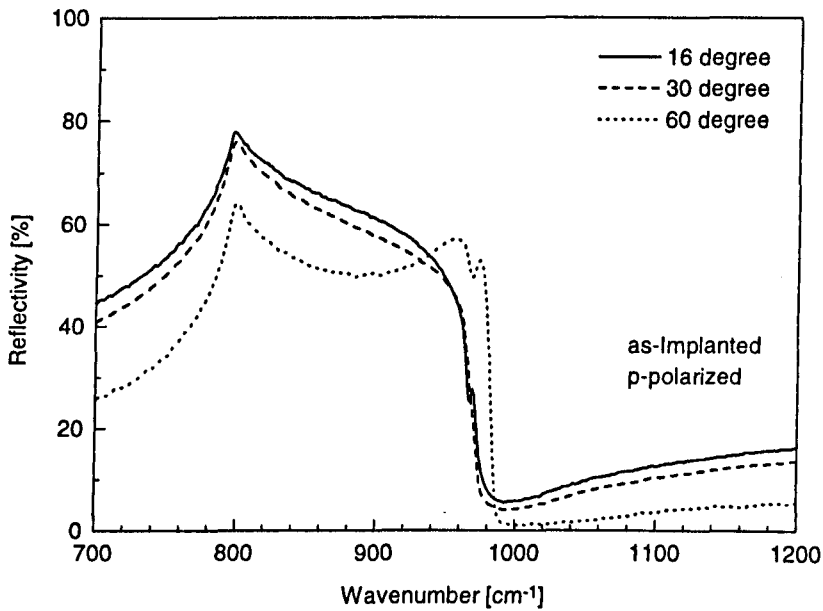


Figure 5.5:15 Reststrahlen reflectivity of as-implanted 6H-SiC illuminated with p-polarised light at 16, 30 and 60 Degrees.

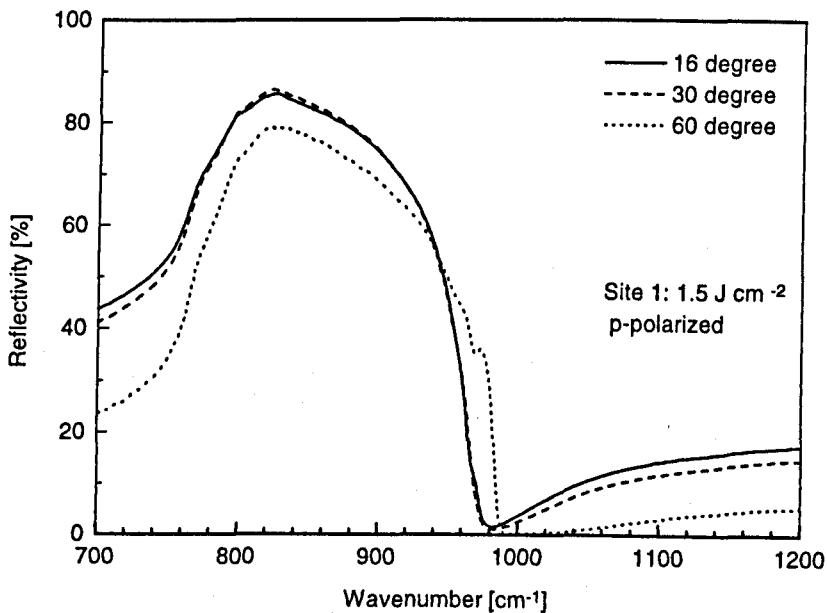


Figure 5.5:16 Reststrahlen reflectivity of laser annealed 6H-SiC at 1.5 J cm^{-2} , illuminated with p-polarised light at 16, 30 and 60 Degrees.

Excimer Laser Annealing of Ion-Implanted 4H- and 6H-Silicon Carbide

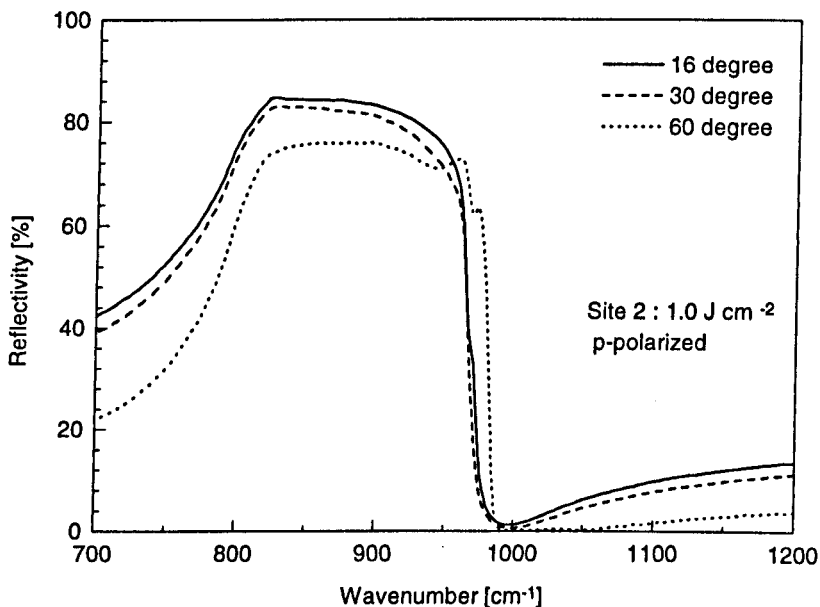


Figure 5.5:17 Reststrahlen reflectivity of laser annealed 6H-SiC at 1.0 J cm^{-2} , illuminated with p-polarised light at 16, 30 and 60 Degrees.

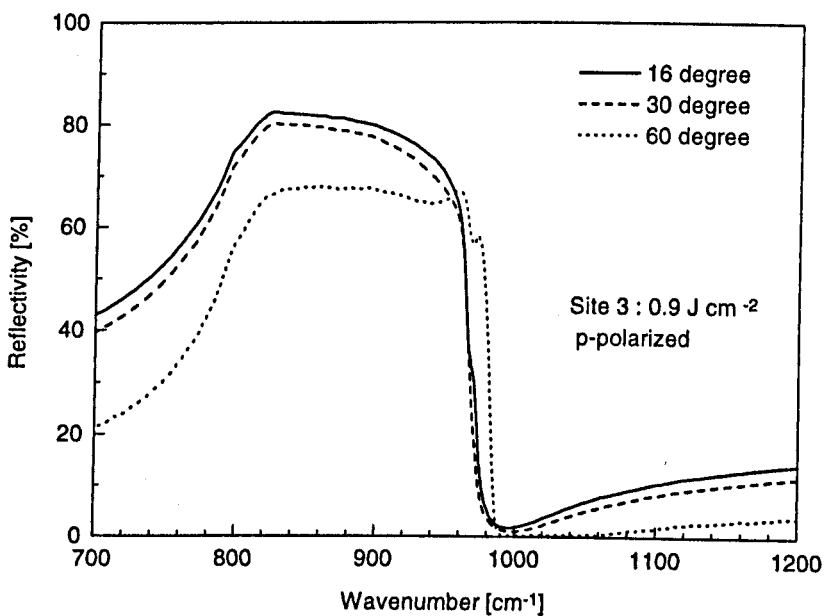


Figure 5.5:18 Reststrahlen reflectivity of laser annealed 6H-SiC at 0.9 J cm^{-2} , illuminated with p-polarised light at 16, 30 and 60 Degrees.

Excimer Laser Annealing of Ion-Implanted 4H- and 6H-Silicon Carbide

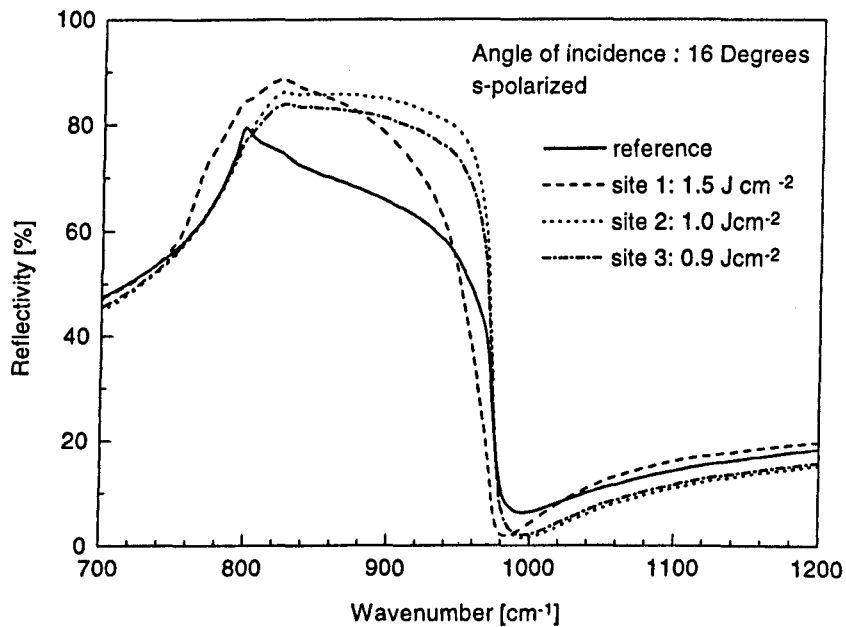


Figure 5.5:19 Reststrahlen reflectivity for laser annealed 6H-SiC, s-polarised light at an angle of incidence of 16 Degrees.

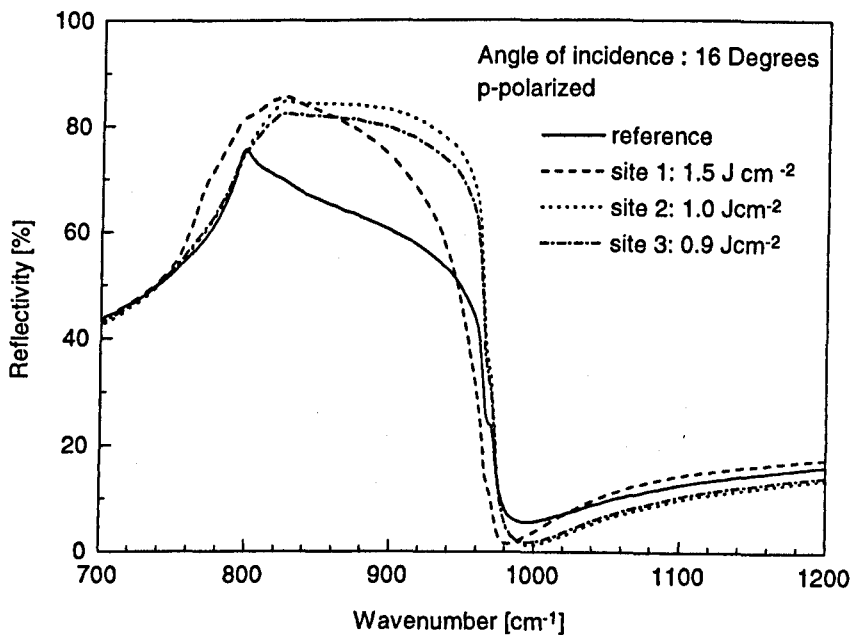


Figure 5.5:20 Reststrahlen reflectivity for laser annealed 6H-SiC illuminated with p-polarised light at an incidence angle of 16 Degrees.

Excimer Laser Annealing of Ion-Implanted 4H- and 6H-Silicon Carbide

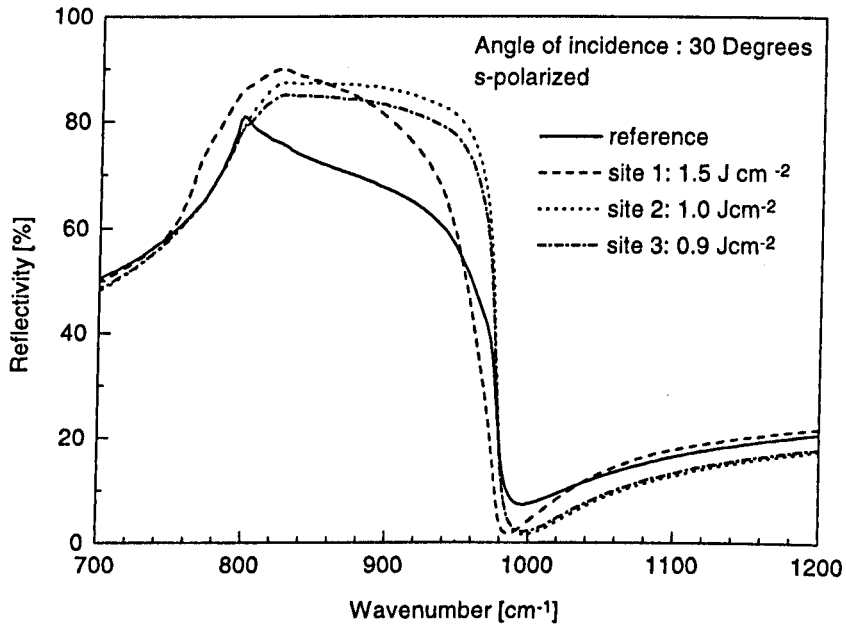


Figure 5.5:21 Reststrahlen reflectivity for laser annealed 6H-SiC illuminated with s-polarised light at an incidence angle of 30 Degrees.

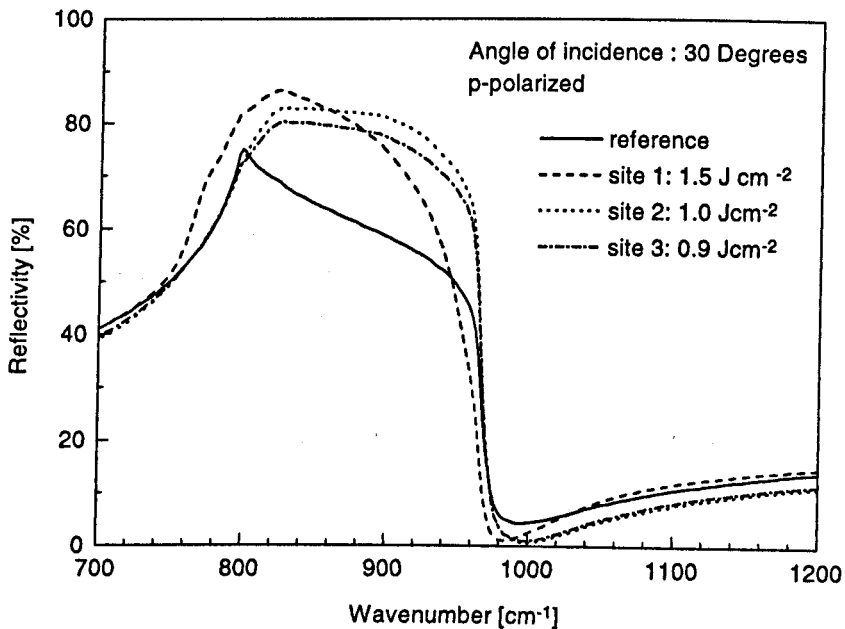


Figure 5.5:22 Reststrahlen reflectivity for laser annealed 6H-SiC illuminated with p-polarised light at an incidence angle of 30 Degrees.

Excimer Laser Annealing of Ion-Implanted 4H- and 6H-Silicon Carbide

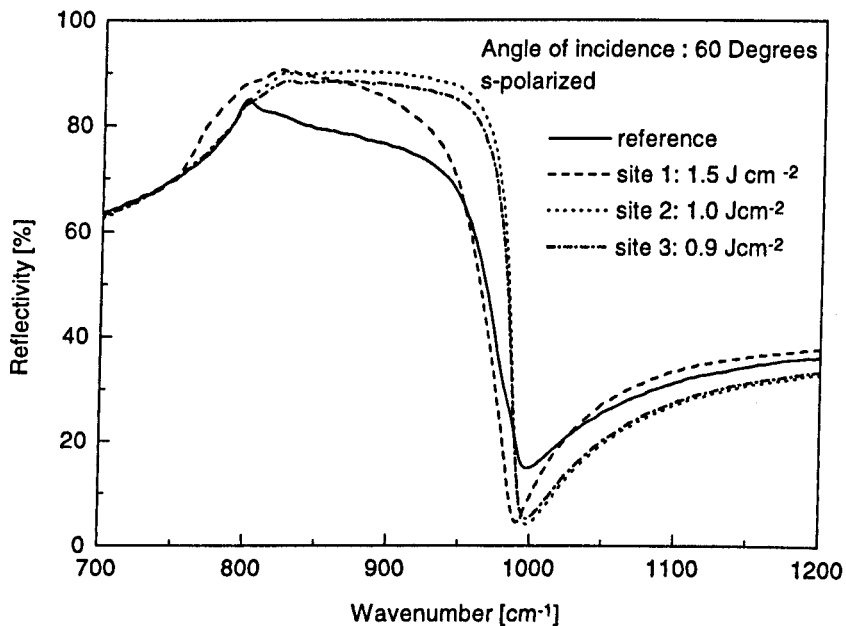


Figure 5.5:23 Reststrahlen reflectivity for laser annealed 6H-SiC illuminated with s-polarised light at an incidence angle of 60 Degrees.

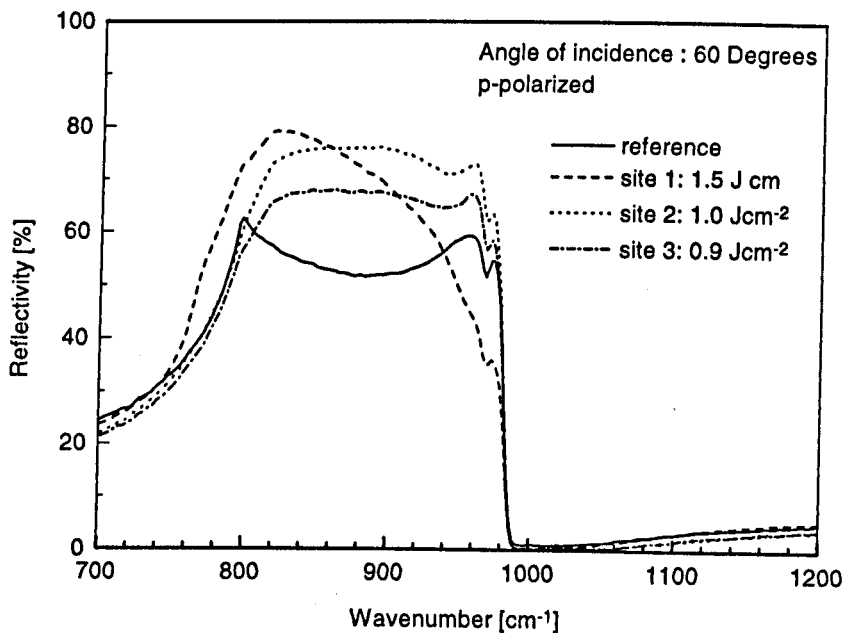


Figure 5.5:24 Reststrahlen reflectivity for laser annealed 6H-SiC illuminated with p-polarized light at an incidence angle of 60 Degrees.

5.5.4 Lorentz-Drude Interpretation of Laser Annealed 4H-SiC

The Lorentz-Drude model is an extremely effective model for simulating the dielectric function. We compare the measured reflectivity for as-received, as-implanted, and excimer laser annealed-ion-implanted material, with the calculated data using the Lorentz-Drude formalism. By interpreting the oscillator parameters we show how the surface modifications subsequent to excimer laser annealing can be understood in terms of the phonon damping constant and plasma frequency.

The complex dielectric was calculated using equation (5:4) using the formalism given in given in references [54,55]. The infrared reflectivity of the Silicon Carbide wafer was modelled as an air/damaged-SiC/bulk-SiC system using the matrix algorithm introduced by Harbecke [56], in which the complex index of refraction and the thickness of the Silicon Carbide layer determine the matrix elements. The samples used for this work were polished on the front side and unpolished on the backside and was modelled as a half-infinite bulk material. The modelled and measured infrared reflectivity spectra were compared and a least square sum was used to assess the quality of the fit. Global minimization of the least square sum was achieved using a simulated annealing algorithm [57] implemented by M. Schlaf⁹.

Fits were carried out for all the as grown and as received and laser annealed samples. Because of the repetitive nature of the spectra only typical spectra of as-grown, as-implanted and laser annealed have been illustrated Figure 5.5:25 and Figure 5.5:26. The Reststrahlen reflectivity spectra shown in Figure 5.5:25 shows the measured and calculated data for a high quality as-received bulk Silicon Carbide sample with a high reflection maximum. The stacked data, Figure 5.5:26, illustrates the changes in reflection maxima and the induced oscillation at the higher wavenumbers for the laser induced damage at 1.3 J cm^{-2} .

Excimer Laser Annealing of Ion-Implanted 4H- and 6H-Silicon Carbide

Real and imaginary refractive index data determined from the Lorentz-Drude model are shown in Figure 5.5:27 and Figure 5.5:28. The high value of the extinction coefficient, hence, optical absorption depth is very shallow, which is typical of the Reststrahlen band and indicative of high quality material. Also shown is the n and k data for implanted samples #3, #4, and #6 with increasing implantation dose respectively. As can be seen there is a decrease in material quality with implantation dose for the low and high dose samples, #3 - #6, however the implanted sample in between the upper and lower implantation dose, #4, is not consistent, appearing slightly higher in both graphs than the low implantation dose, sample #3. One explanation here is that this sample was capped with Si_3N_4 , to suppress sublimed species whilst annealing. The infrared measurements here were taken after having removed the capping layer with an hydrogen fluoride strip and the act of removal might have chemically polished the near surface. Therefore, this will have some effect on the way in which EM radiation couples at this surface

Figure 5.5:29 to 5.5:33 shown the Reststrahlen reflectivity with the associated complex refractive index data for the lowest and highest implantation doses. Also shown in Figure 5.5:29 and Figure 5.5:30 is the as-grown high quality spectra with an extinction coefficient peaking at around 23. For both implantation doses the highest values for n and k subsequent to excimer laser annealing occur between 1.0 and 0.9 J cm^{-2} .

Extracted from the calculated data via simulated annealing is the phonon damping constant, Γ , for each irradiated site. Figure 5.5:35 and Figure 5.5:36 illustrate the calculated phonon damping constants for the laser irradiated Silicon Carbide in the fluence range 0.9 to 1.3 J cm^{-2} . The horizontal line is the calculated phonon damping constant for the as-implanted material. Clearly the as-implanted material for the high implanted dose has suffered a greater amount of damage having a value of, $\Gamma = \sim 65$, compared with that of the lower dose, $\sim \Gamma = 20$. It is also

^o M. Schlaf, Ph.D research student at the University of Hull.

Excimer Laser Annealing of Ion-Implanted 4H- and 6H-Silicon Carbide

clear that when the laser fluence is increased beyond 0.9 and 1.0 J cm^{-2} , the optimum for lattice recovery, the damping constant is also seen to increase systematically with laser fluence.

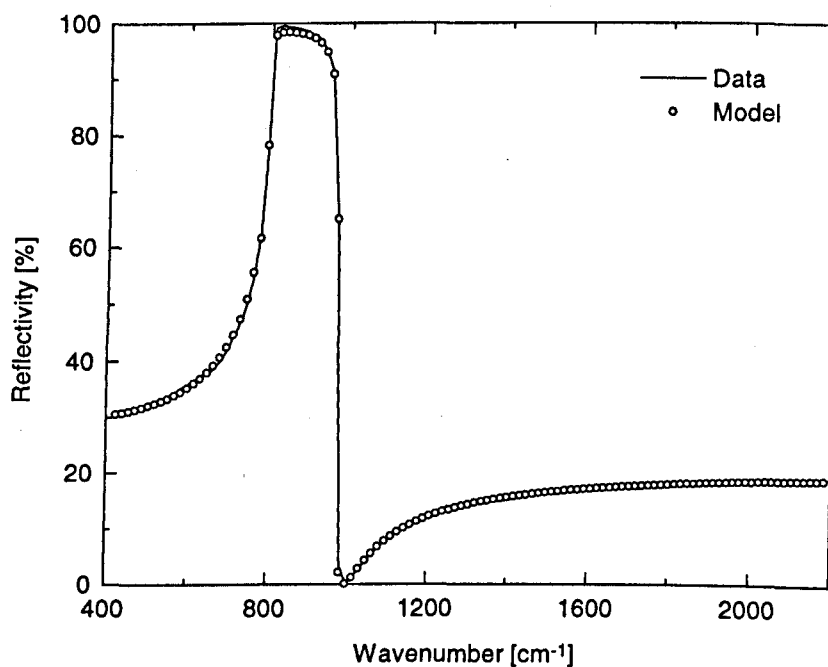


Figure 5.5:25: Measured and calculated infrared reflectivity spectra for high quality as-received bulk 4H-SiC, sample #1.

Excimer Laser Annealing of Ion-Implanted 4H- and 6H-Silicon Carbide

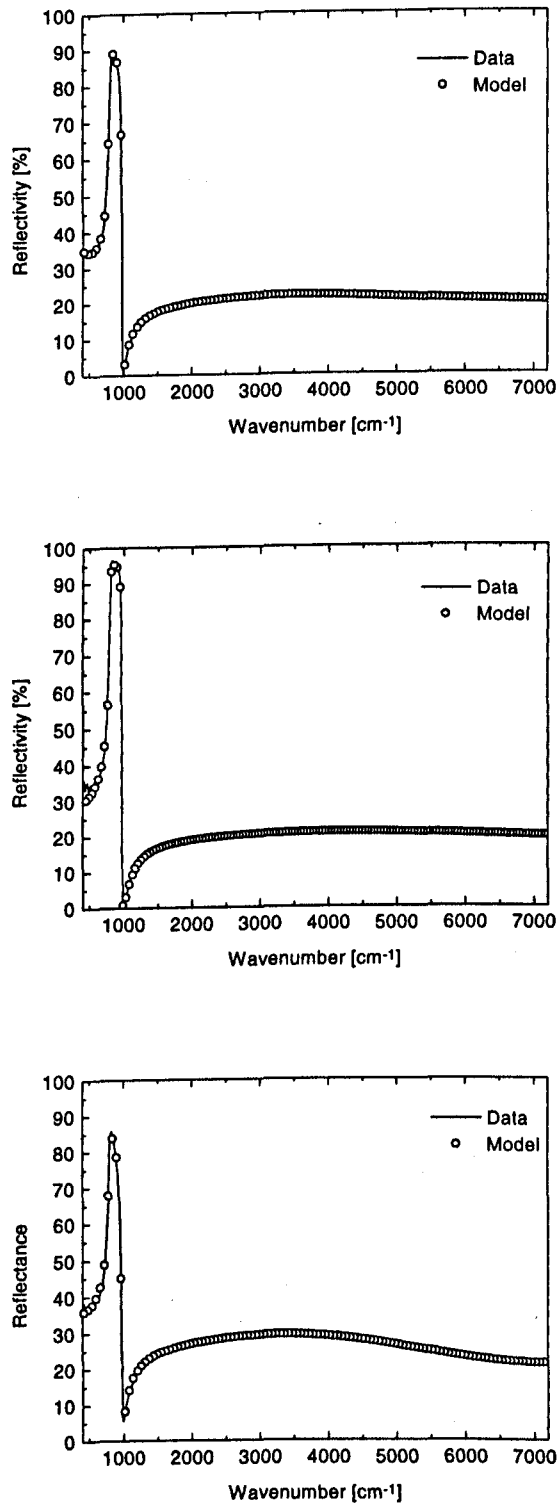


Figure 5.5:26 Measured and calculated infrared reflectivity spectra; (top): as-implanted, (middle): Laser annealed at 1.0 J cm^{-2} and (bottom): Laser annealed 1.3 J cm^{-2} , sample # 3.

Excimer Laser Annealing of Ion-Implanted 4H- and 6H-Silicon Carbide

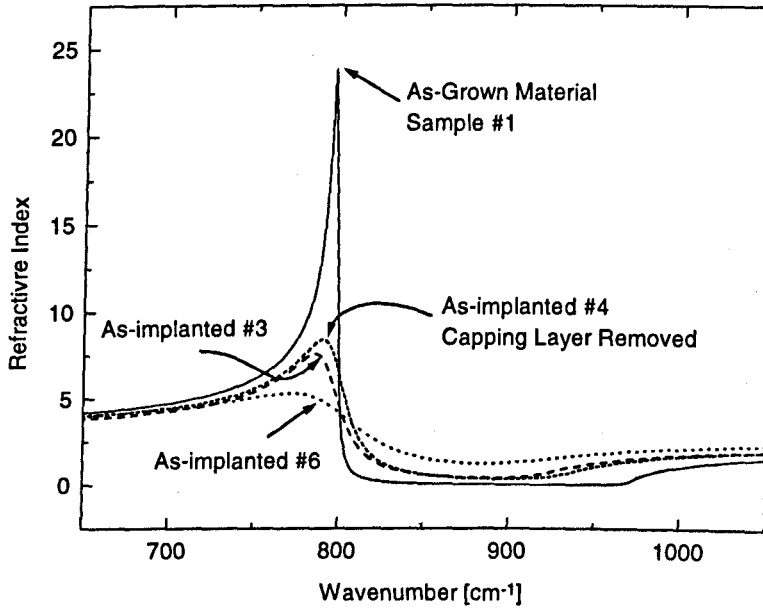


Figure 5.5:27 Calculated real part of the refractive index for as-implanted 4H-Silicon Carbide.

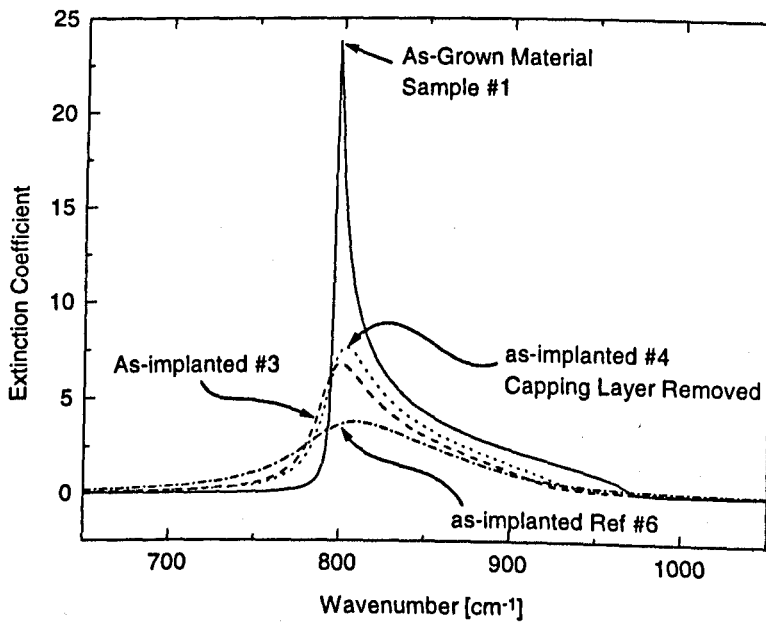


Figure 5.5:28 Calculated imaginary part of the refractive index for as-implanted 4H-Silicon Carbide.

Excimer Laser Annealing of Ion-Implanted 4H- and 6H-Silicon Carbide

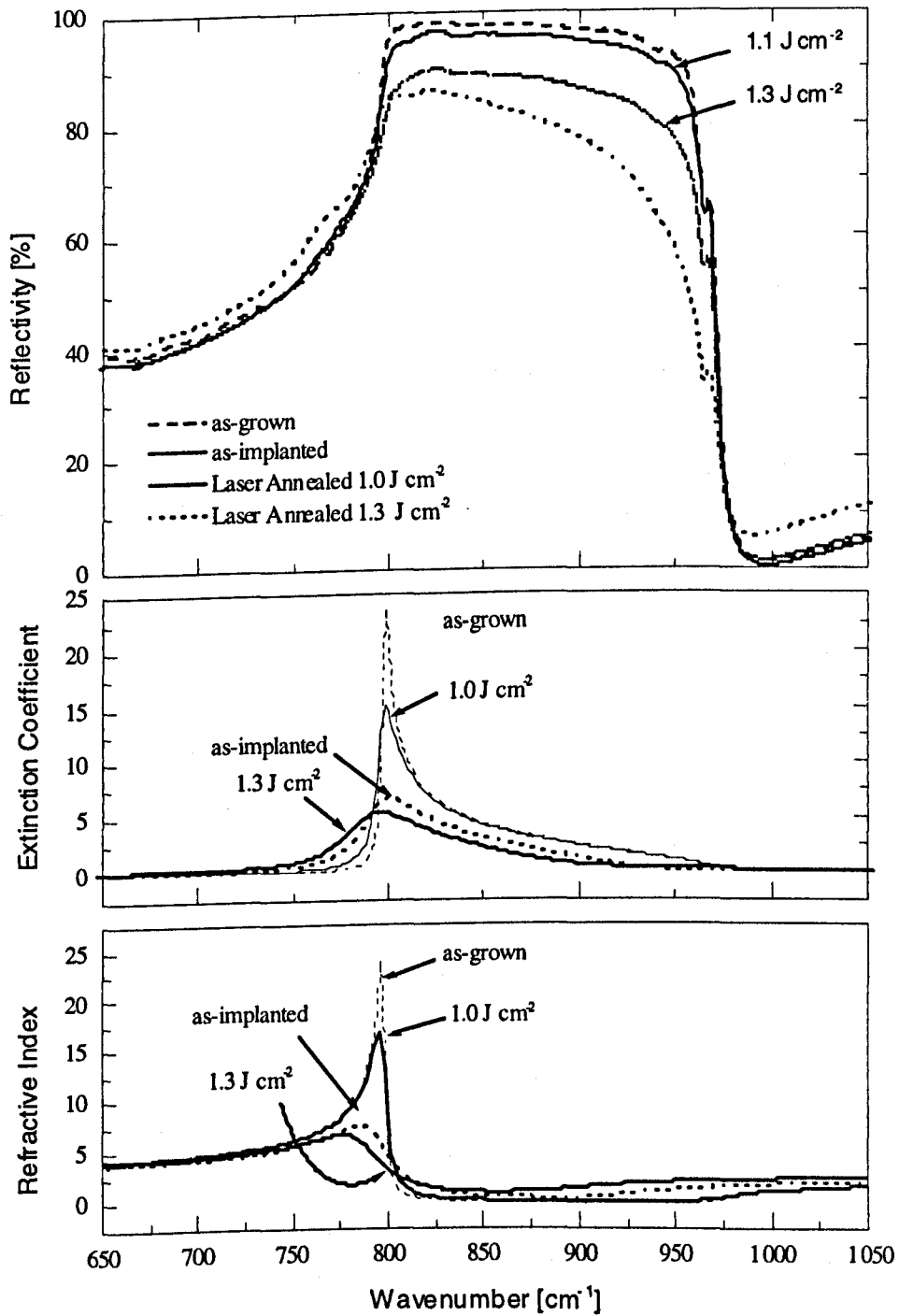


Figure 5.5:29. Calculated real and imaginary refractive index data for excimer laser annealed ion-implanted material, low dose, sample #3.

Excimer Laser Annealing of Ion-Implanted 4H- and 6H-Silicon Carbide

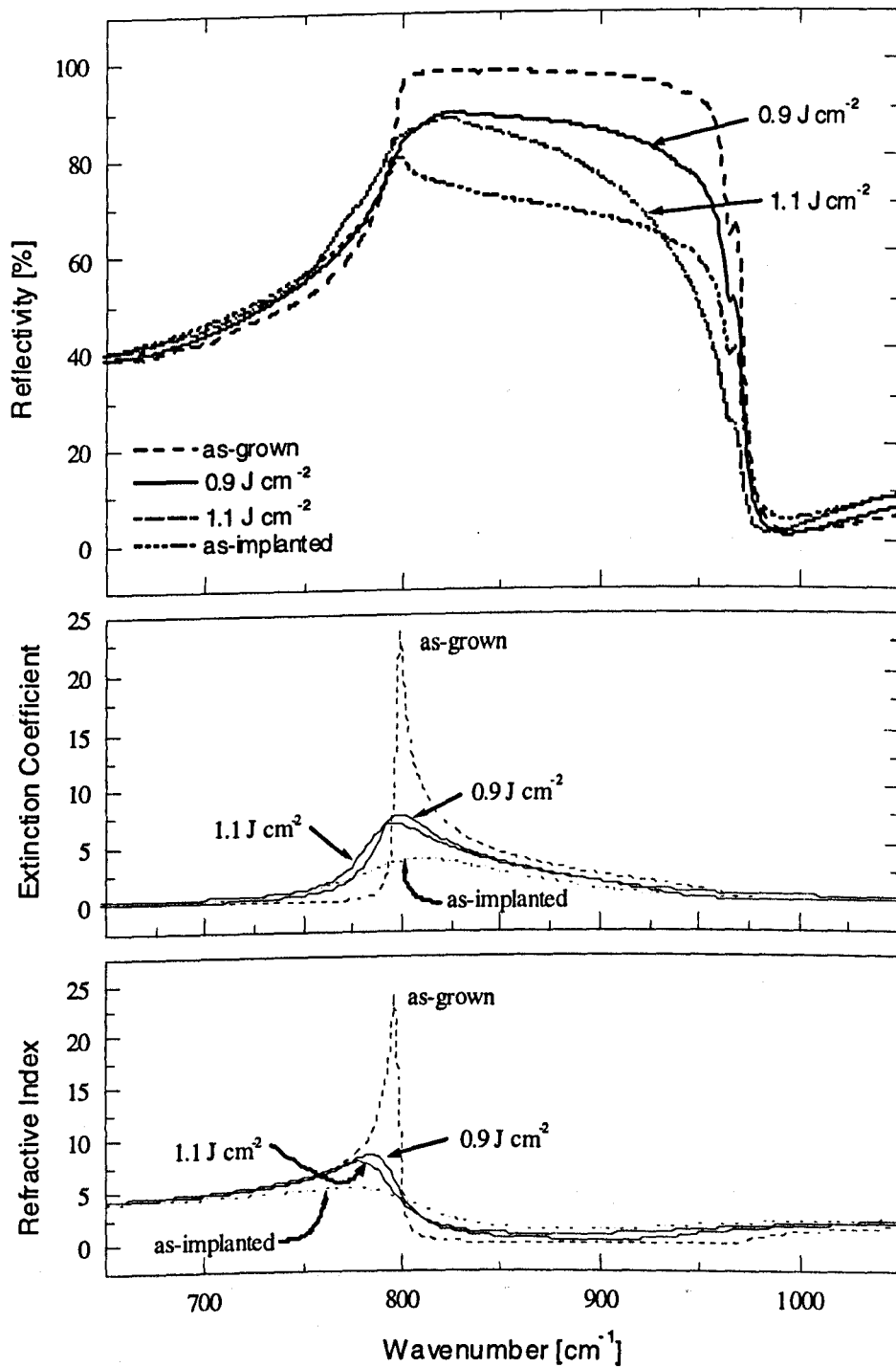


Figure 5.5:30 Calculated real and imaginary refractive index data for excimer laser annealed ion-implanted material, high dose, sample #6.

Excimer Laser Annealing of Ion-Implanted 4H- and 6H-Silicon Carbide

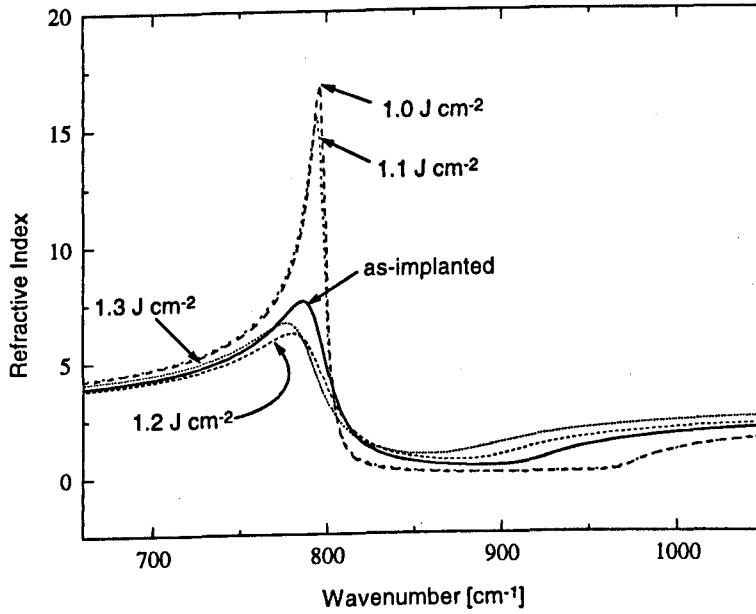


Figure 5.5:31 Calculated real part of the refractive index subsequent to laser annealing, low dose, sample #6.

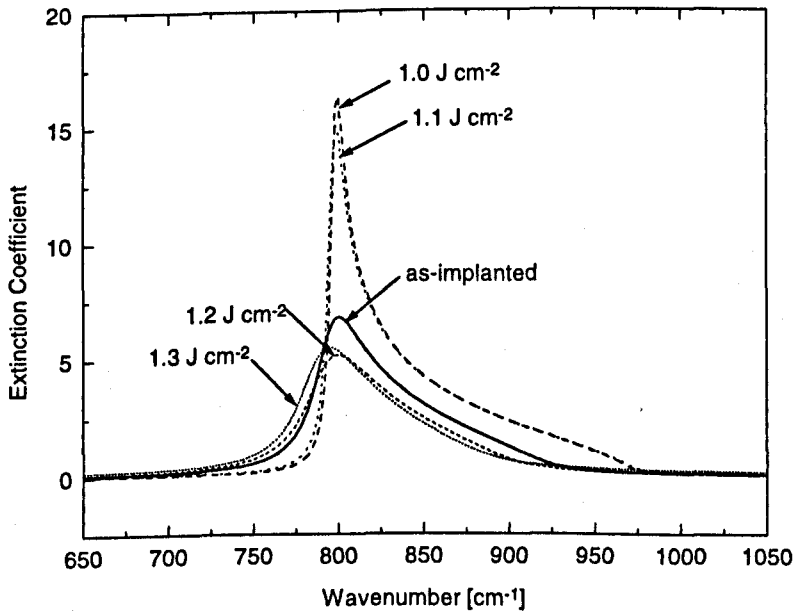


Figure 5.5:32 Calculated imaginary part of the refractive index subsequent to laser annealing for a low dose sample #6.

Excimer Laser Annealing of Ion-Implanted 4H- and 6H-Silicon Carbide

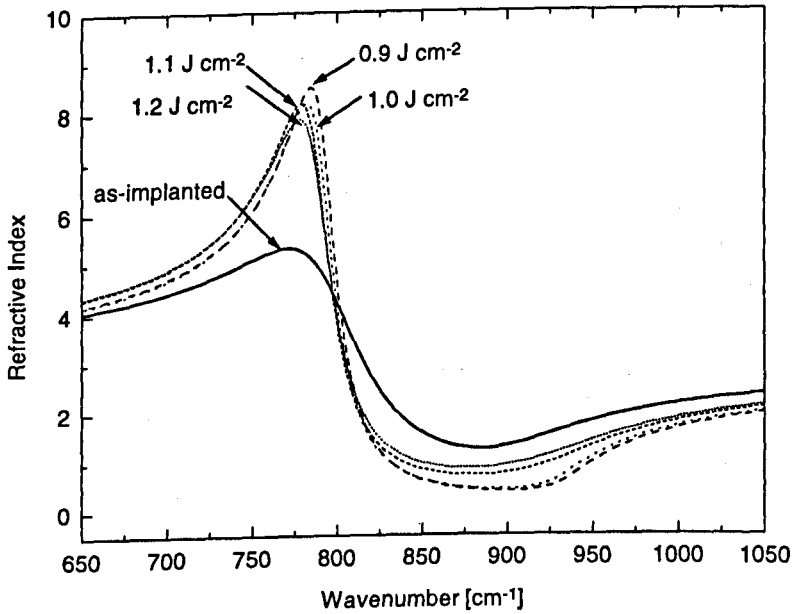


Figure 5.5:33 Calculated real part of the refractive index subsequent to laser annealing, high dose, sample, #6.

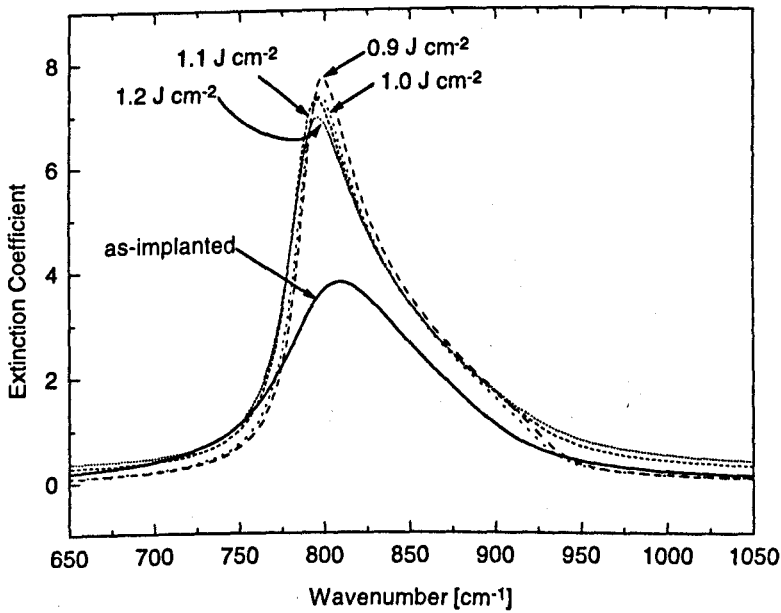


Figure 5.5:34 Calculated imaginary part of the refractive index subsequent to laser annealing, high dose, sample #6.

Excimer Laser Annealing of Ion-Implanted 4H- and 6H-Silicon Carbide

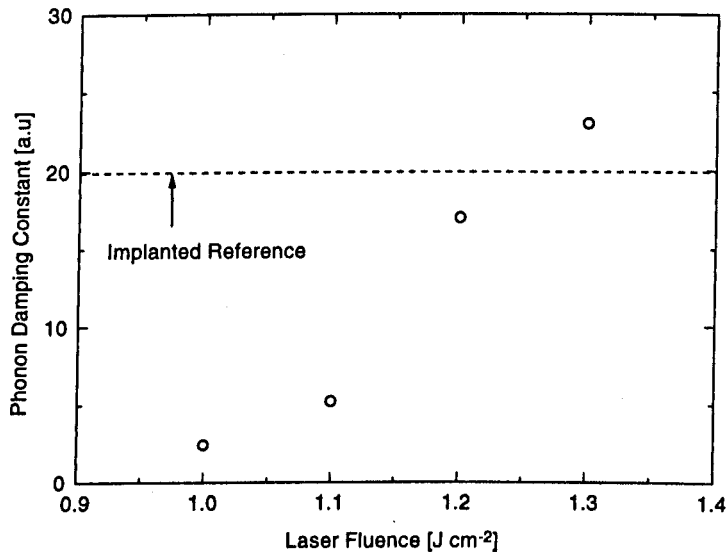


Figure 5.5:35 Calculated phonon damping constants, Γ , using the Lorentz-Drude formalism for the low implantation dose, sample #3.

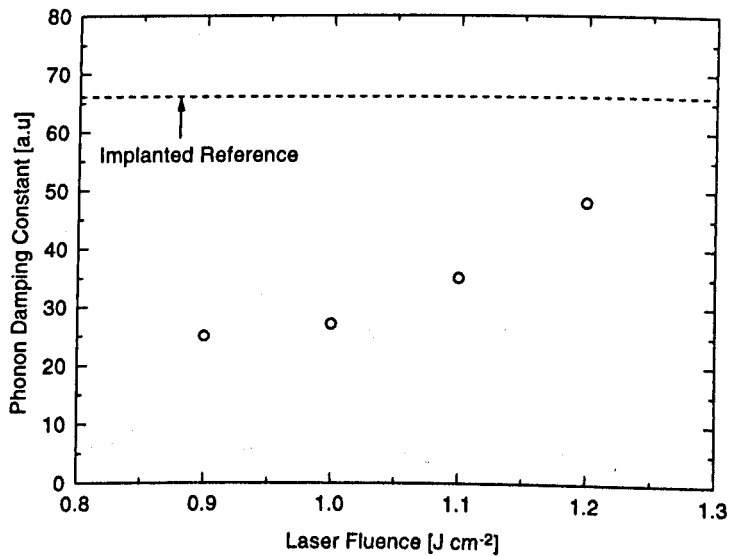


Figure 5.5:36 Calculated phonon damping constants, Γ , using the Lorentz-Drude formalism for the high implantation dose, sample #6.

5.5.5 Dopant Activation.

The optical properties in the Infrared, reflectance and transmittance, can have strong dependencies on the dopant properties. Here, the sensitivity of the reflection minima (plasma edge) situated on the longer wavelength side of the Reststrahlen band, is utilized in order to extract information on the dopant concentration.

An Infrared reflection spectra of an as-received 4H-SiC sample with known differences in the surface concentration of Nitrogen was taken and is illustrated in Figure 5.5:37. The wafer was characteristic having a discoloured spot towards the centre of about 5 mm² in area. The inhomogeneity is inherent in the growth process and is produced by the nucleation of nitrogen. The spectra shown in Figure 5.5:37 was a bulk sample cut from a boule and the 'fall off' in the Reststrahlen maxima, i.e. the Reststrahlen band was not as 'square', indicative of a lower quality sample in comparison with some of the other spectra, particularly the epitaxial grown material. The sample inhomogeneity however, indicated how the plasma edge shifts with a change in nitrogen concentration at the surface. It is well known from early work in silicon that the plasma edge shifts with dopant concentration as

$$\lambda_p^2 = \frac{1}{N} \quad (5:15)$$

where λ_p , is the wavelength of the plasma edge and N being the concentration. Accordingly, the shift in Figure 5.5:37 to higher wavenumbers (shorter wavelength) corresponds to an increase in the surface concentration in the centre portion of the nitrogen rich spot. In view of this, any significant difference in nitrogen concentration should be then evident with a similar shift subsequent to laser annealing.

Figure 5.5:38 shows the infrared spectra for nitrogen implanted silicon carbide at three implantation doses contrasted against a high quality sample. There is no significant correlation

Excimer Laser Annealing of Ion-Implanted 4H- and 6H-Silicon Carbide

between the plasma edge and the implantation dose over the range 1×10^{14} and $3 \times 10^{15} \text{ cm}^{-2}$, however the high quality reference sample indicates a slightly higher plasma edge in comparison of about 5 cm^{-1} .

Figure 5.5:39 shows the infrared reflection spectra of plasma edge versus laser pulse number. This sample was annealed in at 1450 mJ cm^{-2} at 2, 5, and 10 laser pulses in an argon ambient at a pressure of 35 bar. In this case there is a clear shift with pulse number towards lower wavenumbers. A shift in this direction which is in contrast to the shift in Figure 5.5:37 would infer some effect of negating an increase in the nitrogen concentration. Very similar infrared spectra can be seen in Figure 5.5:40, and Figure 5.5:41. The spectra shown in Figure 5.5:40 illustrates when Silicon Carbide is irradiated between 0.9 and 1.0 J cm^{-2} there is a vertical shift in the reflection minima and with a further increase in laser fluence, 1.1 and 1.2 J cm^{-2} , the plasma edge is then shifted towards lower wavenumbers. This directional change from a reduction in the reflectivity minima, which then leads to a translational shift towards the lower wavenumbers, probably indicates some kind of a mechanistic change caused by the increasing laser fluence.

From the work in Chapter 5.5.3, it was pointed out that a shift in the reflection minimum could be observed more clearly using s-polarized light compared to unpolarized light due the superposition of the less sensitive p-polarized reflection spectra. Figure 5.5:41 illustrates s-polarized reflection spectra for a laser annealed 6H-SiC sample. The spectra show two sites which were laser irradiated at a fluence which is thought to induce recrystallization and of a site that had clearly damaged the surface. The shift in the spectra at 1.5 J cm^{-2} towards shorter wavenumbers is strong evidence of laser induced damage. Although it cannot be determined from this experiment alone, using the relationship of the shift in plasma edge in equation (5:15) this infers a reduction in carrier concentration at 1.5 J cm^{-2} .

Excimer Laser Annealing of Ion-Implanted 4H- and 6H-Silicon Carbide

The shift in wavelength and change in the reflectivity in the plasma edge shown in Figure 5.5:37 to Figure 5.5:41 indicate three different modifications taking place in the reflection spectra. When annealed above at a laser fluence of 1.5 J cm^{-2} , there is a shift towards lower wavenumbers and a reduction in the reflectivity minima is seen. At a laser fluence 0.9 and 1.0 J cm^{-1} the main change in spectra is a reduction in the reflectivity minima with a very slight shift towards higher wavenumbers. These changes at the lower laser fluence correspond to increases in the reflectivity within the Reststrahlen region. The reduction in reflectivity can be attributed to an improvement in the crystallization and shift to higher wavenumbers can be tentatively attributed to increased electron-optical coupling. Observation of these three modification are illustrated schematically in Figure 5.5:41. From these observations alone it is not possible to determine exactly the very nature of the modifications that have taken place, however, for identification purposes in Chapter 6, we shall refer to them as being, (I): *Severe Damage*, (II): *Increased Carrier Concentration* and (III): *Improved Crystallization*, respectively. The third modification, (III), has been so named due to the high reflection maxima observed in the Reststrahlen region in Chapter 5.5.4 which also corresponds with the reduced reflection minima.

Briefly, there have been several reports of a reduction in reflectivity close to the plasma edge. Mechanical polishing measurements revealed a reduction in the reflection minima and calculated spectra of a damaged layer depleted of carriers correlated with the increased damage caused by the mechanical abrasive [58] However, if this is the case, the nature of the free surface depletion layer is unknown. The action of the laser might induce acceptor-like defect or defect complexes or create some form of surface oxide which act to reduce the freely available electronic states.

Excimer Laser Annealing of Ion-Implanted 4H- and 6H-Silicon Carbide

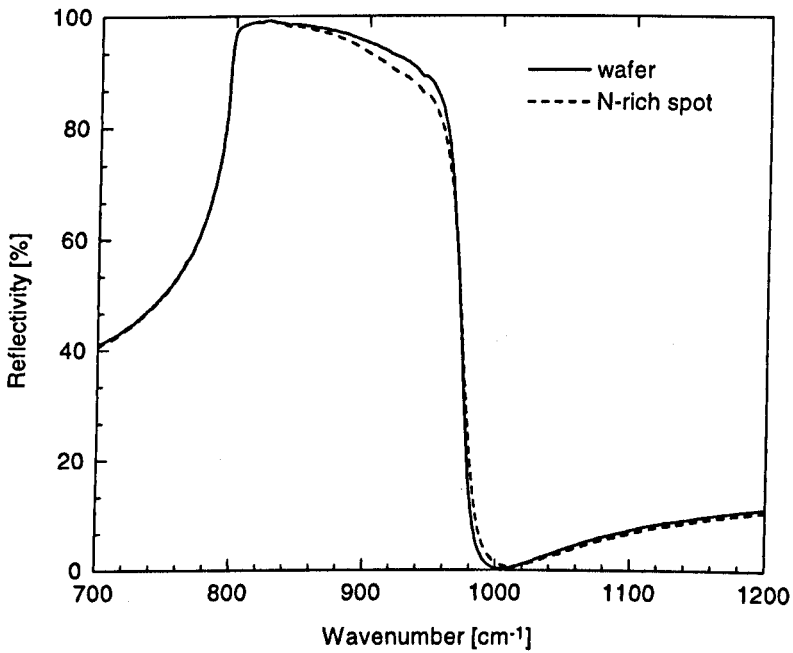


Figure 5.5:37 Infrared spectra of as-received 4H-SiC, sample #9, from two different areas of the same wafer.

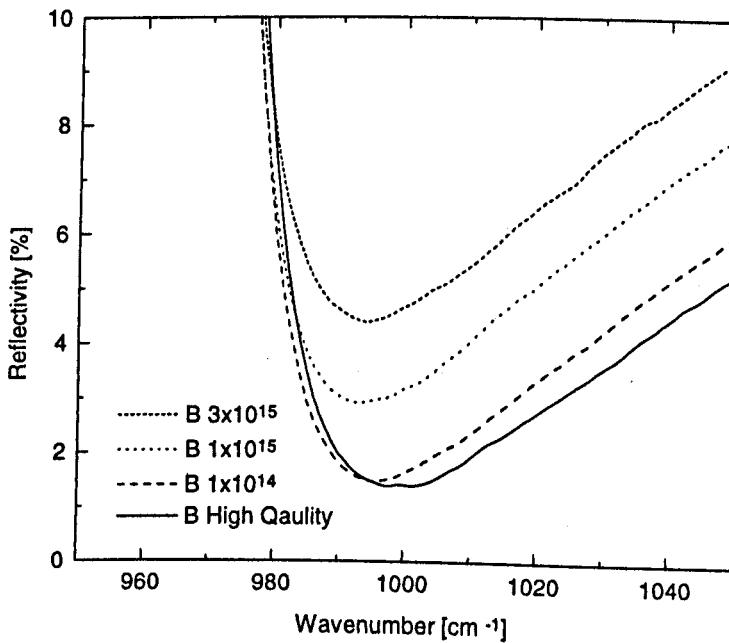


Figure 5.5:38 Plasma edge spectra for nitrogen ion implanted SiC.

Excimer Laser Annealing of Ion-Implanted 4H- and 6H-Silicon Carbide

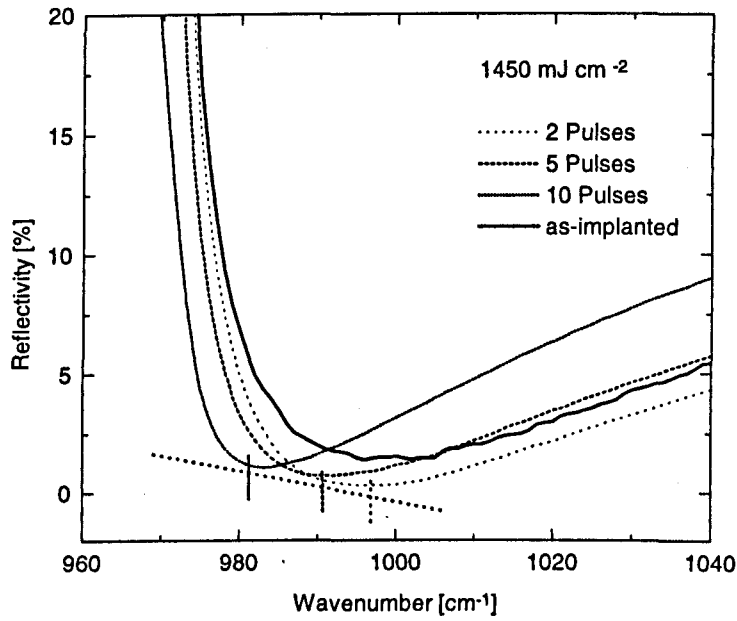


Figure 5.5:39 Infrared spectra of the plasma edge in laser irradiated 4H-SiC, carried out at a laser fluence of 1450 mJ cm^{-2} at a pressure of 35 Bar.

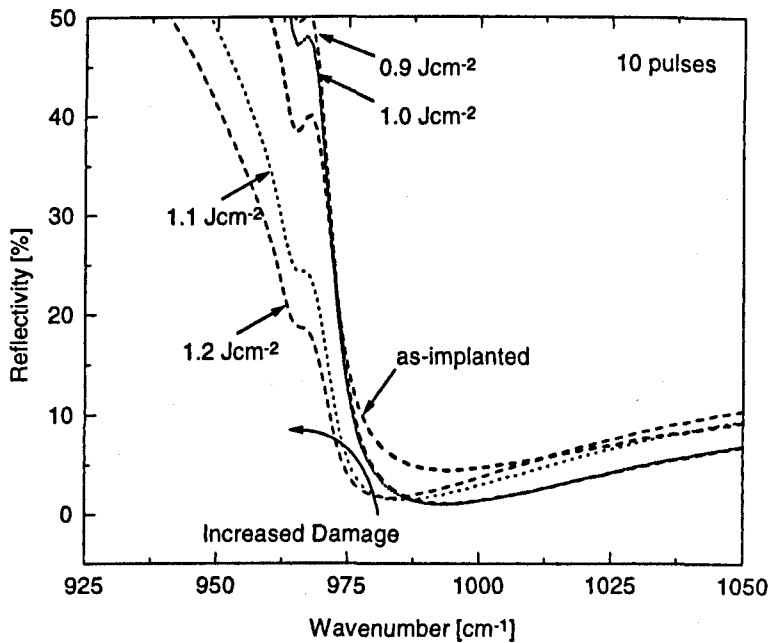


Figure 5.5:40 Infrared reflectivity near to the plasma edge of laser irradiated SiC sample #6.

Excimer Laser Annealing of Ion-Implanted 4H- and 6H-Silicon Carbide

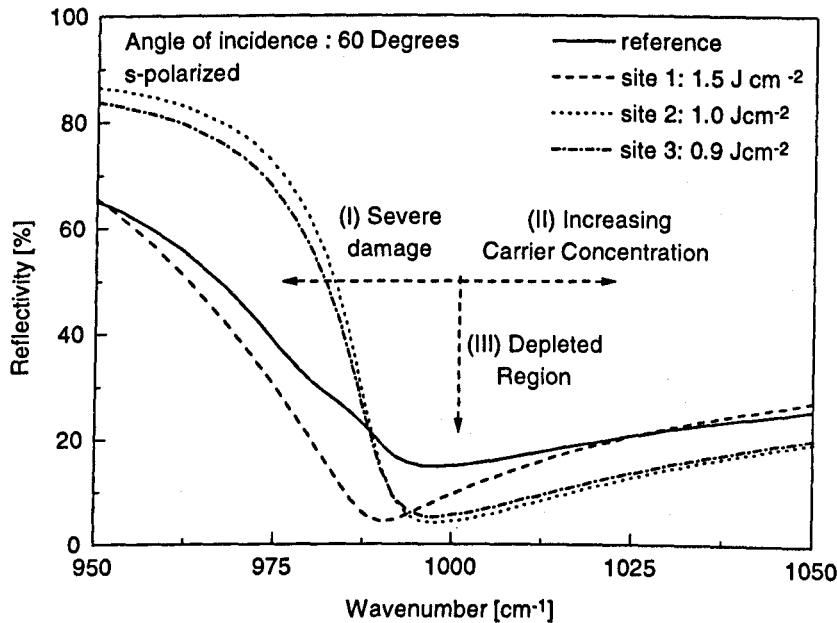


Figure 5.5:41 Infrared reflectivity spectra of laser irradiated 6H-SiC. Measurements were made using s polarised light at an angle of incidence of 60 degrees.

5.5.6 Structural Modifications of XeCl Laser Annealed 4H-SiC

Photoluminescence of radiation induced defects in ion-implanted Silicon Carbide has been a subject of great interest and goes as far back as the late 1960's and early 70's [59]. Qualitative information about the concentrations of extrinsic components are generally carried out by measuring the band edge excitonic emission. Generally, these measurements are carried out at liquid helium temperatures ~ 4.2 k to reduce thermal quenching. However the samples used in the annealing experiments were made on quartered wafers, which would allow more convenient electrical measurements and as a consequence were too large to fit into the liquid helium cryostat. However, the spectrometer previously described in Chapter 3, was capable of holding the larger samples and was used to carry out the experiments described below. Briefly, the

Excimer Laser Annealing of Ion-Implanted 4H- and 6H-Silicon Carbide

optical resolution of this system was 2nm and the Silicon Carbide was excited using an Ar⁺ laser at a wavelength of 351nm.

Figure 5.5:42, illustrates the changes in photoluminescence spectra for a range of laser fluence. It was not possible to detect a luminescent signal from the as-implanted material due to ion-implantation damage (Dose: $1 \times 10^{15} \text{ cm}^{-2}$) and therefore no reference signal is shown. The sample was irradiated at 308 nm with range of laser fluence between 1.0 and 1.6 J cm^{-2} with 5 and 10 laser pulses. From the infrared measurements in Chapter 5.5.2, lattice recovery was evident between 0.9 and 1.0 J cm^{-2} . This is in close agreement with the luminescent intensity in Figure 5.5:42, where a maximum intensity is observed at 1.0 J cm^{-2} . The luminescent intensity decreased with increasing laser fluence, which strongly suggests the material became damaged with increasing laser fluence. The actual laser fluence for optimum lattice recovery cannot be identified exactly because the lowest laser fluence carried out in this actual set of measurements was 1.0 J cm^{-2} and if a lower fluence had have been used then this could have indeed produced a slightly higher intensity, hence improved annealed surface.

Apart from the increased intensity, the spectra indicating lattice recovery in Figure 5.5:42, exhibits two relatively sharp peaks at 3.001 and 3.041 eV. In comparison, the as-received substrate before implantation, in Chapter 3, Figure 3.4:3, showed only one relatively sharp peak at 3.005 eV and the presence of an emission band at $\sim 3.033 \text{ eV}$. From the Free-Acceptor (A_0) and Donor-Acceptor-Pair transitions (B_0 and C_0 peaks), equations (3:3) and (3:5), the assignment of such peaks depend on the values associated with the exciton binding energy, the donor and acceptor ionization energies, and the coulomb energy term; equation (3:6). With the present data it is difficult distinguish between the (A_0) and (B_0) peaks, hence, establish the nature of the evolved peak subsequent to excimer laser annealing. It is however highly probable that the peak is related to the implantation of nitrogen.

Excimer Laser Annealing of Ion-Implanted 4H- and 6H-Silicon Carbide

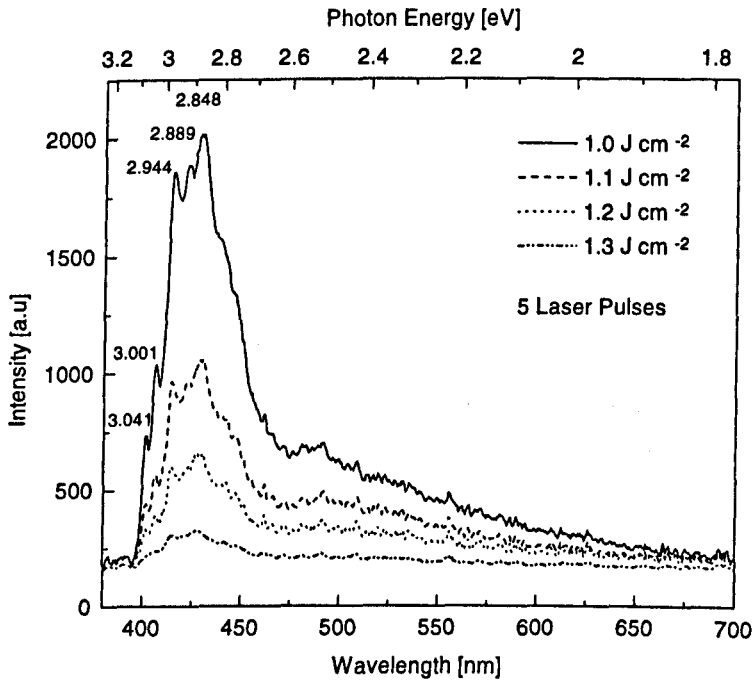


Figure 5.5:42: Photoluminescence spectra of excimer laser annealed ($\lambda = 308$ nm) 4H-SiC, in an argon ambient, at a pressure of 35 bar.

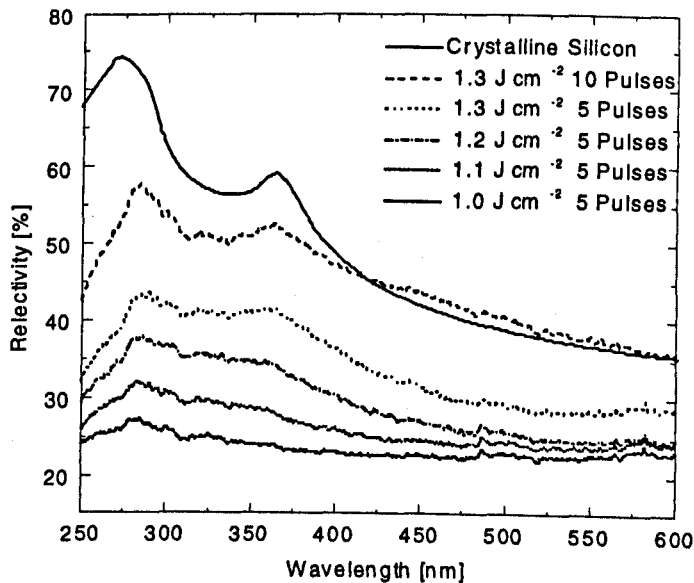


Figure 5.5:43 Visible reflection spectra of excimer laser annealed 4H-SiC (sample #3, in Chapter 3.)

Excimer Laser Annealing of Ion-Implanted 4H- and 6H-Silicon Carbide

Subsequent to laser annealing the reflectivity spectra was measured for the same sample as that shown above, and is illustrated in Figure 5.5:43. By comparing the reflectivity and photoluminescence spectra it can be seen that there is an increase in the reflectivity with a corresponding decrease in the photoluminescence intensity spectra. Also shown in Figure 5.5:43 is a reflectivity spectra for crystalline Silicon which corresponds to the theoretical reflectivity of bare silicon [60], The peak at ~ 360 nm matches the evolving peak in Silicon Carbide. This indicates the existence of elemental polycrystalline silicon which is consistent with the thermodynamic argument that Silicon Carbide dissociates into molten silicon with dissolved Carbon at temperatures close to the melting point [61].

5.6 Conclusion

Infrared reflectivity measurements have been carried out in order to correlate the laser fluence and pulse number with changes in reflectivity subsequent to laser annealing. Measurements were made over the Reststrahlen region over the spectral range $700 - 8000 \text{ cm}^{-1}$. The amount of induced damage on implanted material could be seen as a decrease in reflectivity with increasing implantation dose. An optimum laser fluence at 308nm was identified has being between 0.9 and 1.0 J cm^{-2} , above which, the reflectivity was seen to decrease indicating the evolution of damage.

Spatial dispersion measurements were carried out at 16 , 30 and 60 degrees from the normal using s and p polarisation. The mixed polarisation was separated out into the s and p components and the reflectivity was measured for the different angles of incidence. The reflectivity now measured with the deconvoluted s and p vectors were more sensitive to the changes made subsequent to laser irradiation. Particularly, the sensitivity of the plasma edge, where subtle shifts were more evident when measured with p polarisation.

Excimer Laser Annealing of Ion-Implanted 4H- and 6H-Silicon Carbide

The reflectivity was modeled using the Lorentz-Drude formalism. The phonon damping constant, Γ , which is a measure of the level of crystallinity was in agreement with experimental results, tending to low values between 0.9 and 1.0 J cm⁻² and increasing in value above this laser fluence.

Visible reflectivity measurements also showed an evolution of a peak situated at ~270 nm for Silicon Carbide irradiated over a range of laser fluence and pulse number. This strongly suggested the evolution of silicon rich features and that material was tending to dissociate at the higher laser fluence, typically ~ 1.3 Jcm⁻².

5.7 References.

-
- [1] B. Canut, S. Ramos, J. A. Roger, J. P. Chante, M. L. Locatelli, D. Planson. *Mat. Sci. and Eng* **B46**, 267 (1997).
- [2] N. Ramungul, V. Khemka, Y. Zheng, R. Patel, and T. P. Chow. *IEEE Transactions on Electron Devices*, **43**, 465 (1999).
- [3] K. A. Jones, K. Xie, D. W. Eckart, M. C. Wood, V. Talyansky, T. Venkatesan, K. Wongchotigul and M. Spencer. *J. Appl. Phys.* **83**, (12) 8010 (1998).
- [4] G. Krotz, W. Hellmich, G. Derst, S. Kalbitzer. *Nucl. Instrum. Methods* **B 80/81**, 927 (1993).
- [5] L. Muehlhoff, W. J. Choyke, M. J. Bozach, *J. Appl. Phys.* **60**, 2842 (1986).
- [6] S. Y. Chou, Y. Chang, K. H. Weiner, T. W. Sigmon, and J. D. Parsons. *Apply. Phys. Lett.* **56**(6), 530 (1990).
- [7] L. Ottaviani, M. L. Locatelli, D. Planson, K. Isoird, J. P. Chante, E. Morvan, and P. Godignon. *Materials Science and Engineering* **B61-62**, 424 (1999).
- [8] M. V. Rao, J. Gardner, P. Griffiths, O. W. Holland, G. Kelner, M. Ghezzi, D. S. Simons, and P. H. Chi., *Inst. Phys. Conf. Ser. No* **142**, 521 (1996).
- [9] H. Sonntag and S. Kalbitzer *Apply. Phys. A.* **A61**, 363 (1995).
- [10] E. Valcheva, T. Paskova, I. G. Ivanov, R. Yakimova, Q. Wahab, S. Savage, N. Nordell and C. I. Harris, *J. Vac. Sci. Technol.* **B 17**(3), 1040 (1999).
- [11] R. A. Yankov, M. Voelskow, W. Kreissig, D. V. Kulikov, Jpezoldt, W. Skorupa, Yu. V. Trushin, V. S. Kharlamov and D. N. Tsigankov, *Tech. Phys. Lett.* **23**(8), 627 (1997).
- [12] T. Henkel, V. Heera, R. Kogler and W. Skorupa, *J. Appl. Phys.* **84**(6), 3090 (1998).
- [13] S. Ahmed, C. J. Barbero, T. W. Sigmon, *Apply. Phys. Lett.* **66**(6), 712 (1995).
- [14] T. Kimoto, A. Itoh, H. Matsunami, T. Nakata, M. Wantanabe, *J. Electron Mater.* **24**(4), 325 (1995).
- [15] T. Miyajima, N. Tokura, A. Fukumoto, H. Hayashi, and K. Hara. *Jpn. J. Appl. Phys.* **2B 35**(1), 1231 (1996).
- [16] A. Hallen, A. Henry, P. Pellegrino, B. G. Svensson, and D. Aberg. *Materials Science and Engineering* **B61-62**, 378 (1999).
- [17] S. Fung, M. Gong, C. D. Belling, G. Brauer, H. Wirth, W. Skorupa, *J. Appl. Phys.* **84**, 1152 (1998).
- [18] W. J. Weber, N. Yu, L. M. Wang, N. J. Hess. *Mater. Sci. and Engr. A* **253 142**, (1998).
- [19] E. Wendler, A. Heft, W. Wesch. *Nucl. Instr. And Meth. B* **141**, 105 (1998).
- [20] R. F. Davies, G. Kelner, M. Shur, J. W. Palmour, and J. A. Edmond, *Proc IEEE* **79**, 677 (1991).
- [21] V. Heera, R. Kogler, W. Skorupa. And E. Gaser, *Mater. Res. Soc. Symp. Proc.* **316**, 229 (1994).

Excimer Laser Annealing of Ion-Implanted 4H- and 6H-Silicon Carbide

-
- [22] V. Heera, R. Kogler, W. Skorupa. *J. Stoemenos. Appl. Phys. Lett.* **67**, 1999 (1995).
- [23] E. I. Shtyrkov, I. B. Khaibullin, M. F. Galyautdinov and M. M. Zaripov, *Opt. Spektrosk.* **38**, 1031 (1975).
- [24] E. I. Shtyrkov, I. B. Khaibullin, M. M. Zaripov, M. F. Galyautdinov, and R. M. Bayazitov. *Sov. Phys. Semicond.* **9**, 1309 (1975).
- [25] J. A. Van Vechten, R. Tsu, and F. W. Saris. *Phys. Lett. A.* **74**, 422 (1979).
- [26] Y. Hishida, M. Watanabe, K. Sekine, K. Sugino, and J. Kudo. *Appl. Phys. Lett.* **76**(26), 3867 (2000).
- [27] Y. Hishida, M. Watanabe, K. Nakashima, and O. Eryu. *Material Science Forum* **338-342**, 873 (2000).
- [28] H. Ohyama, T. Suzuki, K. Nishi, T. Mitsuyu, T. Tomimasu. *Appl. Phys. Lett.* **71**, 823 (1997).
- [29] V.V Makarov, T. Tuomi, K. Naukkarinen, M. Luomajarvi and M. Riihonen. *Appl. Phys. Lett.* **35**, 922 (1979).
- [30] H. Rubens and E. F. Nichols, *Weid. Ann.* **60**, 418 (1887).
- [31] C. R. Pidgeon, *Free Carrier Optical Properties of Semiconductor*, T. S. Moss, M. Balkanski (Eds), *Handbook on Semiconductors*, vol 2, North Holland, Amsterdam, (1980), pp227-230.
- [32] T. Zorba, D. I. Siapkas and C. C. Ktsidis, *Microelectronic Engineering* **28**, 229 (1995).
- [33] J. Pezoldt, R. A. Yankov, T. Werninghaus, D. R. T. Zahn, W. Fukarek, G. Teichert, M. Luebbe, and W. Skorupa. *Diamond and Related Materials.* **8**, 346 (1999).
- [34] H. Hobert, H. Dunken, R. Menzel, T. Backmann, and W. Wesch. *J. of. Non-Crystalline Solids.* **220**, 187 (1997).
- [35] *Introductory to Solid State Physics*, C. Kittel, 7th Edition John Wiley and Son 1986.
- [36] M. F. Macmillan, A. Henry, and E. Janzen. *J. of. Elect. Mater.* **27**(4), 300 (1998).
- [37] T. Zorba, D. I. Siapkas, C. C. Hatsidis, *J. Microelectronic. Engineering.* **28**, 229 (1995).
- [38] J. M. Bluet, K. Chourou, M. Anikin, and R. Madar. *Material Science and Engineering.* **B61-62**, 212 (1999).
- [39] K. Pfennighaus, A. Fissel, M. Oehme et-al. In: *Fruhjahrstagung der Deutschen Physikalischen Gesellschaft, Munster* 17.3-21.3.
- [40] H. Hobert, H. H. Dunken, G. Peiter, M. Diegel, and H. Stafast, *Appl. Phys. A.* (1999)
- [41] T. T. Zorba, C. L. Mitsas, I. D. Siapkas, G. Z. Terzakis, D. I. Siapkas. *Appl. Surf. Sci.* **120**, 102 (1996).
- [42] J. P. Biersack and L. Haggmark, *Nucl. Instr. and Methods*, **174**, 257 (1980).
- [43] C. J. McHargue, P. S. Sklad, C. W. White, *Nucl. Inst. and Meth. B.* **46**, 79 (1990).
- [44] W. J. Webber, N. Yu. L. M. Wang, N. J. Hess. *J. Nucl. Mater.* **244**, 258 (1997).

Excimer Laser Annealing of Ion-Implanted 4H- and 6H-Silicon Carbide

-
- [45] T. Troffer, M. Schadt, T. Frank, H. Itoh, G. Pensl, J. Heindl, H. P. Strunk, and M. Maier, *Phys. Stat. Sol. A* **162**, 227 (1997).
- [46] D. Peters, R. Schorner, K. H. Holzein, and P. Friedrichs, *Appl. Phys. Lett.* **71**, 2996 (1997).
- [47] A. Hallen, P. P. A. Persson, A. Yu. Kuznetsov, L. Hultman, and B. G. Svenson, *Material Science Forum* **338-342**, 869 (2000).
- [48] V. Heera and W. Skoupa, *mater. Res. Soc. Symp. Proc.* **438**, 241 (1996).
- [49] L. Muehlhoff, W. J. Choyke, M. J. Bozack and J. T. Yates, Jr. *Appl. Phys.* **60**, 2842 (1986).
- [50] N. Pan, J. A. Cooper, Jr, and M. R. Melloch, *J. Electron. Mater.* **26**, 208 (1997).
- [51] K.A. Jones, K. Xie, D. W. Eckart, M. C. Wood, V. Talyansky, R. D. Vispute, T. Venkatesan, K. Wongchotigul and M. Spensor, *appl. Phys.*, **83**, 8010 (1998).
- [52] D. W. Berreman, *Phys. Rev.* **130**, 2193 (1963).
- [53] F. Engelbrecht, R. Helbig, *Physical Review B*, **48**(21), 15698, (1993).
- [54] S. S. Mitra, in E. D. Palik (Ed.), *Handbook of Optical Constants of Solids*, Academic Press, New York, (1985), p. 547.
- [55] P. Grosse, et al., M. Offenber, *Appl. Phys A.* **39**, 257 (1986).
- [56] B. Harbecke, *Proc. IEEE* **79**, 165 (1993).
- [57] A. D. Rakic, *Phys. Rev. E.* **52**, 6862 (1995).
- [58] *Non Destructive Evaluation of Semiconductor Materials and Devices*, Ed., J. N. Zemel, p. 336.
- [59] L. Patrick and W. J. Choyke, *Physical Review B*, **5**, (8) 3253 (1972).
- [60] S. S. Mitra, in: E. D. Palik., in *Handbook of Optical Constants and Solids*, Academic Press, New York, 1985, p. 547.
- [61] S. V. Baranov, A. G. Vodop'yanov, G. K. Moiseev, and G. N. Kozhevnikov. *J. of Inorganic Materials.* **18** (8), 1097 (1982).

Chapter 6

Summary and Conclusion

6.1 Summary	156
6.2 Conclusion	168
6.3 References	169

Chapter 6

Summary and Conclusion

6.1 Summary

At the time this work was carried out very little research had been carried out on excimer laser processing of 4H-Silicon Carbide. High quality material only became commercially available in 1994, thus, research work in this area was in its infancy. One of the main areas of research in the semiconductor community was aimed at producing devices for high temperature, high frequency and high power applications. An associated requirement for the realisation of such a device is a highly doped p-n junction. The work in this thesis set out to address some of the problems that are associated with the low atomic diffusion of nitrogen dopants and also that of ion implantation induced damage.

Chapter 1 began with a brief introduction and history of events showing how Silicon Carbide is a material that offers promise for the future. It was briefly shown how the utilisation of the material has evolved from rather simple applications such as an abrasive medium to more complex semiconductor device applications. Polytypism was briefly discussed in the introduction because of its fundamental importance. The different arrangement of Silicon and Carbon bi-layers give rise to different band structure, e.g. different bandgap energies being one such property, 4H = 3.26 eV, and 6H = 2.95 eV.

The main emphasis of the thesis was then presented, namely, the difficulties associated with the incorporation and activation of nitrogen dopants into Silicon Carbide. The diffusion process in Silicon Carbide was stressed, because of its fundamental importance throughout this work. The

Initial work in Chapter 2 began with investigations on the response of Silicon Carbide when subjected to optical radiation. This consisted of experimental investigations on optical constants, namely, n and k data, using ellipsometric measurements which were then used to determine the reflection and absorption coefficient for the ArF and XeCl laser wavelengths. A set of ablation experiments were undertaken at 193nm and 308nm to establish a processing 'window' for the annealing and defect studies that followed. Experiments carried out under vacuum conditions revealed interesting structural dependency with pressure. It was seen that for a decreasing pressure the surface features became more ordered, almost columnar like. Subsequent to these 193 nm experiments, the surface topology was measured using a mechanical profileometer which revealed protruding features which extended several microns above the original surface. Thus, the absence of etch pits over the fluence range investigated prevented the determination of the threshold fluence using Beer's Law. Experiments were carried out in a oxygen ambient, over a lower fluence range which produced etch pits thus allowing the determination of an estimated ablation threshold fluence. In a similar manner, ablation experiments were carried out to establish a fluence 'window' at a wavelength of 308nm. Swelling of the Silicon Carbide surface was observed at a laser fluence just above the determined ablation threshold, however as the fluence was increased catastrophic (ablation) predominated and material was expelled from the surface. Irradiated material at 308nm and 193nm suggested structural modifications were taking place close to the ablation threshold which brought about questions concerning the thermodynamics of Silicon Carbide under non equilibrium conditions e.g. does Silicon Carbide melt under the action an excimer laser pulse.

The photoluminescence properties of Silicon Carbide were investigated in Chapter 3. Measurements were made on as-received material to obtain a record of the starting conditions. The main objectives were to measure and identify changes in the luminescence spectra after being subjected to excimer laser radiation, with aim of creating and identifying laser induced defect

centres. Silicon Carbide has a long history of photoluminescence studies, especially the pioneering work carried out by Choyke, but little or no such work existed at this time on excimer laser induced defect luminescence. The photoluminescence measurements were undertaken using above bandgap excitation in order to excite all available transitions.

The as-grown spectra for n and p-type material were very different. The intrinsic n-type material doped with acceptor impurities showed strong Donor-Acceptor pair emission (D-A) just below the band edge, whilst the p-type spectra were characterised by a broad band emission centred at around ~ 2.2 eV indicative of deep level impurities such as boron. The as-grown luminescence spectra measured on epitaxial material purchased toward the beginning of this work was not of the highest quality and consisted of a relatively high number of micro pipe defects ($30\text{-}100\text{ cm}^{-2}$). Two broad peaks at ~ 2.594 eV and 2.530 eV were measured from this material which were probably indicative of defects. The peaks were situated on the low energy side of the donor-acceptor tail in p-type material. These bands were of particular interest since similar emissions were observed subsequent to laser irradiating at 308nm at 800 mJ cm^{-2} and appeared to be annealed out at 1000 mJ cm^{-2} . Photoluminescence spectra were also measured for material irradiated at 193nm with an ArF laser and a similar broad band emission was also seen to emerge at ~ 2.5 eV. When the laser fluence was increased the photoluminescence intensity decreased in intensity suggesting the material was becoming damaged. Hydrogen passivation experiments were performed to investigate the nature of this band. It was shown that the induced emission band could be removed when irradiated at 308nm such that the photoluminescence spectra returned close to the as grown state. The hydrogen incorporation was also checked for its stability with time. The spectra did indicate some subtle changes suggesting the hydrogen diffused out with time, however the changes were minimal when compared to the depassivation experiments using the XeCl laser at 308nm .

Positron annihilation measurements were carried out in Chapter 4. Positrons, sensitive to open volume defects, namely vacancies, were used to help determine the nature of the laser induced emission band. The combined results from the PL and PA experiments helped identify the possible modifications that were taking place subsequent to laser irradiation. Results from the normalised S parameter revealed vacancy agglomerates consisting of about 8 di-vacancies. At 308nm the damage consisted of a buried layer of defects about 70nm wide occurring at depth of about 50nm beneath the surface. The extent of the damage was seen to shift further away from the surface with increasing laser fluence. At 193 nm, the damage was situated closer to the surface compared with the results at 308 nm.

The fifth chapter was devoted to Infrared reflection measurements on excimer laser annealing of ion-implanted material. Infrared reflection measurements at normal and variable angles of incidence were performed in order to ascertain the effects of the laser radiation. Infrared measurements were made both before and after the laser annealing experiments took place. The aim of this work was to repair the lattice using the technique of laser annealing.

The implanted material was irradiated between 0.9 J cm^{-2} and 1.3 J cm^{-2} using 10 and 15 laser pulses in an Argon ambient at 35 bar. The reflectivity in the Reststrahlen region provided a very useful way of evaluating the effects of the laser annealing experiments. In high quality material, the reflectivity of the characteristic Reststrahlen region is very close to 100%. As the material became damaged, for example by ion-implantation or due to laser induced damage, the reflectivity spectrum was seen to change considerably, generally with a reduction in the reflectivity maximum. It was shown that material damaged by ion implantation could be repaired when irradiated at an optimum laser fluence between $0.9 - 1.0 \text{ J cm}^{-2}$ using a XeCl laser at 308nm.

A Lorentz-Drude model was also used to determine the optical constants from the experimental reflectivity data. Information on the real and imaginary refractive index could be extracted to

give a quantitative description on the effects of excimer laser annealing. After laser irradiating ion implanted material the extinction coefficient increased to a value close to that of high quality as-received material, thus indicating lattice recovery was taking place. It was also shown that beyond the optimum laser fluence the material begins to become damaged due to the laser itself. This was observed by a shift in the plasma edge to lower wavenumbers. From the Lorentz-Drude model, the phonon damping constant, which is a representation of the 'quality/crystallinity' of the material could be extracted and was consistent with a lattice recovery process taking place. Recovery was seen to be most effective for samples implanted with the low implantation dose, for a given laser exposure. However, further investigations were not undertaken to 'completely' recover the lattice for more damaged material, i.e. it is thought that for the samples with a higher implantation dose the laser exposure dose would have to be increased accordingly.

Under equilibrium conditions Silicon Carbide is reported not to melt at atmospheric pressure. However, the heating of a material such as Silicon Carbide under the action of nano second duration laser pulses is inevitably different to equilibrium heating. The thermodynamics of Silicon Carbide were not investigated directly in this work but the possibility of Silicon Carbide melting when subjected to laser irradiation previously raised some debate between other researchers in the field.

The photoluminescence and positron annihilation studies were complimentary and were carried out on excimer laser irradiated Silicon Carbide to investigate the feasibility of inducing vacancy defects. The main thrust of the interest stemmed from the broad emission band at ~ 2.5 eV that was observed predominately when irradiated at 193nm. The nature of the emission band could not be identified solely from the photoluminescence experiments, but taken in conjunction with the positron annihilation experiments at both 193 and 308nm, it was possible to speculate on the nature of the band. Positron annihilation measurements revealed a damaged structure on Silicon Carbide irradiated at both 193nm and 308nm. It was shown that damage occurs above a threshold

fluence with the creation of di-vacancy clusters, the size of which consisted of ~8 di-vacancies per cluster. To some extent the intention of this work was to introduce single vacancy defects homogeneously spread within the lattice in order to assist migration between nearest or next nearest neighbour. The fact of large di-vacancy clusters renders the "laser induced defect mediated diffusion" mechanism ineffective. Large di-vacancies such as this are effectively large holes in the solid and nitrogen diffusion might well be enhanced but effectively the surface of a large open volume defect will passivate. The energy level will probably not be the same as that of substitutional nitrogen and thus affect the electrical characteristic from a device point of view. The creation of large open volume defects, particularly at the highest laser fluence used here (1.8 J cm^{-2}), is consistent with the photoluminescence data, and showed spectra similar to that which might be expected from porous Silicon Carbide.

However, some caution is necessary. Two distinct behaviours were observed in the PA spectra. A threshold at $\sim 1.4 \text{ J cm}^{-2}$ was evident but also the spectrum changed markedly at 1.8 J cm^{-2} . The fluence used here to irradiate the as-received material was higher than those used in the annealing of implanted material. In order to test a simple hypothesis, a single piece of relatively poor quality, but un-implanted 4H-Silicon Carbide was irradiated and no noticeable effect on the surface was apparent until the incident fluence exceeded 1.6 J cm^{-2} . Here it is argued that the melting of Silicon Carbide is associated with the formation of silicon droplets which, as was briefly pointed out in Chapter 3, manifest themselves as a silver/blue colouration of the surface. It is then apparent from this simple experiment that significant melting does not occur in un-implanted, crystalline material, at the fluence threshold observed in PAS measurements on implanted material. The formation of di-vacancy clusters appears to be a solid state phenomenon probably associated with the tendency of Silicon Carbide to sublime at about $1700 \text{ }^\circ\text{C}$. The surface temperature will far exceed this and significant numbers of atoms may have sufficient energy to be removed from the lattice. However, at 1.8 J cm^{-2} , the lattice has almost certainly

melted (2700 C) and the different behaviour seen in PAS will probably be associated with this transition. However, it is apparent from the PAS (figures 4.6:2, 4.6:3) that large open volume defects do exist, more so than at lower fluences, and the creation of a structure resembling porous Silicon Carbide is quite likely.

The open volume defects created by sub-melting fluences $< 1.4 \text{ Jcm}^{-2}$ may well be the same as those giving rise to the new band in laser irradiated Silicon Carbide. Since this band exists in untreated material to a greater or lesser extent, it is likely to be associated with a common defect in Silicon Carbide, and the possibility that it is a surface defect of some sort cannot be ruled out. The micro-pipe defect density of Silicon Carbide available today has been reduced very significantly, but at the time this work commenced micro-pipes were still a common feature of Silicon Carbide. The presence of surface defects randomly positioned over the wafer is therefore quite likely, and we suggest that these surface defects have essentially the same structure as the defects created by laser irradiation. By way of illustration, Figure 6.1:1 shows the photoluminescence signal as a function of position across a particular piece of Silicon Carbide. Note how the characteristic defect band emerges as the exciting radiation is scanned across the sample to the point where this band is the dominant band in the spectrum. This particular defect at $\sim 2.55 \text{ eV}$, not visible to the naked eye, also existed in the as-purchased material.

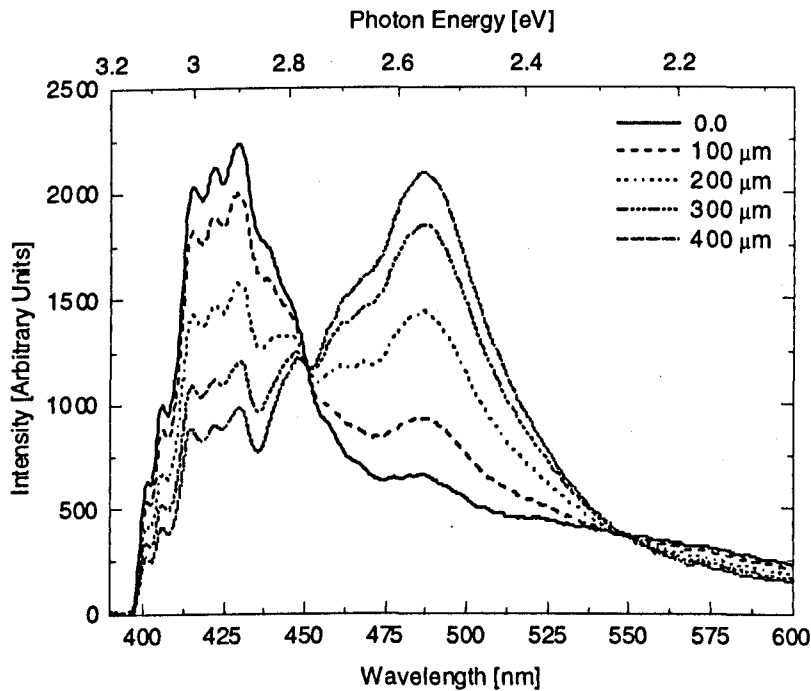


Figure 6.1:1 Spatially resolved photoluminescence spectra for as-received 4H-Silicon Carbide. The legend indicates the spectra measured at different spatial separations on the sample surface.

It was shown that when irradiated at 308nm a buried layer of defects extended deeper than at 193nm. Although at 193nm the value of the normalised S parameter implied a similar number of defects, they were existed closer to the surface. This is in some agreement with the optical absorption depth at 193 nm which was much smaller than at 308nm. It is not certain why the damage extends to a greater depth beneath the surface. However, one possibility might be due to the higher temperature experienced at the surface leading to preferential damage recovery. The temperature will be higher at the surface and it is possible not only that vacancies are created but also that vacancy migration can occur which repairs the damage to some extent. Beneath the surface, however, the maximum temperature reached will depend on the depth and there will probably be a point where vacancies are created but significant migration and repair cannot occur

before the temperature drops below a critical value. Alternatively, if Silicon Carbide has in fact melted, the melt depth would increase with laser fluence and during solidification the Silicon Carbide might re-grow epitaxially, effectively annealing out any defects. This argument can only apply if stable melting of Silicon Carbide is possible, and it is not clear yet that this is the case.

It was shown in Chapter 5 that a damaged lattice could be recovered by the application of excimer radiation at 308nm with a laser fluence of 0.9 Jcm^{-2} to 1.0 Jcm^{-2} in an Argon ambient at 35 bar. Visible reflection measurements for laser annealed material as a function of laser fluence were measured and illustrated in Chapter 5, Figure 5.5:43. The evolving reflectivity spectra strongly suggested that at the high laser fluence, higher than that required for optimum lattice recovery, the Silicon Carbide was beginning to decompose. As the laser fluence or pulse number was increased a peak in the reflectivity spectra at $\sim 370 \text{ nm}$ emerged with increasing strength. This feature is evidence for the presence of crystalline silicon in the surface since nothing in the optical constants for Silicon Carbide will explain it, but the refractive index of crystalline silicon will. It is therefore suggested that as the Silicon Carbide decomposes the silicon components begin to nucleate forming silicon droplets. This is consistent with thermodynamic arguments [1] that Silicon Carbide dissociates into molten Si with dissolved carbon at temperatures close to the melting point. This strongly suggests that the lattice recovery occurring at lower fluences does not involve melting.

The fluences at which lattice recovery occurs in implanted material are significantly lower than those used in the PAS and some comment is necessary. Implanted material is noticeably darker in colour than virgin Silicon Carbide, and the infrared spectra show very clearly that the implanted surface region has a different refractive index. Implanted material appears to have a lower band gap and to be more absorbing. Furthermore, since it is damaged the thermal conductivity might be adversely affected. It is reasonable to assume, whether it is because of optical effects alone or combined with thermal effects, that laser radiation is coupled into the material more effectively

and at a given fluence that the surface temperature is higher than in un-implanted material. Therefore the implanted material is repaired at a lower fluence than virgin material. Furthermore, the PL signal from material where the lattice has recovered shows no sign of an increase in the characteristic defect band in the PL. Therefore lattice recovery appears to take place without significant damage to the material, unless the initial fluence is too high and melting occurs.

It only remains to deal with the activation of the dopants and possible future work. Electrical measurements are required to determine whether or not the activation is taking place in the samples that were laser annealed at 308 nm. It is possible to estimate whether activation should occur during a laser pulse from the known variation of the diffusion coefficient with temperature. Such data is extremely scarce but work has been published which indicates the temperature dependence of the diffusion coefficient [1]. Using this in combination with cooling curves will yield an estimate of the total nitrogen diffusion. The validity of this approach has been demonstrated by [2] at Hull. It has been shown that while pulsed laser annealing is a highly non-equilibrium process many of the conventional equilibrium thermodynamic concepts can be applied. Thus phase segregation on solidification can occur, as can diffusion. Extrapolation of the known diffusion coefficients of Mn in CdTe to the melting point of CdTe in conjunction with a simple theoretical heating and cooling cycle yields integrated diffusions which agree remarkably well with the experimentally observed total diffusion.

Accordingly, theoretical calculations were carried out to estimate the diffusion length of Nitrogen dopants in Silicon Carbide. The amount of atomic diffusion is strongly dependent on the laser fluence owing to the strong temperature dependence of atomic diffusion coefficients. The variation of the diffusion coefficient with time is illustrated in Figure 6.1:2, which is simply a transformation of the temperature during the laser heating and subsequent cooling.

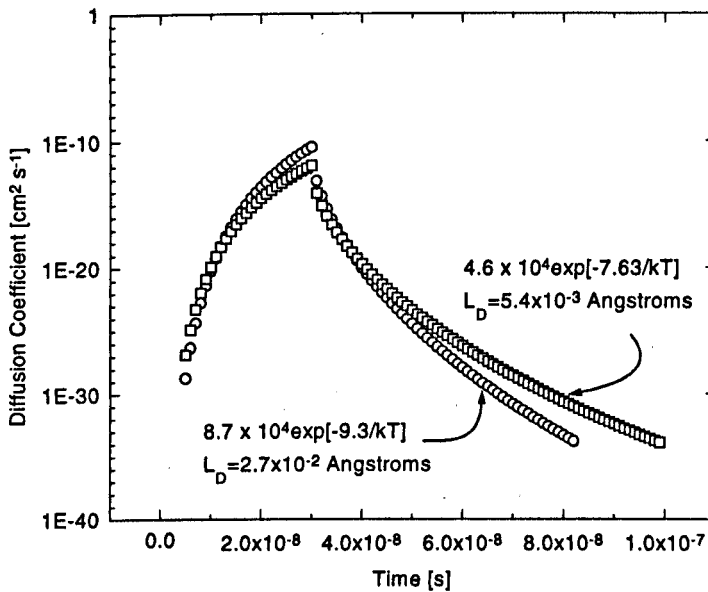


Figure 6.1:2 Calculated Integrated diffusion length for Nitrogen dopants in Silicon Carbide, activation energies taken from [1]

A laser pulse of uniform irradiance over the pulse duration was assumed in these calculations. The heating cycle is calculated such that the surface temperature just reaches melting point. The activation energy for nitrogen in Silicon Carbide taken from Ref [1], are 7.63eV and 9.3eV. The atomic diffusion length was then estimated by integrating under the whole curve. The predictions suggest that the amount of atomic diffusion that takes place is far less than the inter-atomic lattice spacing (~3 Angstroms), which can be thought of as the minimum distance that is needed for activation to occur. In short, then, it would appear that effective lattice recovery occurs, for which the self-diffusion coefficients must be significantly higher than for nitrogen, but the nitrogen atoms effectively remain in the interstices.

Because of the exponential form of the diffusion equation and the statistical nature of diffusion, there is the possibility that some of the diffusing species migrate further. Even if the calculated diffusion length is an order of magnitude too low, the migrating dopants will still not reach the host lattice site. This is especially true if the nitrogen dopants are situated at an interstitial site several atomic spacings away from a convenient vacant lattice site.

6.2 Conclusion

The interaction of Silicon Carbide with radiation from an ArF and XeCl excimer laser has been investigated and approached from two different directions. Firstly, to investigate a way of enhancing the dopant diffusion, a process referred to as “laser induced defect mediated diffusion”, and secondly, to recover the lattice in nitrogen ion-implanted Silicon Carbide. In conclusion;

- ◆ Positron annihilation measurements of excimer laser irradiated Silicon Carbide revealed the creation of large open volume defects. These defects occur at and above a laser threshold fluence of 1.4 J cm^{-2} and consist of ~ eight Silicon-Carbon di-vacancies. The defect clusters are considered to be too large for the efficient enhancement of Nitrogen diffusion. This is also supported by simple integrated diffusion calculations where the nitrogen dopants are predicted to diffuse less than the atomic lattice spacing.

- ◆ Excimer laser annealing at 308 nm has been successfully employed to recover the damage induced by nitrogen ion implantation. Utilizing infrared reflection measurements, lattice recovery is seen to be most effective in the fluence range $0.9 - 1.0 \text{ J cm}^{-2}$.

- ◆ When irradiated above the optimum laser fluence for lattice recovery, visible reflectivity data suggests that Silicon Carbide decomposes with the formation of Silicon droplets.

6.3 References

-
- [1] S. V. Baranov, A. G. Vodop'yanov, G. K. Moiseev, and G. N. Kozhevnikov. *J. of Inorganic Materials*. **18**(8), 1097 (1982).
- [2] H. Howari, D. Sands, J. E. Nicholls, J. H. C. Hogg, T. Stirner, and W. E. Hagston. *J. of Appl. Phys.* **88**, (3) 1373 (2000).

Publications

Positron Annihilation Spectroscopy of Laser Irradiated 4H-SiC.

P. G. Coleman, F. Malik, M. J. Uren, K. M. Brunson, D. Sands and C. D. Walton. *Applied Surface Science*, **149** 144-147 (1999).

Infrared Reflectivity of Ion-Implanted and Pulsed Excimer Laser

Irradiated 4H-SiC. P. H. Key, D. Sands, M. Schlaf, C. D. Walton, C. J. Anthony, K.M. Brunson, M. J. Uren. *J. of Thin Solid Films*, **364** 200-203 (2000).

Optical Characterization of Lattice Damage and Recovery in Ion-Implanted and Pulsed Excimer Laser Irradiated 4H-SiC.

D. Sands, P. H. Key, M. Schlaf, C. D. Walton, C. J. Anthony, and M. J. Uren. *Material Science Forum*, **338-342** 655-658 (2000).

Presentations.

Ion-Beam Analysis of Excimer Laser Irradiated 4H-SiC.

D. Sands, C. D. Walton, C. Jeynes, A. P. Knights, M. J. Uren, K. M. Brunson, C. J. Anthony, P. G. Coleman, and F. Malik. Presented at the Ion Beam Users Meeting. University of Surrey, March 23th 1999.

Optical Characterization of Lattice Damage and Recovery in Ion-Implanted and Pulsed Excimer Laser Irradiated 4H-SiC.

D. Sands, P. H. Key, M. Schlaf, C. D. Walton, C. J. Anthony, and M. J. Uren. Presented at the International Conference on Silicon Carbide and Related Materials (ICSCRM99) Raleigh, North Carolina 10th -15th Oct. 1999.